NASA Technical Paper 1163

Effect of Winglets on a First-Generation Jet Transport Wing

V - Stability Characteristics of a Full-Span Wing With a Generalized Fuselage at High Subsonic Speeds

Peter F. Jacobs

MARCH 1978

NASA

NASA Technical Paper 1163

Effect of Winglets on a First-Generation Jet Transport Wing

V - Stability Characteristics of a Full-Span Wing With a Generalized Fuselage at High Subsonic Speeds

Peter F. Jacobs
Langley Research Center
Hampton, Virginia

SUMMARY

This paper presents the effects of winglets on the static aerodynamic stability characteristics of a KC-135A jet transport model at high subsonic speeds. The investigation was conducted in the Langley 8-foot transonic pressure tunnel using 0.035-scale wing panels mounted on a generalized research fuselage.

Data were taken over a Mach number range from 0.50 to 0.95 at angles of attack ranging from -12° to 20° and sideslip angles of 0°, 5°, and -5°. The model was tested at two Reynolds number ranges to achieve a wide angle-of-attack range and to determine the effect of Reynolds number on stability.

Results of the investigation indicate that adding the winglets to the basic-wing configuration produces small increases in both lateral and longitudinal aerodynamic stability and that the model stability increases slightly with Reynolds number. The winglets do increase the wing bending moments slightly but the buffet onset characteristics of the model are not affected by the winglets.

INTRODUCTION

Winglets are intended to provide a substantially greater reduction in induced drag at cruise conditions than that obtained with a simple wing-tip extension which was designed to impose the same bending-moment increments on the wing structure as the winglets. The National Aeronautics and Space Administration (NASA) has been conducting extensive experimental investigations of the effects of winglets on first- and second-generation jet transport wings. (See refs. 1 to 7.)

As a result of the cruise performance benefits shown in the wind-tunnel investigation of reference 1, NASA and the U.S. Air Force have initiated a joint flight research and demonstration program to examine the application of winglets to the KC-135A transport aircraft. In support of the program, extensive wind-tunnel investigations have been conducted on semispan and full-span models of the KC-135A. Performance, loads, stability and control, and buffet data have been obtained over the aircraft operational envelope.

This paper, which is one of a series, presents force and moment data at high subsonic speeds for a 0.035-scale full-span model of the KC-135A wing on a representative fuselage. Two separate wind-tunnel entries were made with this model. The first entry was concerned mainly with stability characteristics at cruise conditions over a limited angle-of-attack range from -8° to 11° for a Reynolds number range from 12.5×10^6/m (3.8×10^6/ft) to 18.7×10^6/m (5.7×10^6/ft). The second entry was made specifically to achieve a wider angle-of-attack range from -12° to 20° for a Reynolds number of 10.8×10^6/m (3.3×10^6/ft). Data were taken over a Mach number range

from 0.50 to 0.95 and at sideslip angles of 0°, 5°, and -5°. Data from both wind-tunnel entries are presented herein. For some of the Mach numbers, the angle-of-attack range presented varies as a result of the inclusion of data from the two wind-tunnel entries. The tests were conducted in the Langley 8-foot transonic pressure tunnel.

SYMBOLS

The results presented in this paper are referred to the stability-axis system for the longitudinal aerodynamic characteristics and to the body-axis system for the lateral-directional aerodynamic characteristics. Force and moment data have been reduced to conventional coefficient form based on the geometry of the basic wing planform. Moments are referenced to the quarter-chord point of the mean aerodynamic chord of the basic wing. All dimensional values are given in both the International System of Units (SI) and U.S. Customary Units; however, all measurements and calculations were made in U.S. Customary Units. (See ref. 8.)

Coefficients and symbols used herein are defined as follows:

b wing span, 138.7 cm (54.6 in.)

C_B wing bending-moment coefficient, $\dfrac{\text{Bending moment}}{q_\infty(S/2)(b/2)}$

$C_{B,rms}$ wing root-mean-square (rms) bending-moment coefficient (obtained from an integration of rms deviations about steady-state bending-moment value), $\dfrac{\text{rms bending moment}}{q_\infty(S/2)(b/2)}$

C_D drag coefficient, $\dfrac{\text{Drag}}{q_\infty S}$

C_L lift coefficient, $\dfrac{\text{Lift}}{q_\infty S}$

C_{L_α} lift-curve slope, $\dfrac{\Delta C_L}{\Delta \alpha}$, per degree

C_l rolling-moment coefficient (C_1 on computer-drawn figures), $\dfrac{\text{Rolling moment}}{q_\infty Sb}$

C_{l_β} rate of change of rolling-moment coefficient with sideslip angle (effective-dihedral parameter), $\dfrac{\Delta C_l}{\Delta \beta}$, per degree

C_m pitching-moment coefficient, $\dfrac{\text{Pitching moment}}{q_\infty S \bar{c}}$

$C_{m_{C_L}}$ longitudinal stability derivative, $\dfrac{\Delta C_m}{\Delta C_L}$

$C_{m,o}$ pitching-moment coefficient at zero lift

C_n yawing-moment coefficient, $\dfrac{\text{Yawing moment}}{q_\infty S b}$

C_{n_β} rate of change of yawing-moment coefficient with sideslip angle (directional-stability parameter), $\dfrac{\Delta C_n}{\Delta \beta}$, per degree

C_Y side-force coefficient, $\dfrac{\text{Side force}}{q_\infty S}$

C_{Y_β} rate of change of side-force coefficient with sideslip angle (side-force parameter), $\dfrac{\Delta C_Y}{\Delta \beta}$, per degree

c local streamwise chord of wing

$\bar{c}$ mean aerodynamic chord of basic reference wing panel, 21.03 cm (8.28 in.)

c_t tip chord of basic reference wing panel, 9.96 cm (3.92 in.)

h span of winglet from chord plane of wing tip (see fig. 2(b)), cm (in.)

M_∞ free-stream Mach number

q_∞ free-stream dynamic pressure, kPa (psf)

R Reynolds number per unit length, per m (per ft)

S basic wing planform reference area, 0.270 m^2 (2.91 ft^2)

x chordwise distance from leading edge, positive aft, cm (in.)

z   vertical coordinate of airfoil, positive upward, cm (in.)

α angle of attack, deg

β angle of sideslip, deg

Δ incremental value

Subscript:

basic   basic wing

EXPERIMENTAL APPARATUS AND PROCEDURES

Test Facility

The investigation was conducted in the Langley 8-foot transonic pressure tunnel, a continuous-flow, single-return tunnel with a slotted, rectangular test section. The longitudinal slots in the floor and ceiling of the test section reduce wall interference effects and allow relatively large models to be tested through the subsonic speed range. Available controls permit independent variation of Mach number, stagnation pressure and temperature, and dew point. A more detailed description of the tunnel is found in reference 9.

Model Description

The wind-tunnel model used in this investigation consisted of 0.035-scale KC-135A wing panels mounted on a representative fuselage. Photographs of the model in the wind tunnel are shown in figure 1. Drawings of the model are shown in figure 2.

Fuselage.- A generalized research fuselage without a tail was used to represent the KC-135A fuselage in this investigation. A comparison of the two is shown in figure 3.

The fuselage used in this investigation has a maximum diameter of 14.58 cm (5.74 in.) and is 125.88 cm (49.56 in.) long. The fuselage wetted area is approximately 0.52 m^2 (5.63 ft^2). The fineness ratio of the fuselage is about 14 percent less than that typical of narrow-body first-generation jet transports like the KC-135A.

The lower surface of the wing was faired into the fuselage, producing a relatively flat bottom that extended from near the wing leading edge to approximately the trailing edge of the wing. This lower-surface fillet did not increase the maximum diameter of the fuselage.

Wing.- The wing of the model has 7° dihedral, 2° of incidence at the root chord, and no geometric twist. A typical outboard airfoil section is shown in figure 4 and its coordinates are presented in table I. The wing thickness ratio varies nonlinearly from 15 percent at the wing-fuselage juncture to

9 percent at the trailing-edge break station (0.54(b/2)) and then remains constant to the wing tip. The trapezoidal planform of the basic wing (extended to the fuselage center line) has a sweep at the quarter-chord of 35°, an aspect ratio of 7.0, and a taper ratio of 0.35. For all data analysis, the reference geometry parameters S, b, and $\bar{c}$ are based on the trapezoidal planform of the basic wing.

Winglet.- A detailed drawing of the winglet used in this investigation is given in figure 2(b). The winglet was derived from a 9-percent-thick general aviation airfoil. The lower-surface coordinates of this airfoil were then scaled to produce an 8-percent-thick airfoil with greater camber. Winglet airfoil coordinates are presented in table II.

The winglet has a span equal to the wing-tip chord, a root chord equal to 65 percent of the wing-tip chord, a leading-edge sweep of 38°, a taper ratio of 0.32, and an aspect ratio of 2.33. The total area of both winglets is 3.2 percent of the trapezoidal planform area of the basic wing. The winglet is canted outboard 15° from vertical (75° dihedral) and toed out 4° (leading edge outboard) relative to the fuselage center line. The winglet is untwisted and therefore has constant negative geometric incidence across its span. The "upper surface" of the winglet is the inboard surface.

To smooth the transition from the wing to the winglets, fillets were added to the inside corners at those junctures and the outside corners were rounded.

Nacelles.- Flow-through nacelles were used with an inlet diameter of 2.90 cm (1.14 in.) and an exit diameter of 2.08 cm (0.82 in.). The inlet diameter was maintained back to approximately 0.66 of the nacelle length and then tapered linearly to the exit.

Boundary-Layer Transition Strips

Boundary-layer transition strips were placed on both surfaces of the wing and winglets. These strips were comprised of a 0.159-cm (0.06-in.) wide band of carborundum grains set in a plastic adhesive. The grains were sized on the basis of reference 10. No. 220 grains were applied to the wing upper and lower surfaces at 0.05c. No. 240 grains were placed on the upper (inboard) surfaces of the winglets at 0.05c and No. 220 grains were applied at 0.35c on the winglet lower (outboard) surfaces.

The transition strips on the lower surface of the winglets were located rearward in an attempt to simulate full-scale Reynolds number boundary-layer conditions (ref. 11). The strips on the upper surface of the winglets were located forward to insure transition ahead of the shock wave for the various test conditions. The fluorescent-oil film flow visualization technique described in reference 12 was employed to verify the presence of laminar flow ahead of the transition strip for the wing and winglets.

Transition strips of the same width as for the wing were also placed on the fuselage, nacelles, and pylons. A strip of No. 220 carborundum grains was applied to the fuselage 3.81 cm (1.50 in.) aft of the nose. No. 240 grains

were applied to the nacelles and pylons 0.635 cm (0.25 in.) downstream of the leading edges of those surfaces.

Measurements

Force and moment data were obtained by use of a six-component electrical strain-gage balance housed within the fuselage cavity. Angle of attack was measured by an accelerometer that was also housed within the fuselage. Static pressures were measured in the model sting cavity by using differential-pressure transducers referenced to free-stream static pressures. Wing buffet and bending-moment data were measured by an electrical strain gage in the wing. The gage was located at approximately 0.30c of the 0.23(b/2) station of the left wing panel.

Corrections

The angle of attack of the model was correctd for flow angularity in the tunnel test section. This correction was obtained from upright and inverted tests of the basic wing configuration. The lift and pitching-moment coefficients have been adjusted to correspond to the condition of free-stream static pressure in the sting cavity. No Mach number correction was made for blockage effects.

Test Conditions

Throughout the entire test, stagnation temperature was maintained at 322 K (120° F), and the air was dried until the dew point was sufficiently low to prevent condensation effects. The test conditions for which data were taken are presented in the following table:

M_∞	α, deg	β, deg	R		q_∞	
			per m	per ft	kPa	psf
0.50	-2 to 11	0, 5, -5	14.4×10^6	4.4×10^6	23.9	500
.70	-12 to 20	0, 5, -5	10.8	3.3	23.6	493
.70	-8 to 6	0, 5, -5	18.7	5.7	40.7	850
.75	-2 to 6	0	17.7	5.4	40.7	850
.78	-12 to 20	0, 5, -5	10.8	3.3	26.6	534
.78	-8 to 6	0, 5, -5	17.1	5.2	40.7	850
.80	-2 to 6	0	17.1	5.2	40.7	850
.82	-2 to 6	0, 5, -5	16.7	5.1	40.7	850
.85	-2 to 6	0	16.1	4.9	40.7	850
.90	-12 to 20	0, 5, -5	10.8	3.3	28.1	587
.90	-8 to 7	0, 5, -5	15.7	4.8	40.7	850
.95	-12 to 16	0, 5, -5	10.8	3.3	29.6	618
.95	-8 to 9	0, 5, -5	12.5	3.8	33.9	707

PRESENTATION OF RESULTS

The results of this investigation are presented in the following figures:

RESULTS AND DISCUSSION

Previous experimental investigations of the effects of winglets on the KC-135A jet transport (refs. 4 to 6) were mainly concerned with performance parameters at cruise and second-segment-climb conditions. For those investigations, a 0.07-scale semispan model was used to obtain the highest possible winglet Reynolds numbers. The purpose of the present investigation was to determine the effects of winglets on the static aerodynamic stability characteristics of the KC-135A at subsonic speeds. In this investigation a sting-mounted full-span model was used.

Both the semispan and full-span models were tested at approximately the same combinations of Mach number and dynamic pressure. However, the smaller size of the winglets on the full-span model produces skin-friction-drag penalties which are a greater percentage of the total drag than those for the semispan model. This effect is due to the difference in winglet Reynolds number between the two models. In addition, the wing panels for the full-span model were not designed to deflect to the actual full-scale shape at cruise conditions as was the semispan model wing. Unpublished chordwise pressure and

---

[1]Note that some of the data obtained exceeds the range of values presented in figure 5. While these data points have been omitted in figure 5, the computer fairings through these points have been retained within the range presented.

spanwise load distributions from this investigation verify that at cruise conditions the wing tips of the full-span model were more highly loaded than those of either the semispan model or the full-scale aircraft. For these reasons, the performance data obtained in this investigation are not considered representative. More applicable performance data are found in reference 4. The performance data presented herein are included for reference only.

During cruise, the KC-135A cargo/tanker aircraft can fly at a wide range of wing loadings and lift coefficients. Much of the data analysis herein is centered around $C_{L,basic}$ = 0.44, which corresponds to an overall trimmed airplane lift coefficient of about 0.4, an average value for a representative mission.

Longitudinal Aerodynamic Characteristics

The static longitudinal aerodynamic characteristics of the model with and without winglets are presented in figures 5 and 6 and summarized in figure 7. As shown in reference 3, the general effect of adding a lifting surface such as a winglet behind the center of gravity is an increase in the static aerodynamic stability of the model. This trend can be seen in figure 7 as more positive C_{L_α} values and more negative $C_{m_{C_L}}$ values for the winglet configuration.

Estimates have indicated, however, that the increments in pitching moment due to the addition of the winglets would not result in any appreciable trim drag penalties over the range of conditions tested. There is very little change in zero-lift pitching-moment coefficients for the two configurations over the Mach number range tested. The stability of the model tends to increase slightly up to the drag-rise Mach number of about 0.79 because of the addition of the winglets, and the increments between the basic-wing and winglet configurations remain nearly constant up to the drag-rise Mach number.

Comparison of figures 7(a) and 7(b) shows that the increment in longitudinal stability of the model due to the winglets increases slightly with Reynolds number.

Lateral-Directional Aerodynamic Characteristics

The static lateral-directional aerodynamic characteristics of the model, with and without winglets, are presented in figure 8 and are summarized in figure 9. Because the winglets are nearly vertical, the lateral stability of the model is affected more than the longitudinal stability. Definite increases in the lateral stability of the model due to the winglets are shown in figure 9. As in the longitudinal case, the increments between the basic-wing and winglet configurations tend to remain constant up to the drag-rise Mach number. Note that both configurations become laterally unstable $\left(\text{positive } C_{l_\beta}\right)$ between

M_∞ = 0.85 and M_∞ = 0.95. At these conditions, the forward wing (right wing if β is positive) stalls first, resulting in a destabilizing rolling moment.

A very slight positive increase in stability parameter increments due to the winglets is shown with increasing Reynolds number (figs. 9(a) and 9(b)). The absolute values of the increments in longitudinal and lateral stability parameters due to the winglets are small for the Reynolds number range of this investigation. However, experience suggests that the stability increments exhibited by the winglets will continue to increase with further increases in Reynolds number.

Wing Bending-Moment Increments

Wing bending-moment increments due to the addition of the winglets are summarized in figure 10 for both the nominal ($\beta = 0^o$) and the "worst case" conditions. For this investigation, the worst case occurs with the model at a sideslip angle of -5° (nose right). In this position, the sweep of the wing panel on which the bending-moment gage is mounted (left panel) is reduced 5° and the incidence of the left winglet is increased by 5°. Therefore, both the left wing and winglet experience higher loads, and the wing bending moments increase accordingly. Up to Mach 0.85, only small variations in bending-moment increment with lift coefficient and Mach number are shown in figure 10 for the nominal case. In general, the bending-moment increments due to the winglets are 5 to 6 percent higher than for the basic wing for this range of Mach number. At Mach numbers above 0.85, the bending-moment increments are strongly influenced by shock-induced separation at the wing tips and, therefore, tend to vary significantly with lift coefficient.

Bending-moment increments for the worst case ($\beta = -5^o$) range from 12 to 20 percent at low lift coefficients but decrease rapidly with increasing lift coefficient because of winglet stall. As previously mentioned, the wing-tip loads for this model are higher than for the full-scale aircraft; consequently, the bending-moment increments shown are also higher than would be expected for the full-scale aircraft.

Buffet Onset

Wing buffet characteristics were obtained from integrations of root-mean-square deviations about the steady-state bending-moment value from the bending-moment gage mounted on the left wing panel. Figure 11 presents the wing buffet characteristics for the nominal and worst-case conditions. For Mach 0.50 and 0.70 (figs. 11(a) and 11(b)), no change in wing buffet characteristics due to the winglets is shown for either $\beta = 0^o$ or $\beta = -5^o$. For both configurations, buffet onset occurs for the nominal case at lift coefficients of 0.6 and 0.4 at Mach 0.78 and 0.82 (figs. 11(c) and 11(d)), respectively. At both these Mach numbers, buffet onset for the worst case occurs at a lift coefficient 0.2 less than for the nominal case because of high wing and winglet loads on the panel with reduced sweep. At Mach numbers above 0.85 (figs. 11(e) and 11(f)), widespread boundary-layer separation results in wing buffet for both configurations across the lift-coefficient range presented. The buffet data presented are considered conservative, again because of absence of aeroelastic deformation of the model wing panel.

SUMMARY OF RESULTS

A wind-tunnel investigation of winglets on 0.035-scale KC-135A jet transport wing panels has been conducted at high subsonic speeds. The wing panels were mounted on a generalized fuselage that approximates the fuselage of the KC-135A airplane. Data are presented for two separate wind-tunnel entries which indicate the following:

1. Adding the winglets to the basic-wing configuration produced small increases in static longitudinal and lateral aerodynamic stability.

2. The stability increases due to the winglets increased slightly with Reynolds number.

3. The winglets produced small increases in the wing bending moments measured at the 23-percent semispan station.

4. The buffet onset characteristics of the model were not affected by the winglets.

Langley Research Center
National Aeronautics and Space Administration
Hampton, VA 23665
February 23, 1978

REFERENCES

1. Whitcomb, Richard T.: A Design Approach and Selected Wind-Tunnel Results at High Subsonic Speeds for Wing-Tip Mounted Winglets. NASA TN D-8260, 1976.

2. Flechner, Stuart G.; Jacobs, Peter F.; and Whitcomb, Richard T.: A High Subsonic Speed Wind-Tunnel Investigation of Winglets on a Representative Second-Generation Jet Transport Wing. NASA TN D-8264, 1976.

3. Jacobs, Peter F.; and Flechner, Stuart G.: The Effect of Winglets on the Static Aerodynamic Stability Characteristics of a Representative Second Generation Jet Transport Model. NASA TN D-8267, 1976.

4. Jacobs, Peter F.; Flechner, Stuart G.; and Montoya, Lawrence C.: Effect of Winglets on a First-Generation Jet Transport Wing. I - Longitudinal Aerodynamic Characteristics for a Semispan Model at Subsonic Speeds. NASA TN D-8473, 1977.

5. Montoya, Lawrence C.; Flechner, Stuart G.; and Jacobs, Peter F.: Effect of Winglets on a First-Generation Jet Transport Wing. II - Pressure and Spanwise Load Distributions for a Semispan Model at High Subsonic Speeds. NASA TN D-8474, 1977.

6. Montoya, Lawrence C.; Jacobs, Peter F.; and Flechner, Stuart G.: Effect of Winglets on a First-Generation Jet Transport Wing. III - Pressure and Spanwise Load Distributions for a Semispan Model at Mach 0.30. NASA TN D-8478, 1977.

7. Meyer, Robert R., Jr.: Effect of Winglets on a First-Generation Jet Transport Wing. IV - Stability Characteristics for a Full-Span Model at Mach 0.30. NASA TP-1119, 1978.

8. Mechtly, E. A.: The International System of Units - Physical Constants and Conversion Factors (Second Revision). NASA SP-7012, 1973.

9. Schaefer, William T., Jr.: Characteristics of Major Active Wind Tunnels at the Langley Research Center. NASA TM X-1130, 1965.

10. Braslow, Albert L.; and Knox, Eugene C.: Simplified Method for Determination of Critical Height of Distributed Roughness Particles for Boundary-Layer Transition at Mach Numbers From 0 to 5. NACA TN 4363, 1958.

11. Blackwell, James A., Jr.: Preliminary Study of Effects of Reynolds Number and Boundary-Layer Transition Location on Shock-Induced Separation. NASA TN D-5003, 1969.

12. Loving, Donald L.; and Katzoff, Samuel: The Fluorescent-Oil Film Method and Other Techniques for Boundary-Layer Flow Visualization. NASA MEMO 3-17-59L, 1959.

TABLE I.- COORDINATES OF TYPICAL OUTBOARD WING SECTION

[Wing section at 2° incidence]

Upper surface		Lower surface	
x/c	z/c	x/c	z/c
0	0	0	0
.0011	.0042	.0020	-.0054
.0022	.0056	.0035	-.0063
.0034	.0071	.0061	-.0073
.0058	.0090	.0092	-.0081
.0095	.0116	.0201	-.0097
.0132	.0136	.0391	-.0116
.0180	.0161	.0631	-.0139
.0234	.0186	.0950	-.0168
.0324	.0221	.1016	-.0174
.0415	.0253	.1445	-.0212
.0536	.0291	.1826	-.0245
.0716	.0338	.2235	-.0284
.0897	.0377	.2597	-.0314
.0990	.0394	.2950	-.0341
.1132	.0417	.3326	-.0366
.1408	.0454	.3726	-.0391
.1589	.0471	.4276	-.0418
.1740	.0483	.4690	-.0429
.1861	.0492	.5110	-.0433
.2011	.0501	.5560	-.0430
.2192	.0510	.5967	-.0424
.2342	.0516	.6386	-.0414
.2584	.0522	.6818	-.0406
.3432	.0522	.7243	-.0397
.3729	.0524	.7620	-.0389
.4090	.0513	.7951	-.0381
.4572	.0489	.8308	-.0377
.5054	.0454	.8662	-.0371
.5416	.0420	.9029	-.0363
.5897	.0367	.9392	-.0358
.6379	.0304	.9790	-.0348
.6862	.0226	.9999	-.0350
.7343	.0153		
.7582	.0108		
.7823	.0065		
.8040	.0027		
.8344	-.0023		
.8642	-.0076		
.8874	-.0119		
.9223	-.0180		
.9492	-.0229		
.9718	-.0269		
.9920	-.0308		
1.0001	-.0347		

TABLE II.- AIRFOIL COORDINATES FOR WINGLETS

x/c	z/c for -	
	Upper surface	Lower surface
0	0	0
.0020	.0077	-.0032
.0050	.0119	-.0041
.0125	.0179	-.0060
.0250	.0249	-.0077
.0375	.0296	-.0090
.0500	.0333	-.0100
.0750	.0389	-.0118
.1000	.0433	-.0132
.1250	.0469	-.0144
.1500	.0499	-.0154
.1750	.0525	-.0161
.2000	.0547	-.0167
.2500	.0581	-.0175
.3000	.0605	-.0176
.3500	.0621	-.0174
.4000	.0628	-.0168
.4500	.0627	-.0158
.5000	.0618	-.0144
.5500	.0599	-.0122
.5750	.0587	-.0106
.6000	.0572	-.0090
.6250	.0554	-.0071
.6500	.0533	-.0052
.6750	.0508	-.0033
.7000	.0481	-.0015
.7250	.0451	.0004
.7500	.0419	.0020
.7750	.0384	.0036
.8000	.0349	.0049
.8250	.0311	.0060
.8500	.0270	.0065
.8750	.0228	.0064
.9000	.0184	.0059
.9250	.0138	.0045
.9500	.0089	.0021
.9750	.0038	-.0013
1.0000	-.0020	-.0067
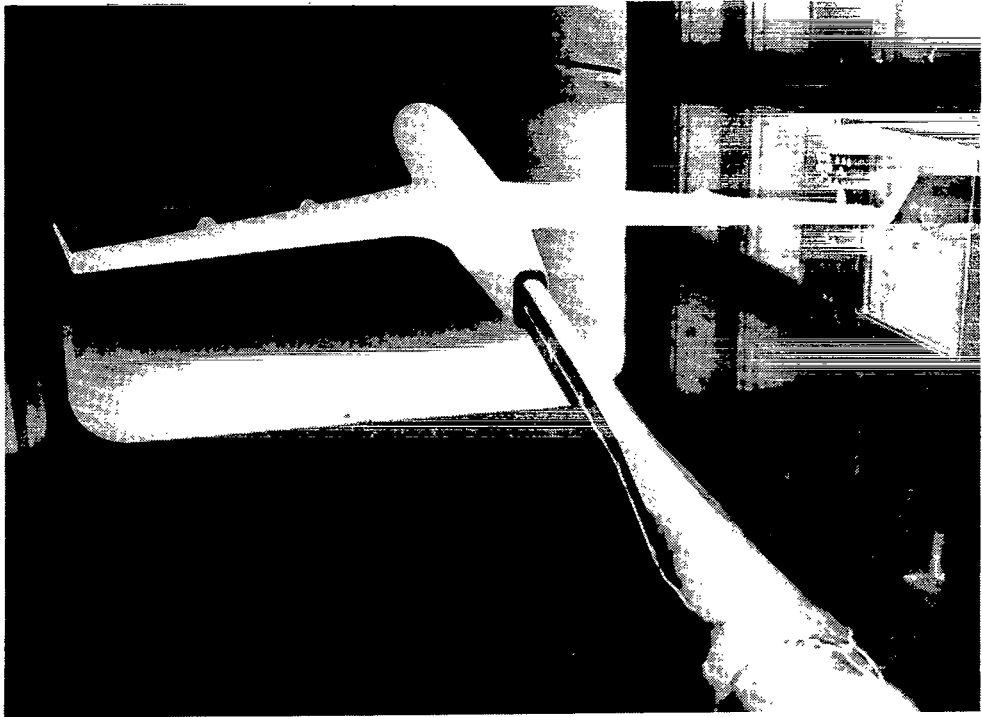
L-76-4416

L-76-4415

Figure 1.- Wind-tunnel model.

28.98 (11.41)

Moment reference center

70.41 (27.72)

37.55°

27.99
(11.02)

37.64
(14.82)

48.44
(19.07)

Trailing-edge
break

69.34
(27.30)

9.96 (3.92)

125.88 (49.56)

Moment reference center

7.29 (2.87) Radius
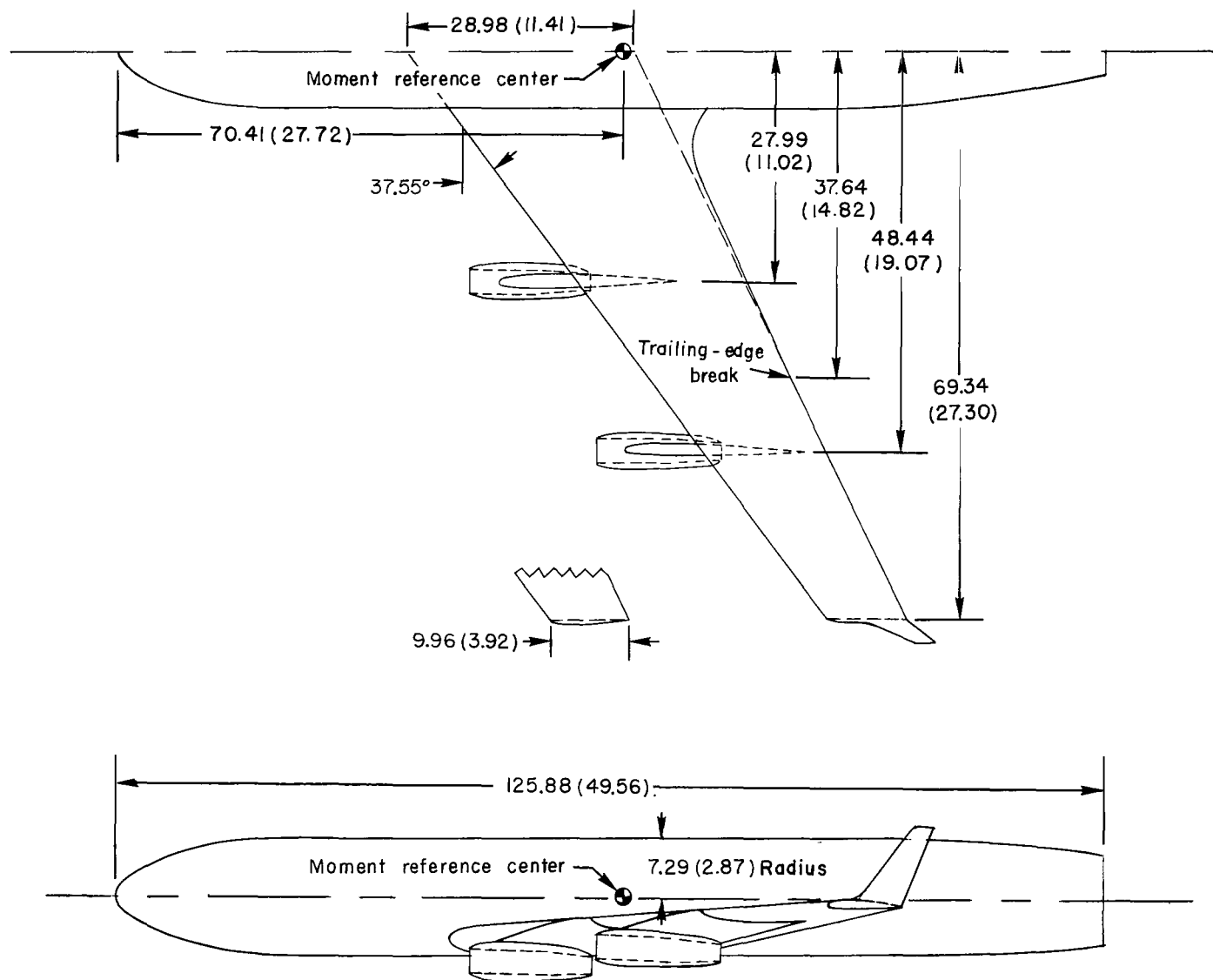
(a) General layout of model.

Figure 2.- Drawings of model. Dimensions are in centimeters (inches).

Typical winglet section

Upper surface

$-4°$

Section A—A

$.21c_t$

Span, $h = c_t$

$38°$

$.65c_t$

c_t

Upper surface

$15°$

Dihedral

$7°$

A

A
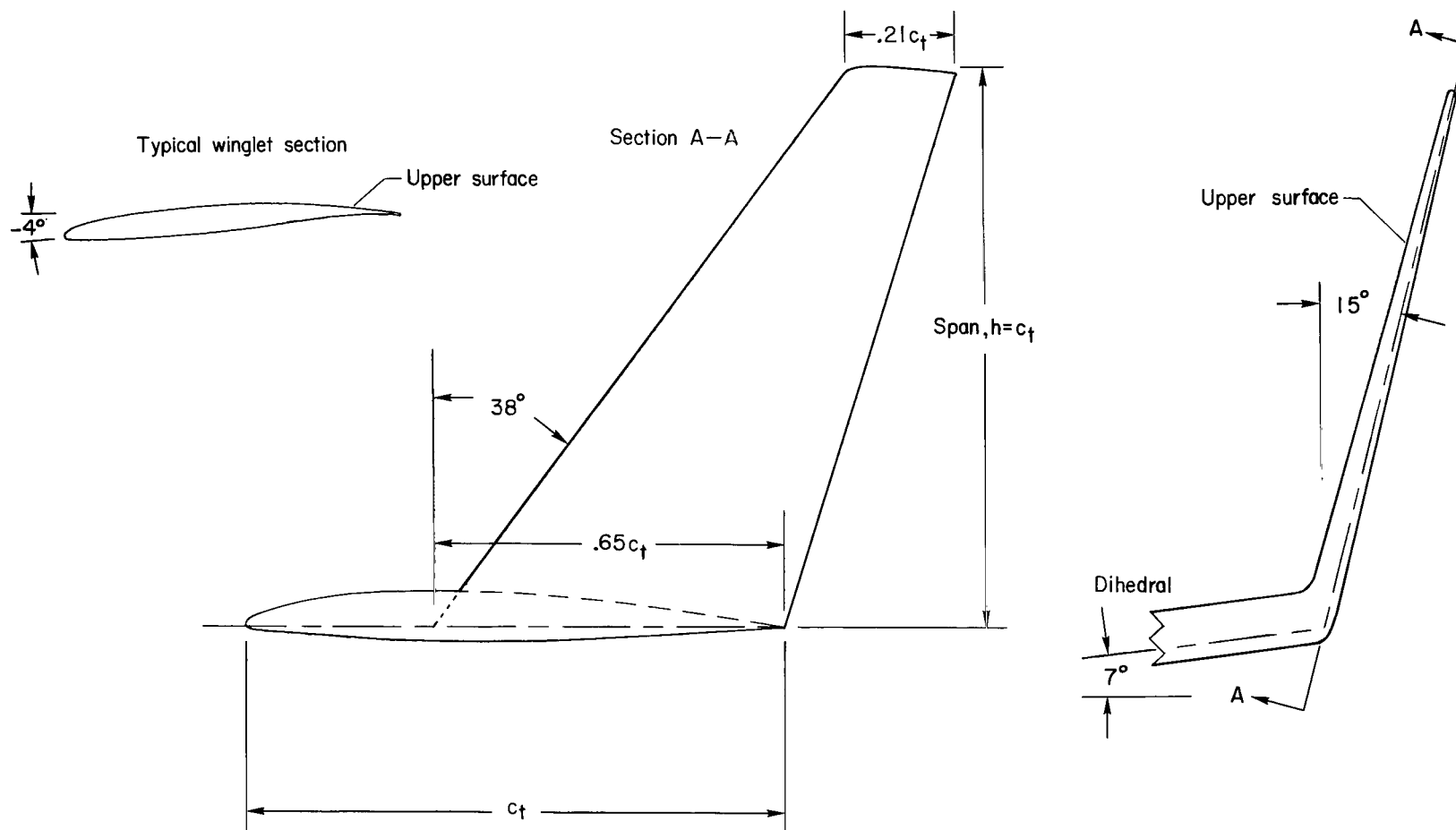
(b) Details of winglets.

Figure 2.- Concluded.

Generalized fuselage ————

KC-I35A fuselage — — —
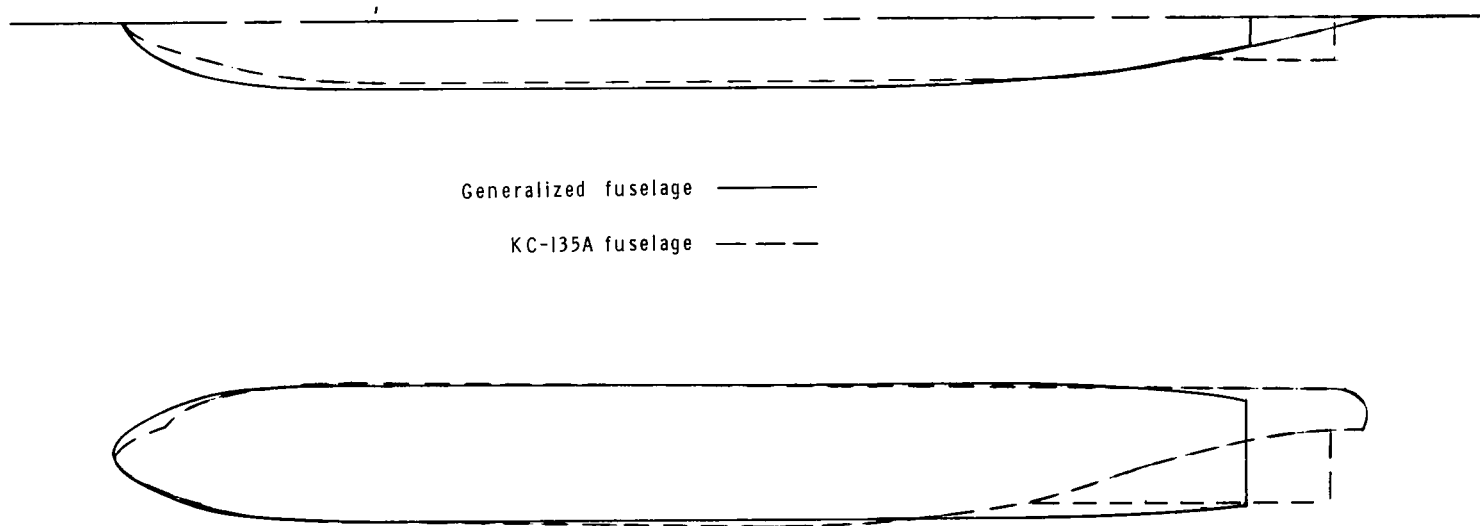
Figure 3.- Comparison of generalized fuselage with actual KC-135A model fuselage.
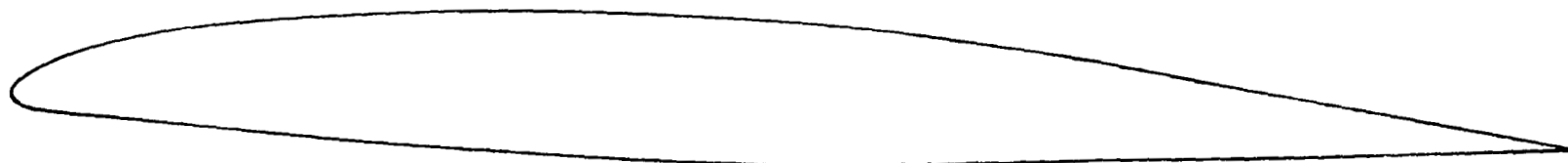
Figure 4.- Typical outboard wing airfoil section.
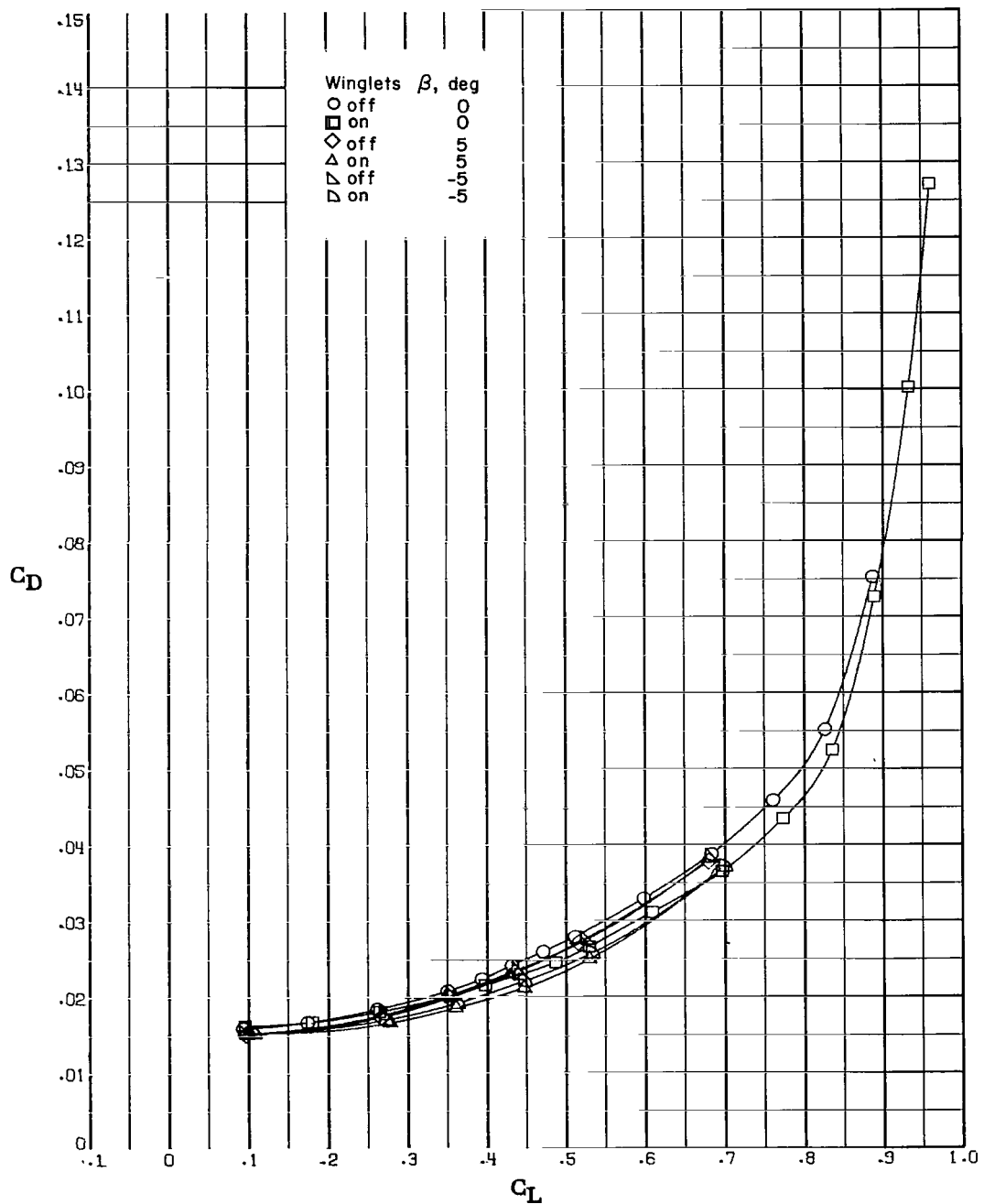
(a) $M_\infty = 0.50$; $R = 14.4 \times 10^6$ per m (4.4×10^6 per ft).

Figure 5.- Variation of drag coefficient with lift coefficient.
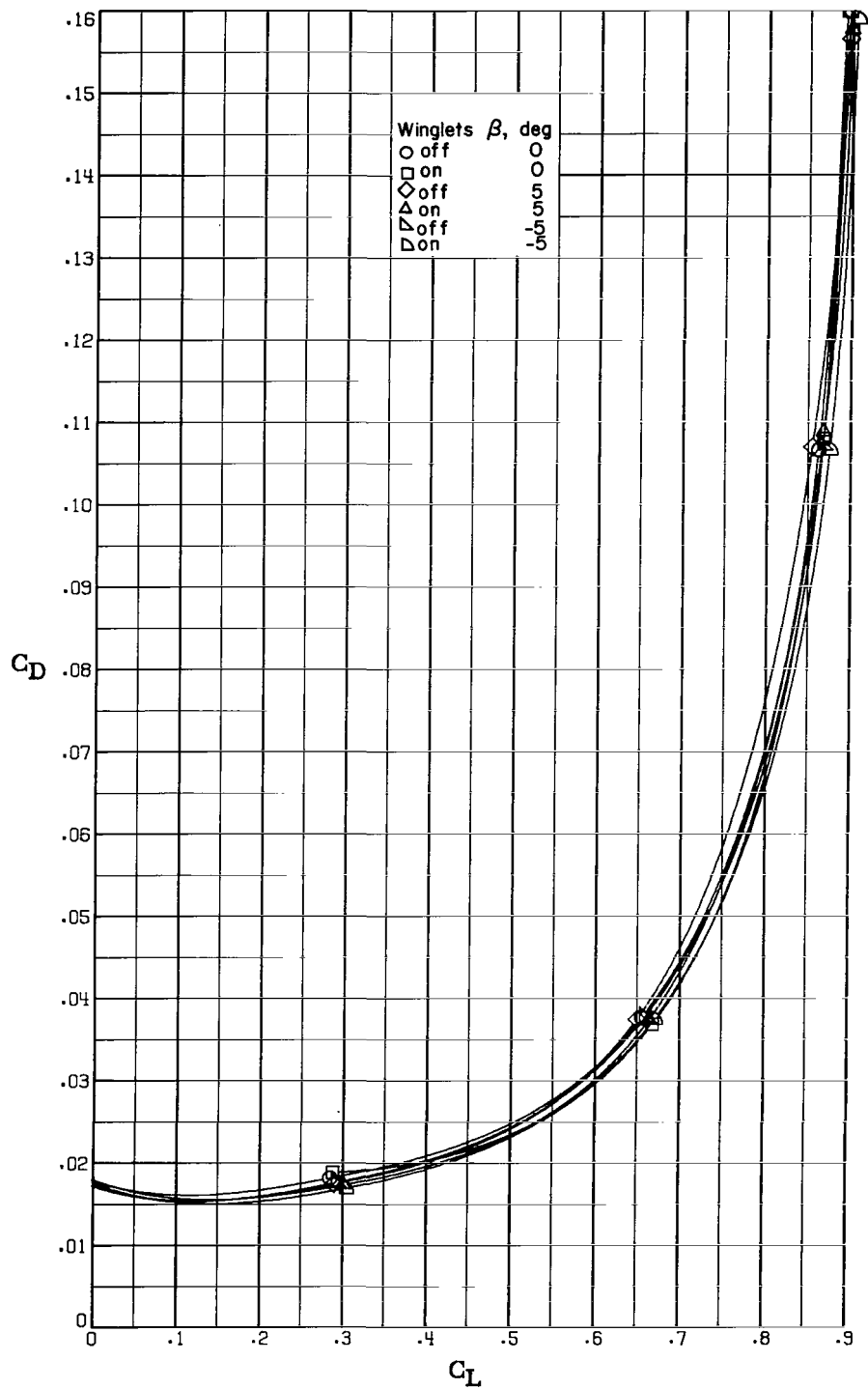
(b) $M_\infty = 0.70$; $R = 10.8 \times 10^6$ per m (3.3×10^6 per ft).
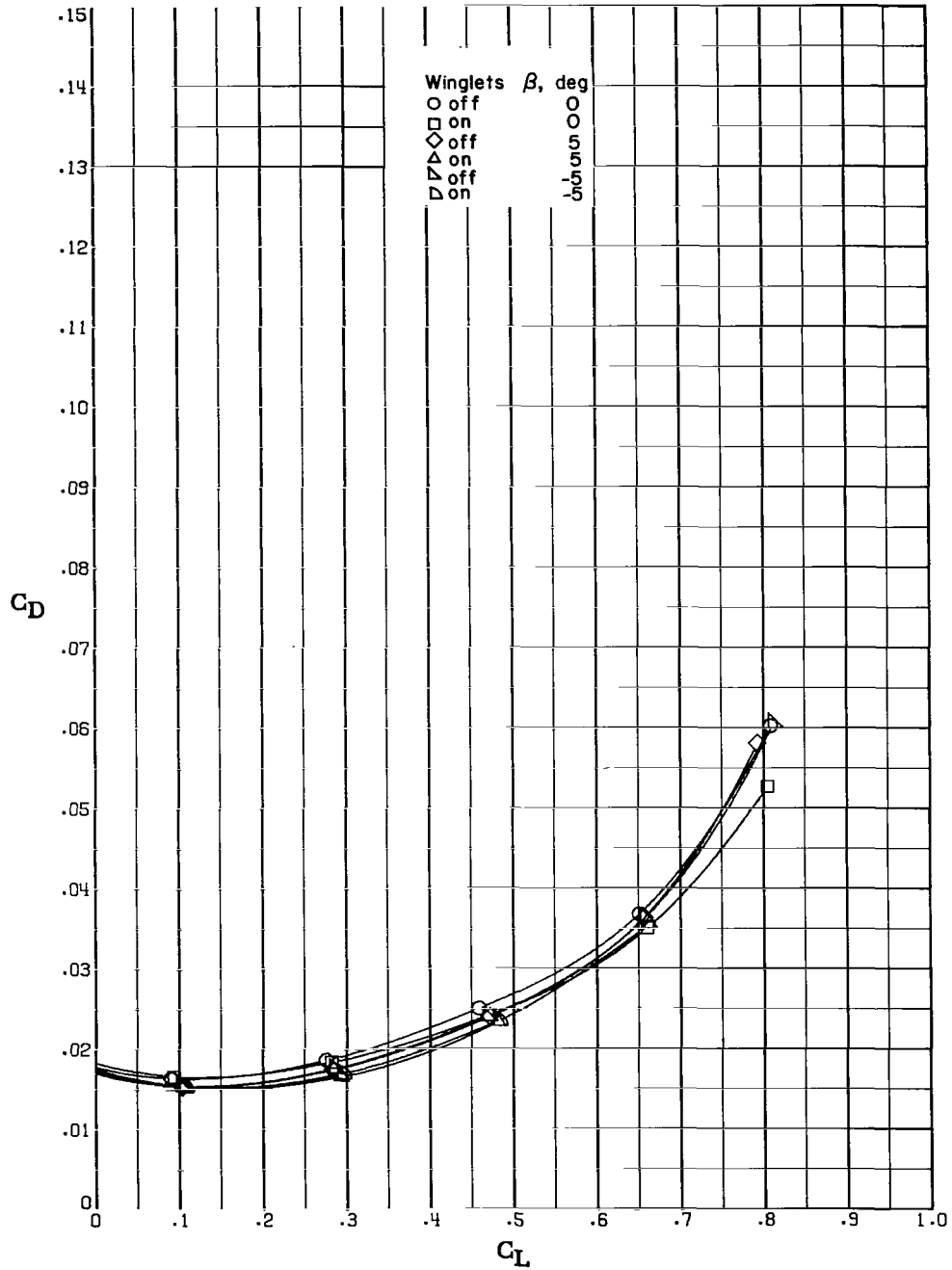
Figure 5.- Continued.

(c) $M_\infty = 0.70$; $R = 18.7 \times 10^6$ per m (5.7×10^6 per ft).
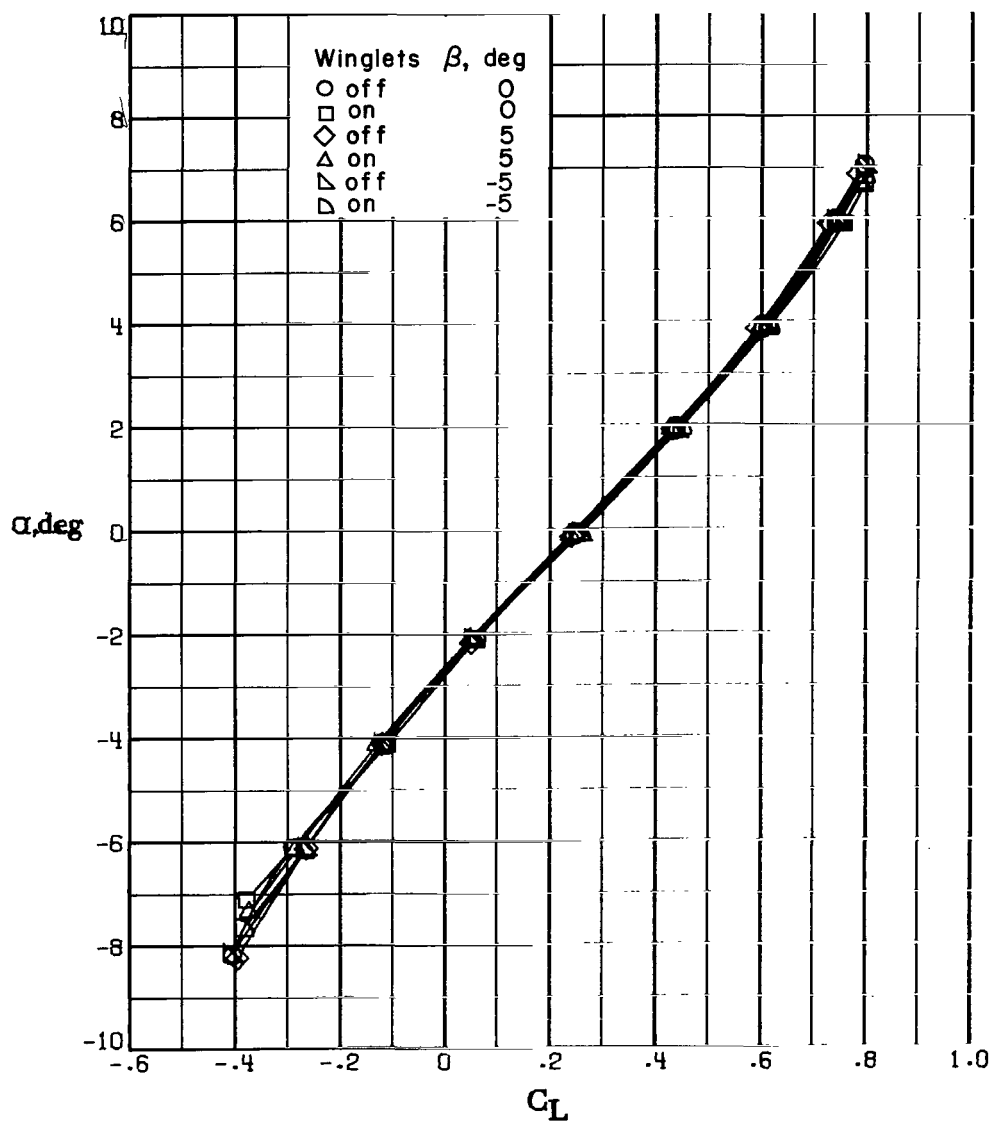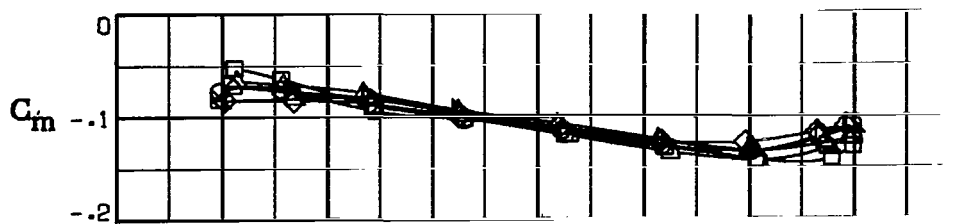
Figure 5.- Continued.
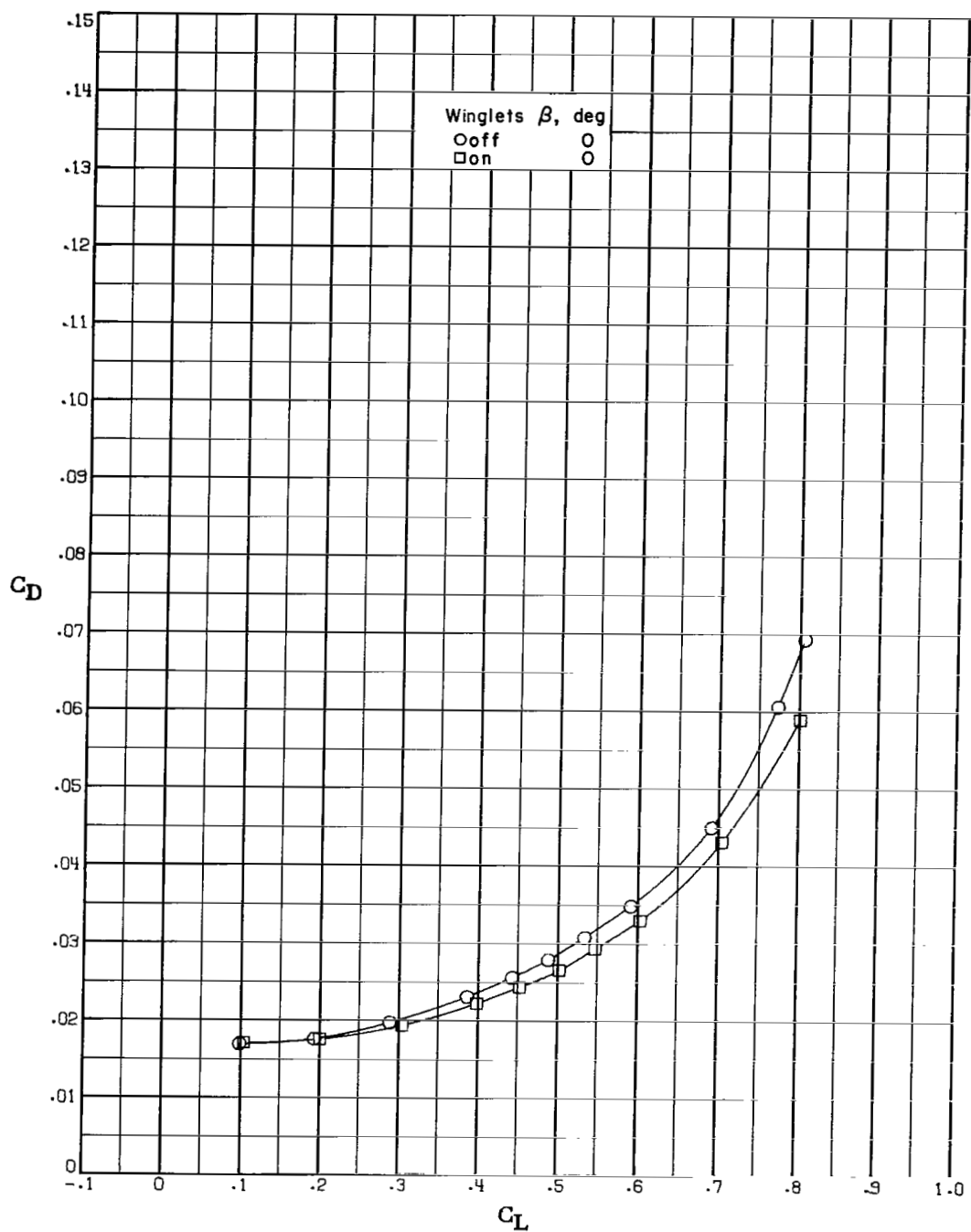
(d) $M_\infty = 0.75$; $R = 17.7 \times 10^6$ per m $(5.4 \times 10^6$ per ft).
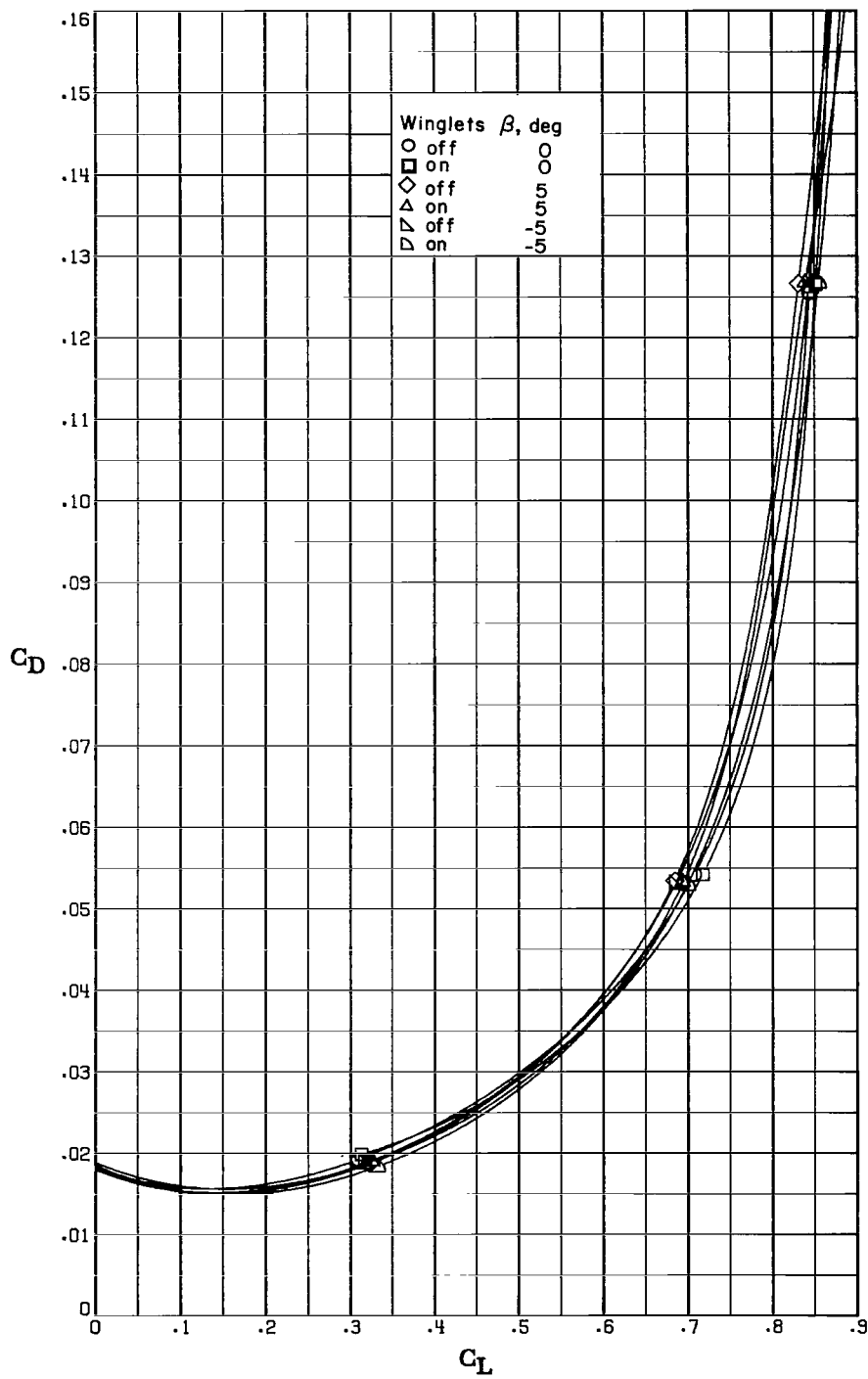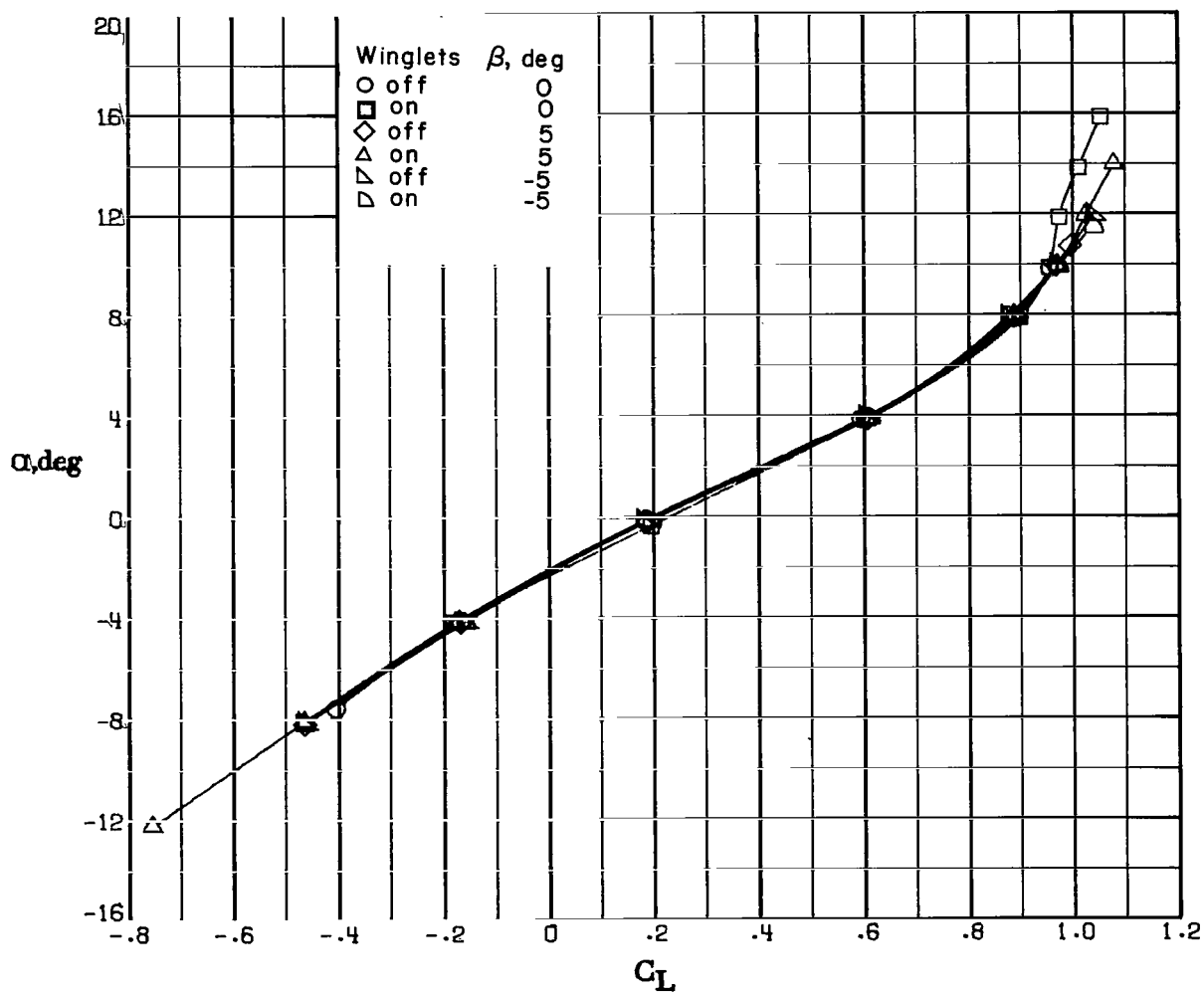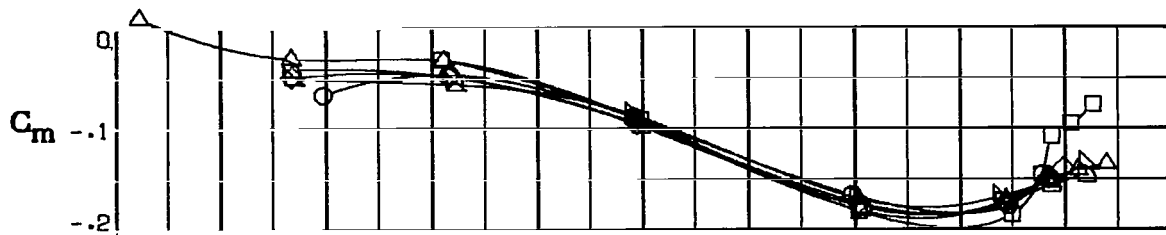
Figure 5.- Continued.

(e) $M_\infty = 0.78$; $R = 10.8 \times 10^6$ per m $(3.3 \times 10^6$ per ft).
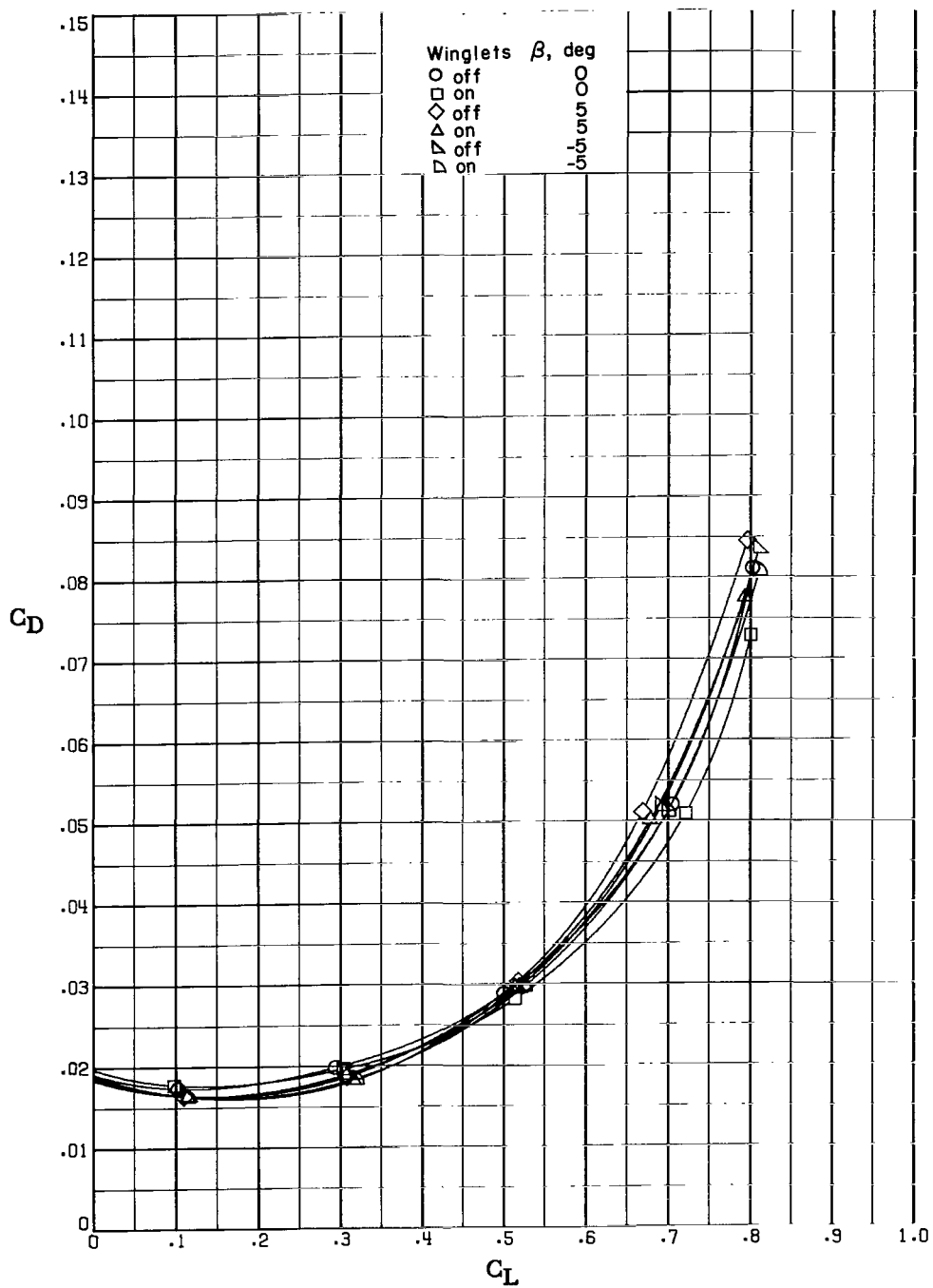
Figure 5.- Continued.

(f) $M_\infty = 0.78$; $R = 17.1 \times 10^6$ per m (5.2×10^6 per ft).
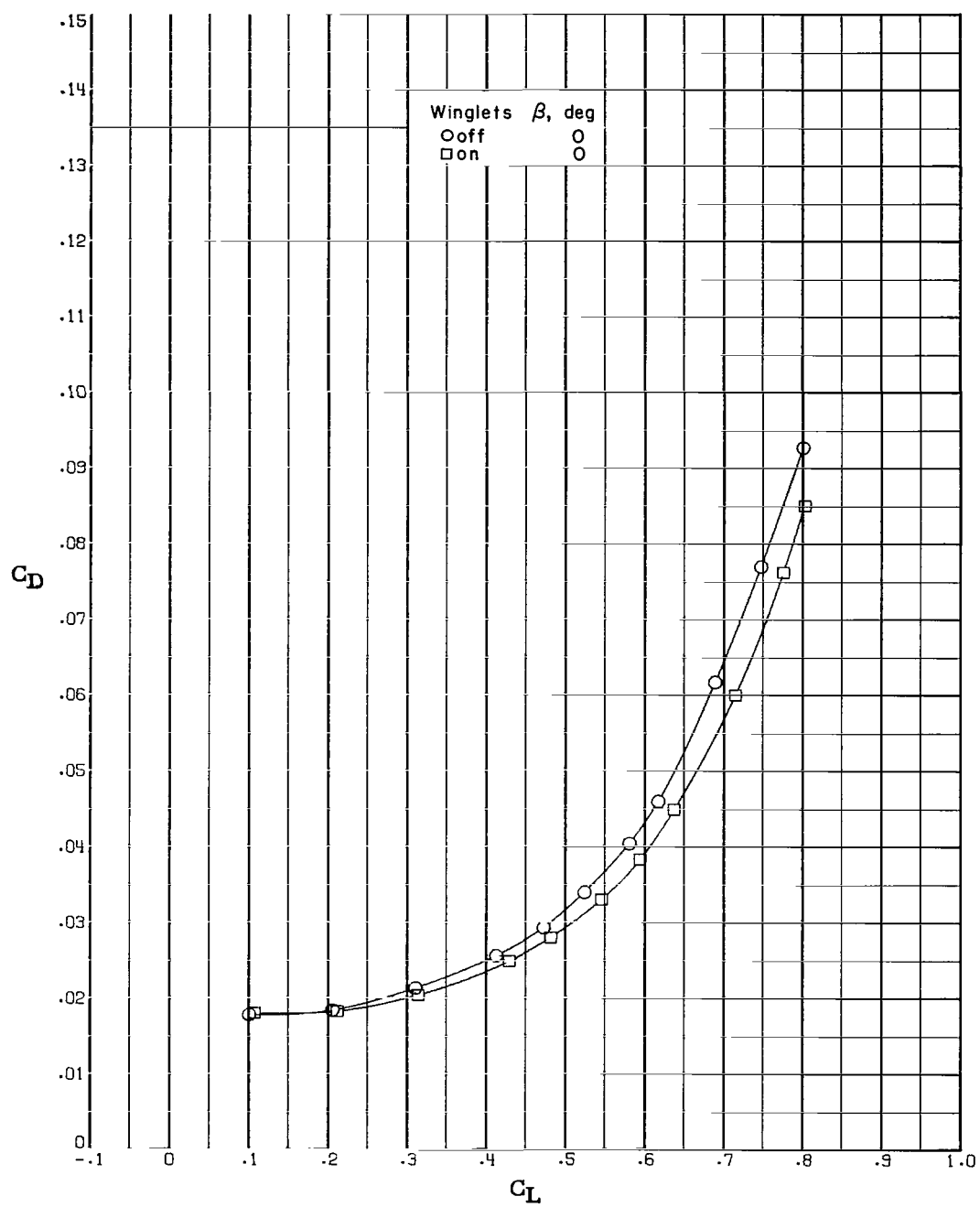
Figure 5.- Continued.

(g) $M_\infty = 0.80$; $R = 17.1 \times 10^6$ per m (5.2 $\times$ 10^6 per ft).
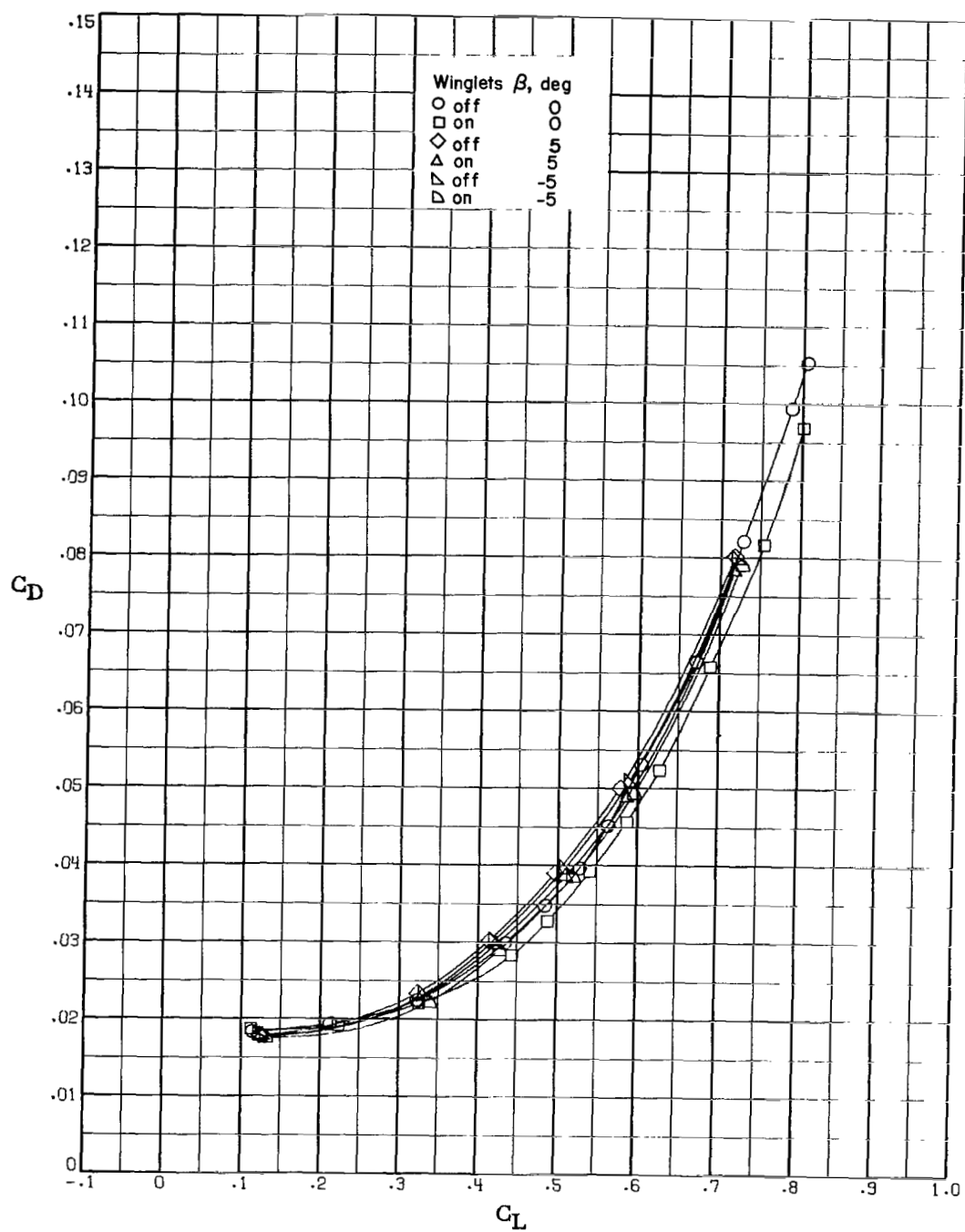
Figure 5.- Continued.

(h) $M_\infty = 0.82$; $R = 16.7 \times 10^6$ per m (5.1×10^6 per ft).

Figure 5.- Continued.
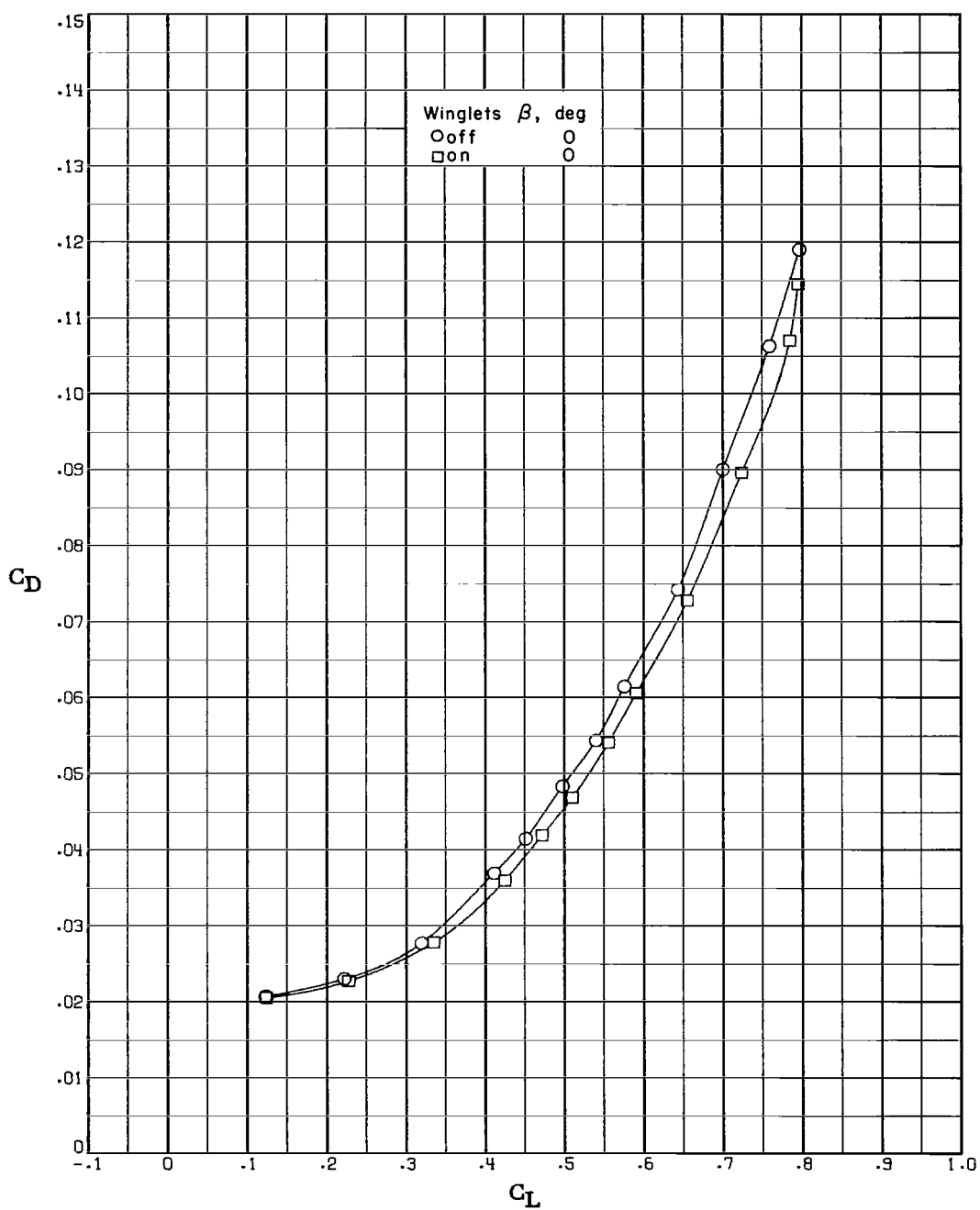
(i) $M_\infty = 0.85$; $R = 16.1 \times 10^6$ per m (4.9×10^6 per ft).

Figure 5.- Continued.
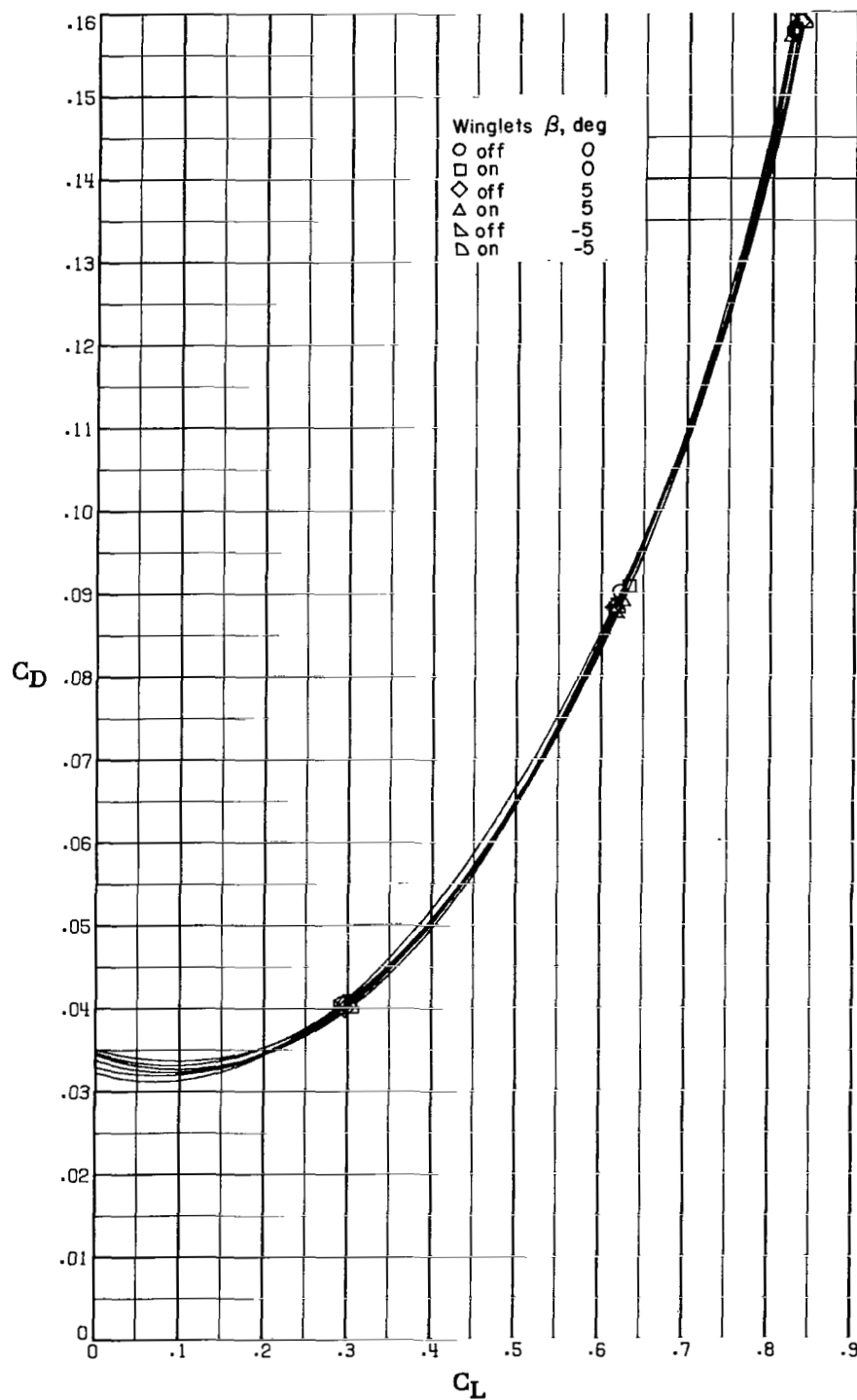
(j) $M_\infty = 0.90$; $R = 10.8 \times 10^6$ per m (3.3×10^6 per ft).
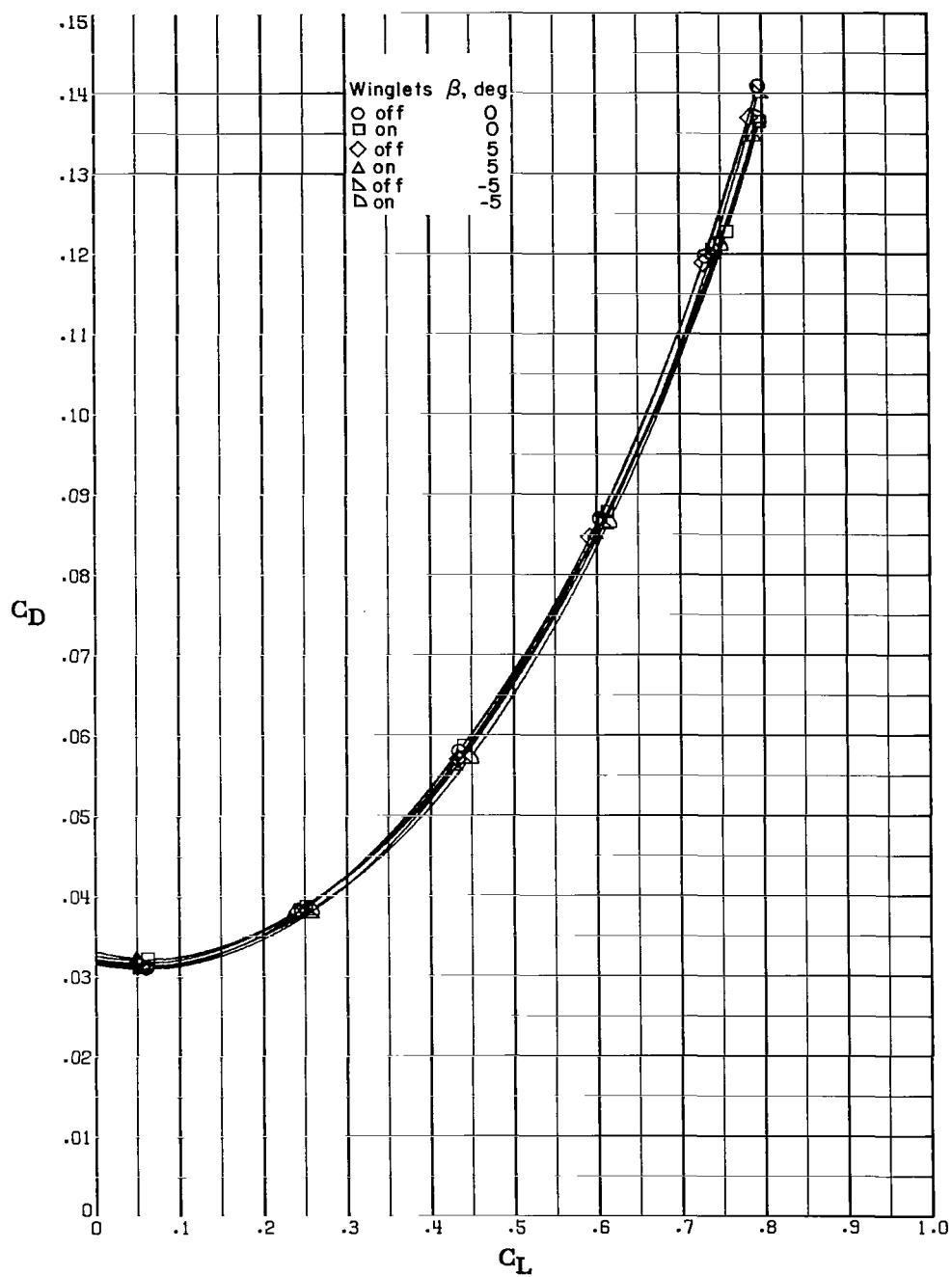
Figure 5.- Continued.

(k) $M_\infty = 0.90$; $R = 15.7 \times 10^6$ per m $(4.8 \times 10^6$ per ft).
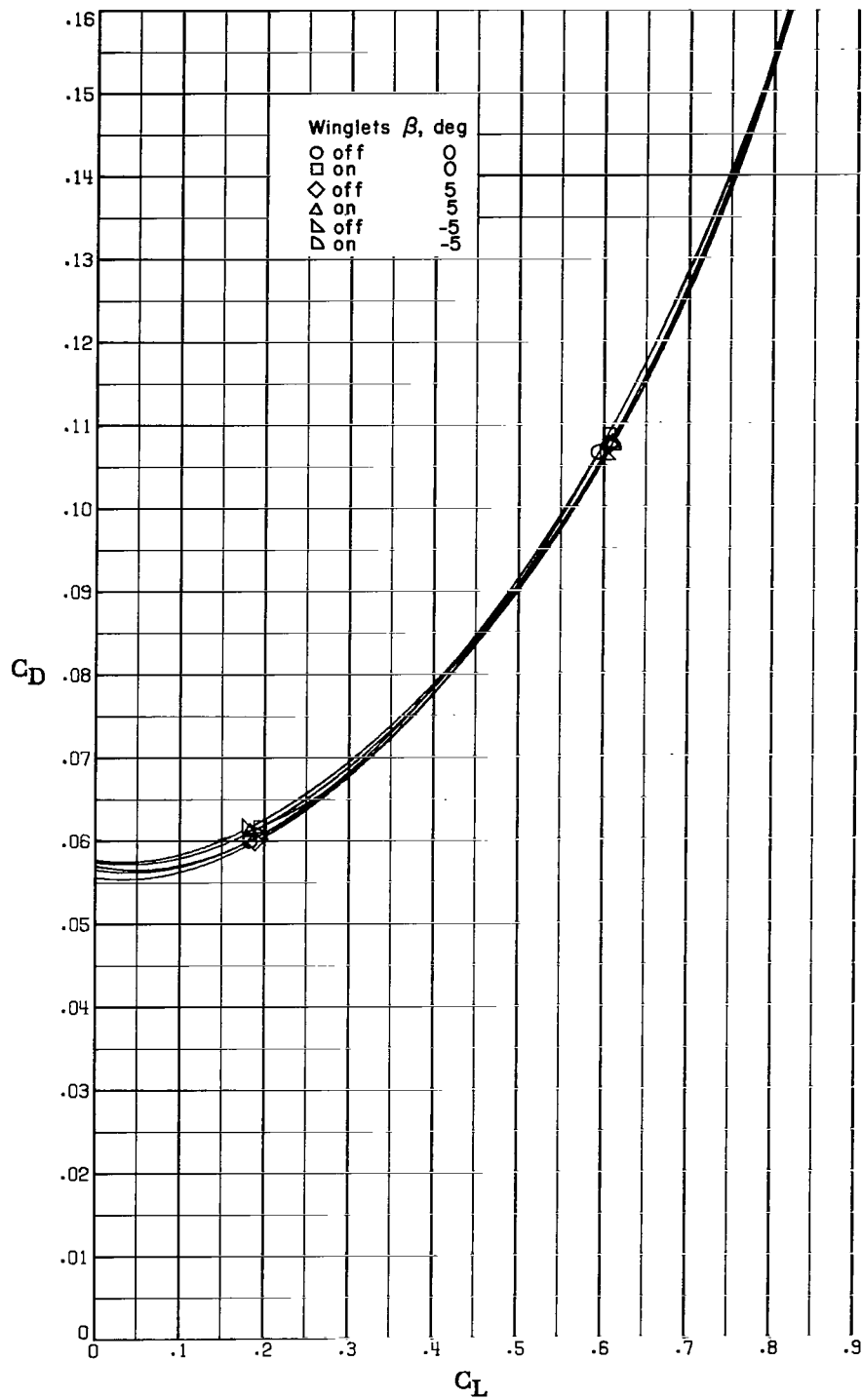
Figure 5.- Continued.

(1) $M_\infty = 0.95$; $R = 10.8 \times 10^6$ per m (3.3×10^6 per ft).
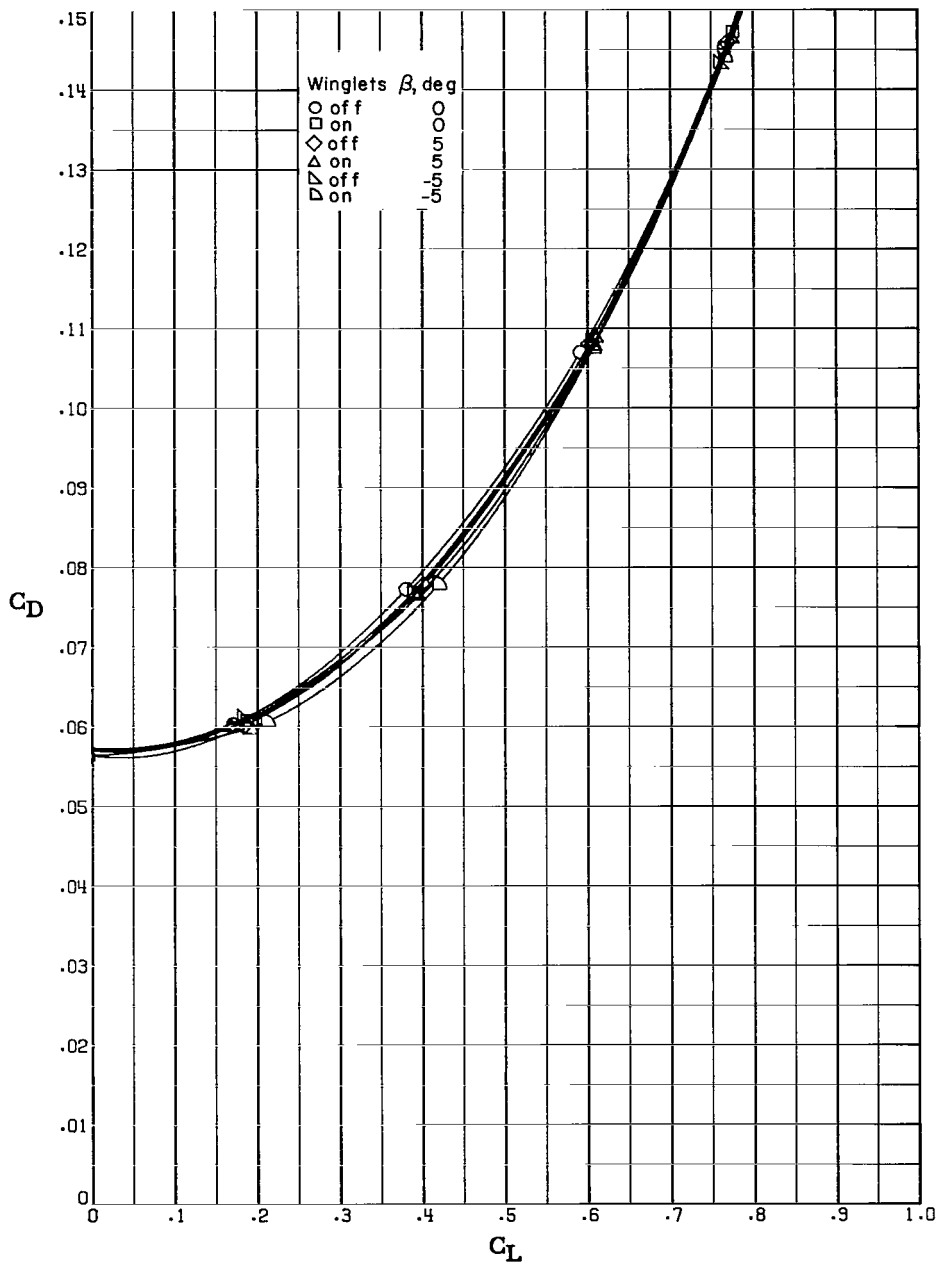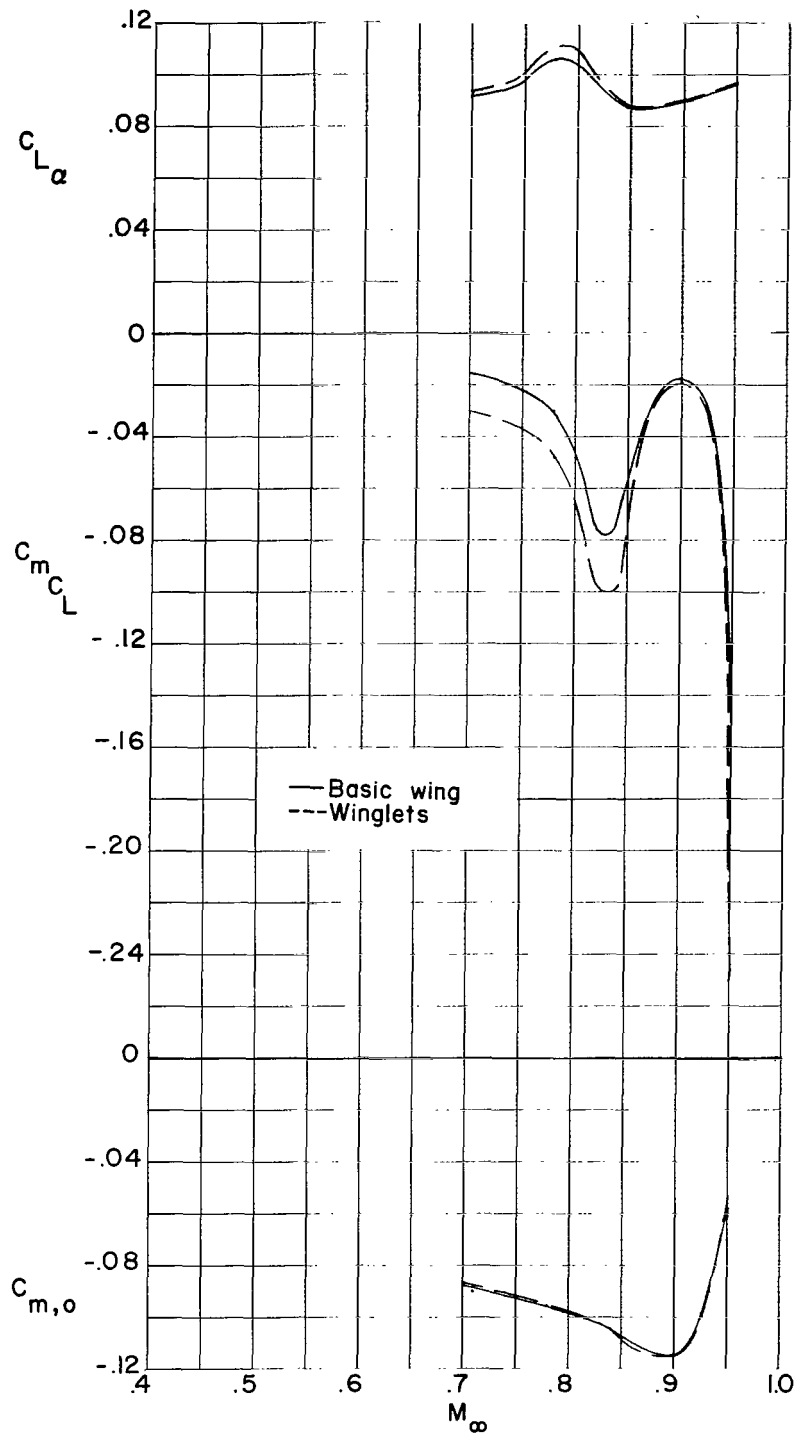
Figure 5.- Continued.

(m) $M_\infty = 0.95$; $R = 12.5 \times 10^6$ per m (3.8×10^6 per ft).

Figure 5.- Concluded.
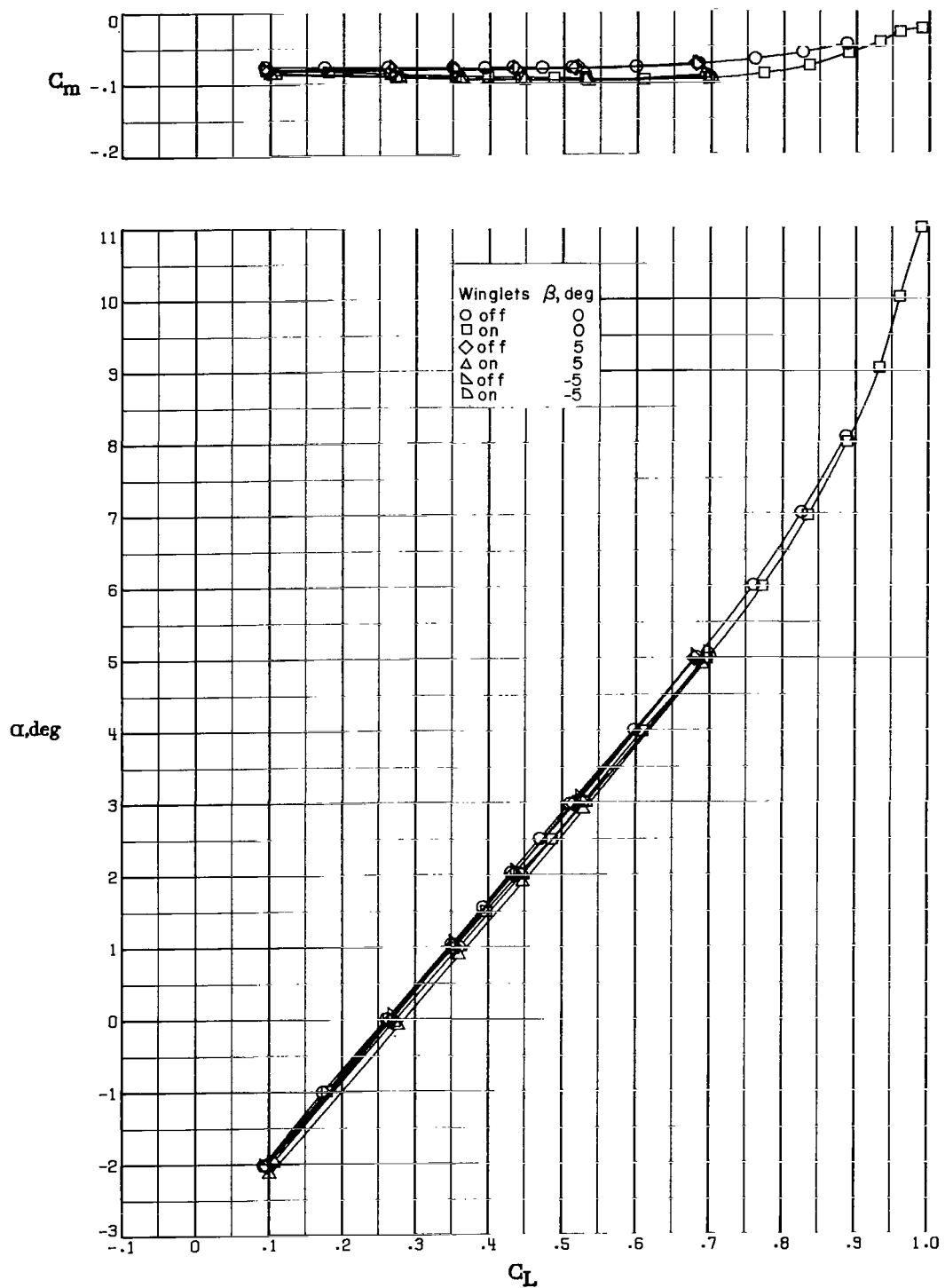
(a) $M_{\infty} = 0.50;$ $R = 14.4 \times 10^6$ per m $(4.4 \times 10^6$ per ft).

Figure 6.- Variation of pitching-moment coefficient and angle of attack
with lift coefficient.
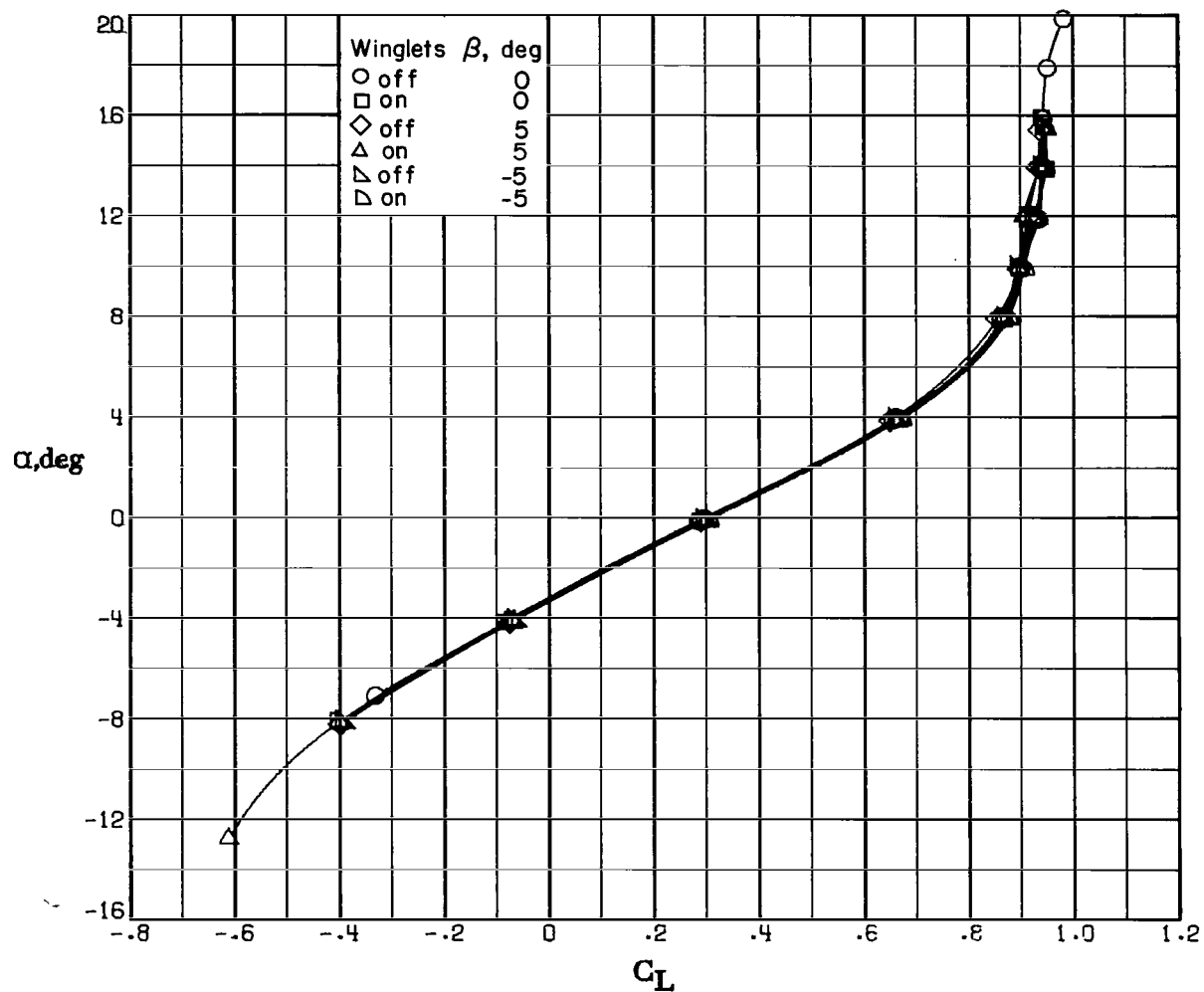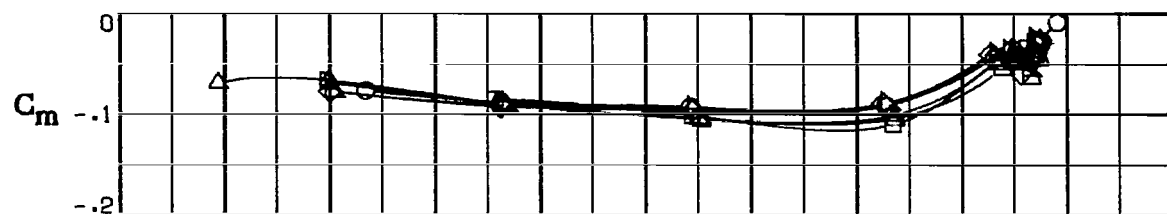
(b) $M_\infty = 0.70$; $R = 10.8 \times 10^6$ per m $(3.3 \times 10^6$ per ft).
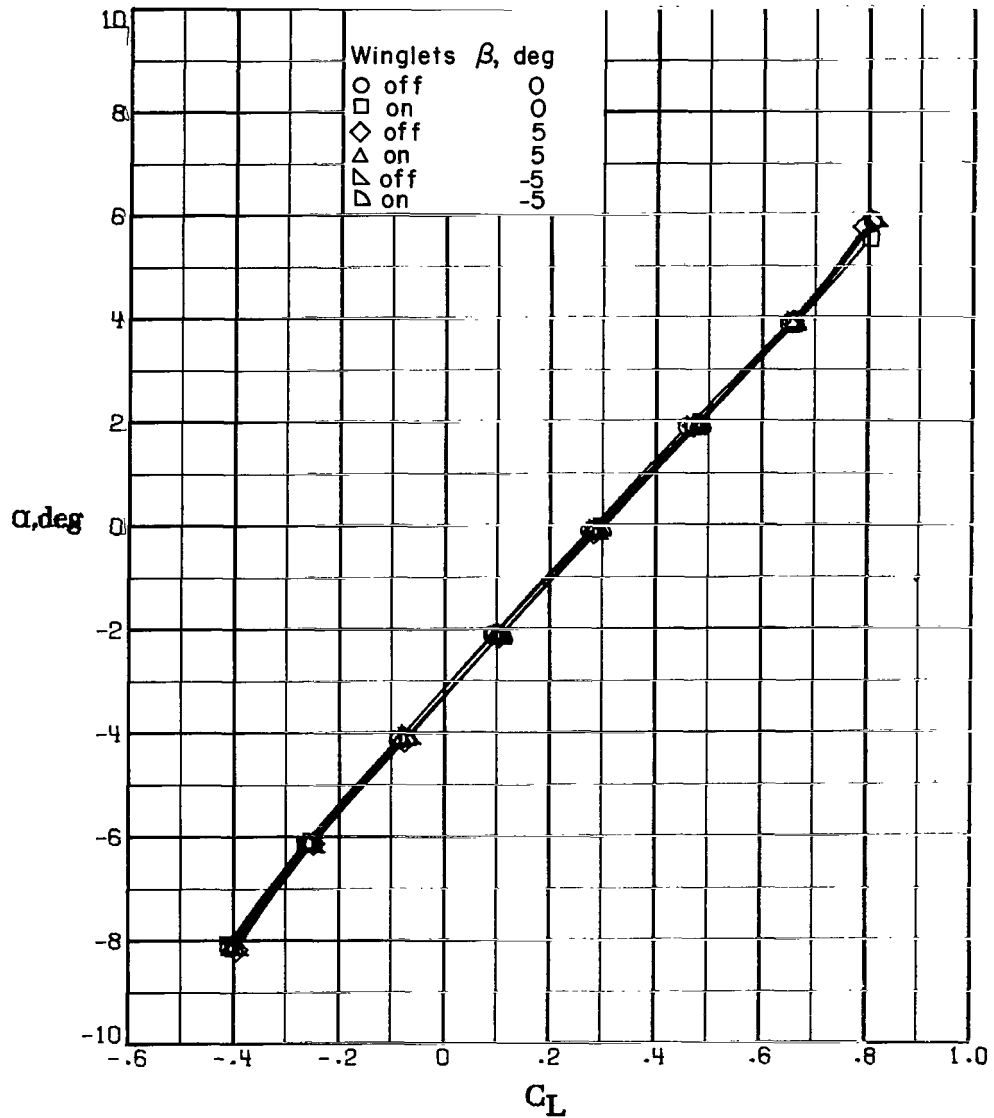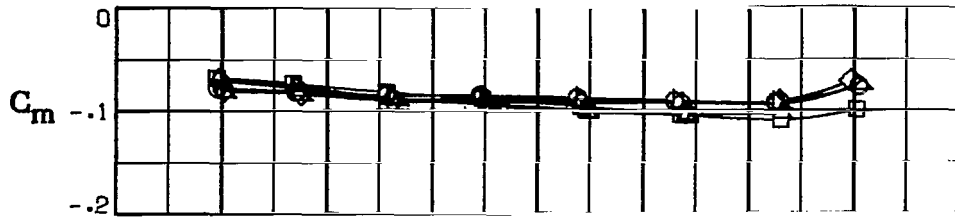
Figure 6.- Continued.

(c) $M_\infty = 0.70$; $R = 18.7 \times 10^6$ per m (5.7×10^6 per ft).

Figure 6.- Continued.
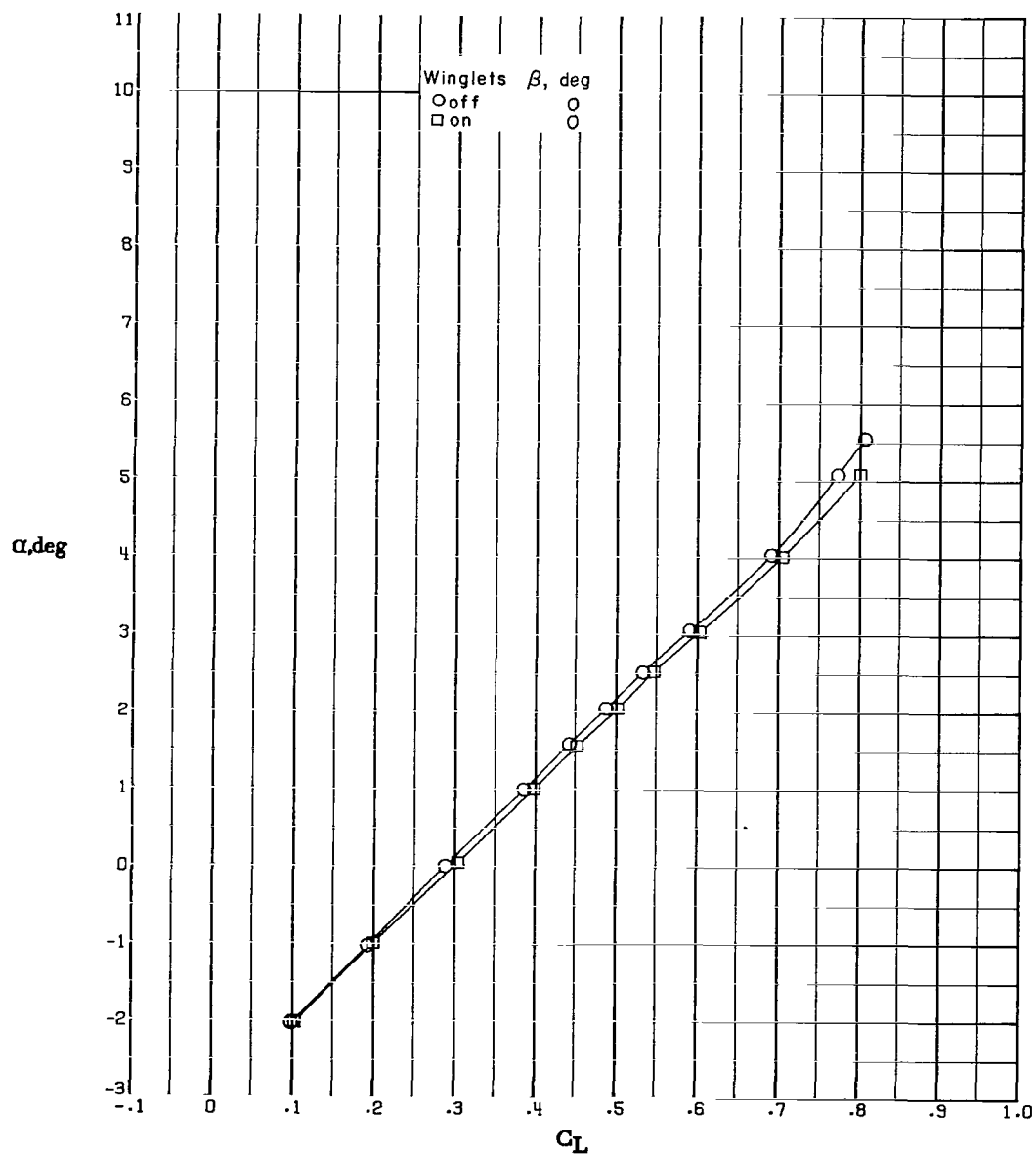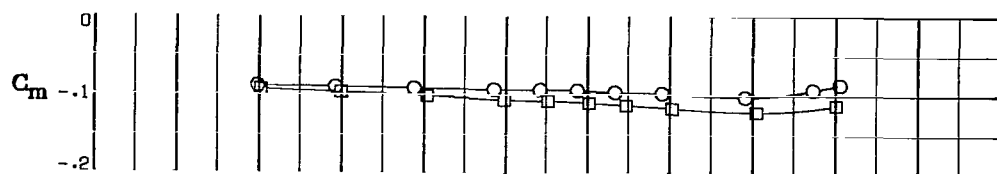
(d) $M_\infty = 0.75$; $R = 17.7 \times 10^6$ per m $(5.4 \times 10^6$ per ft$)$.
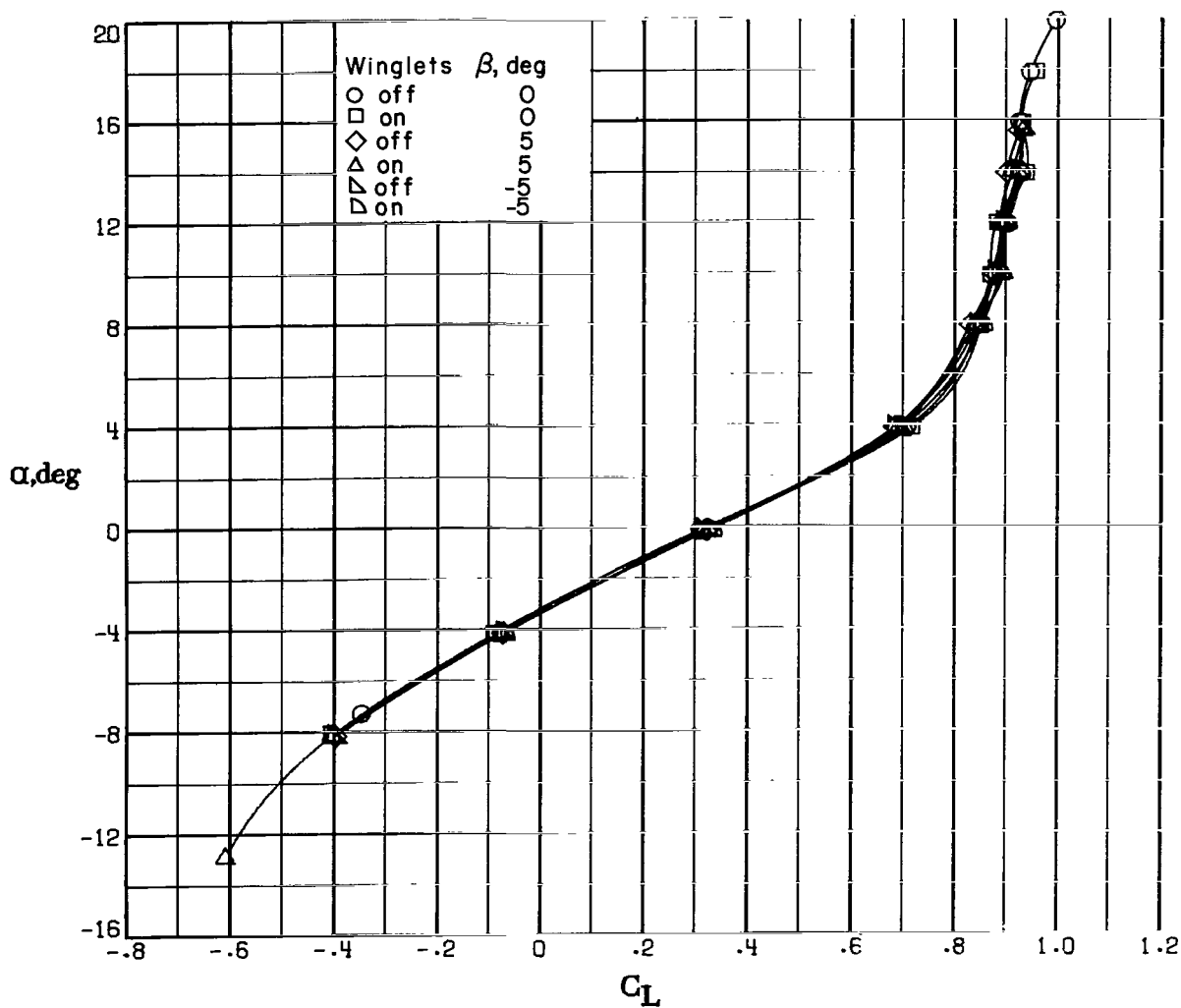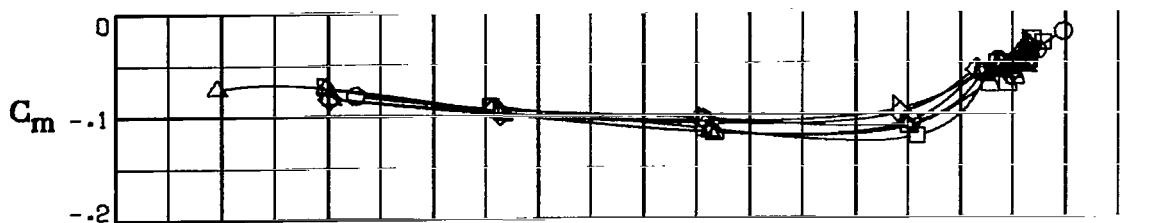
Figure 6.- Continued.

(e) $M_{\infty} = 0.78$; $R = 10.8 \times 10^6$ per m (3.3×10^6 per ft).
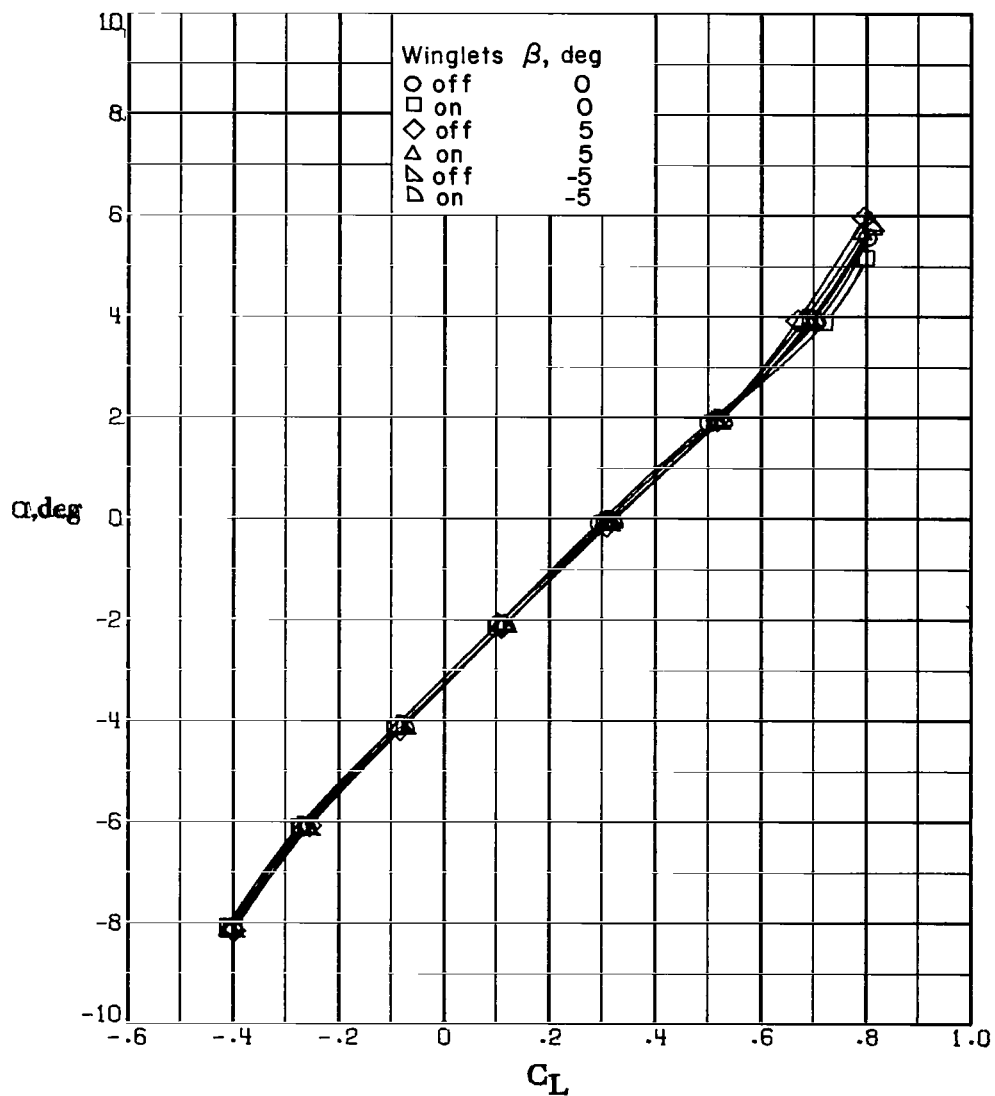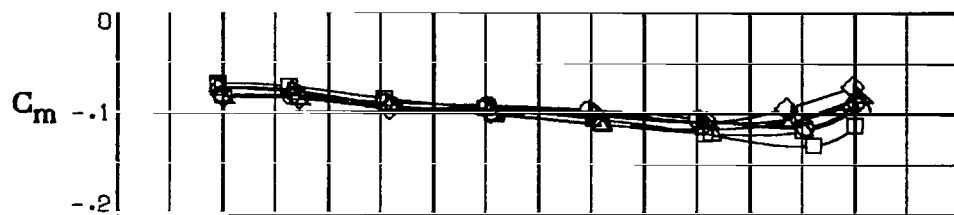
Figure 6.- Continued.

(f) $M_{\infty} = 0.78$; $R = 17.1 \times 10^6$ per m $(5.2 \times 10^6$ per ft$)$.
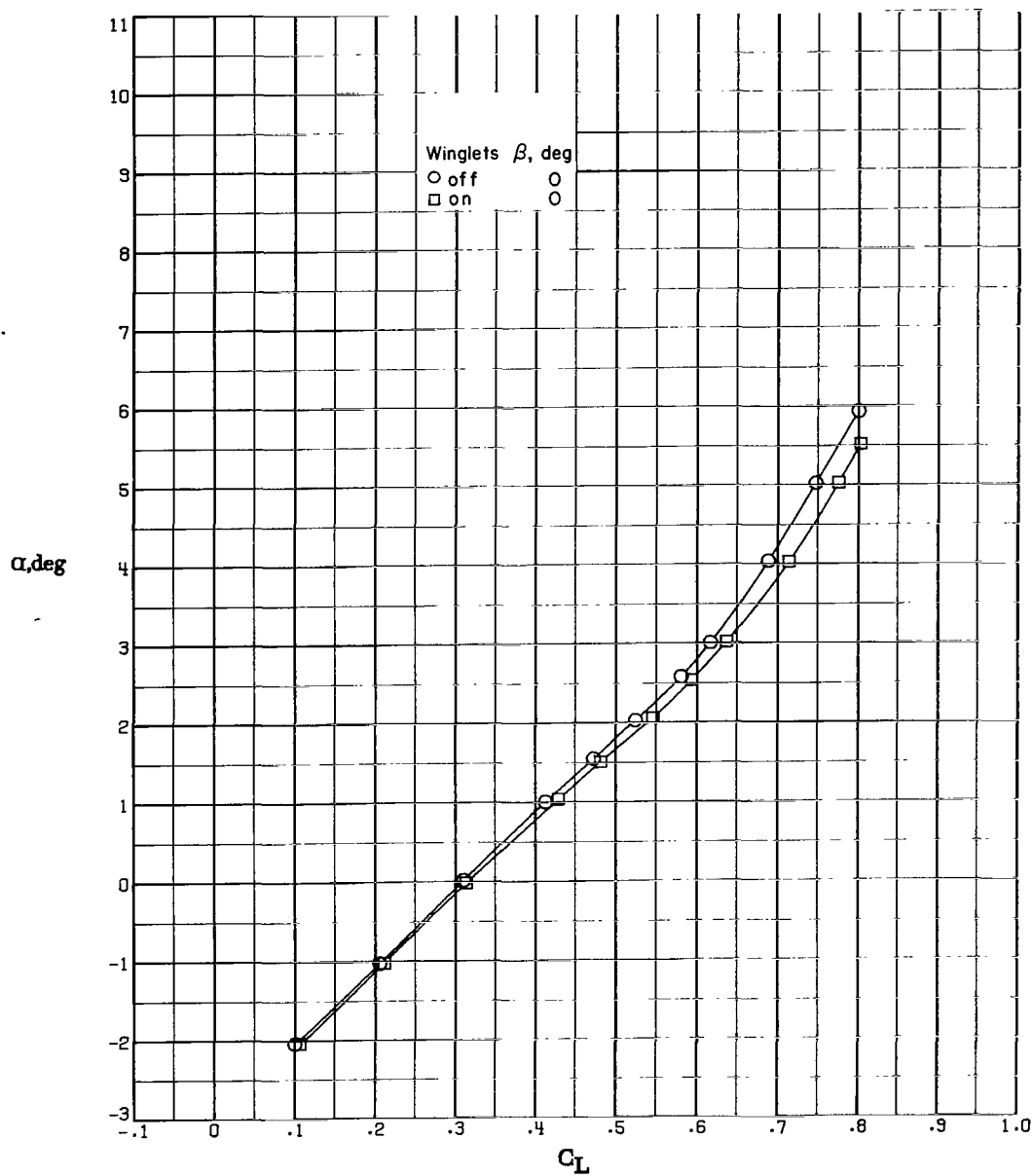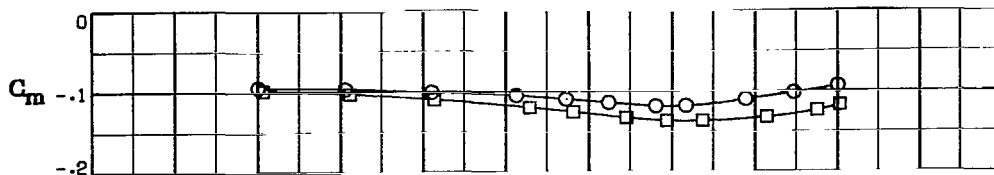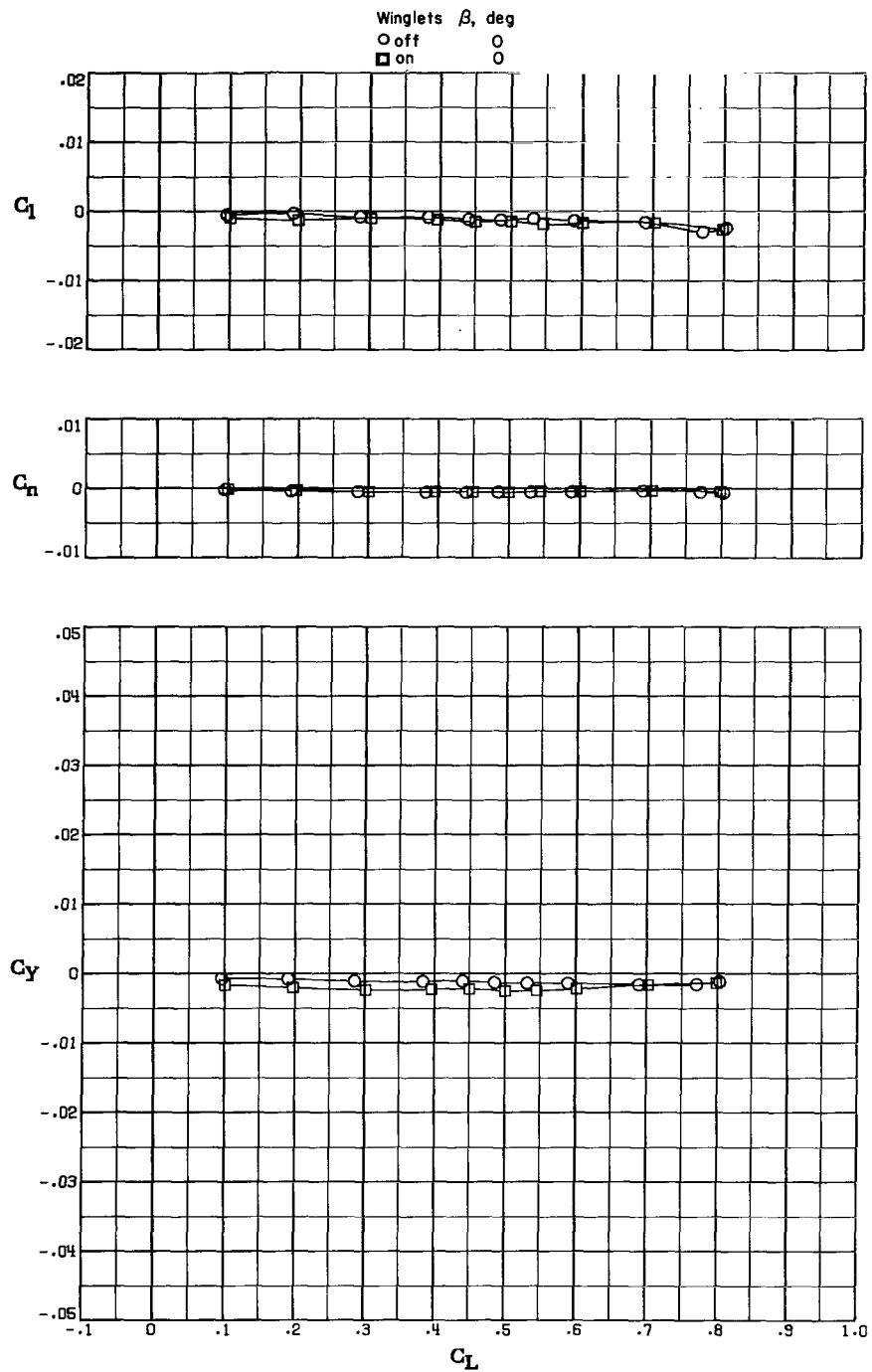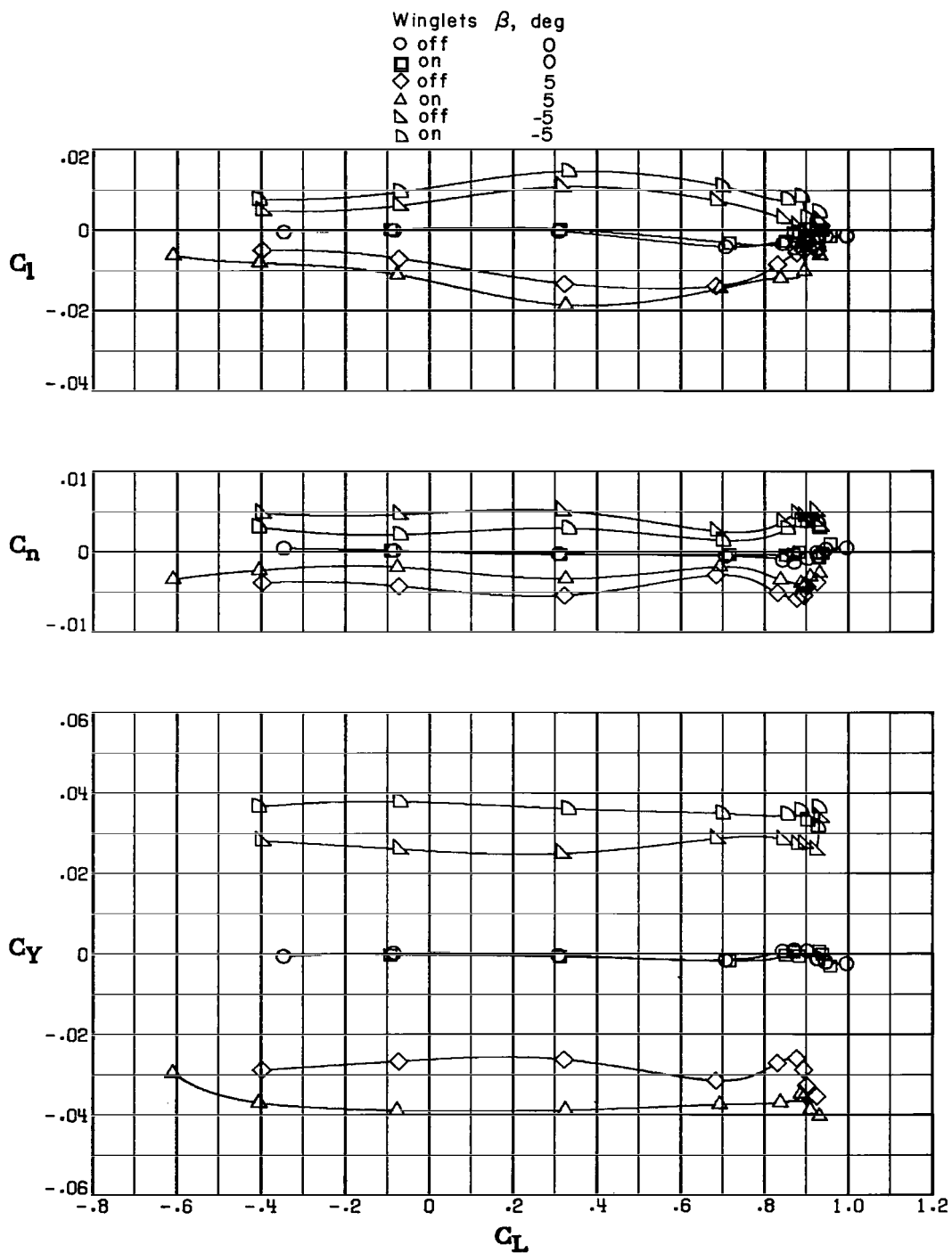
Figure 6.- Continued.

(g) $M_\infty = 0.80$; $R = 17.1 \times 10^6$ per m (5.2×10^6 per ft).
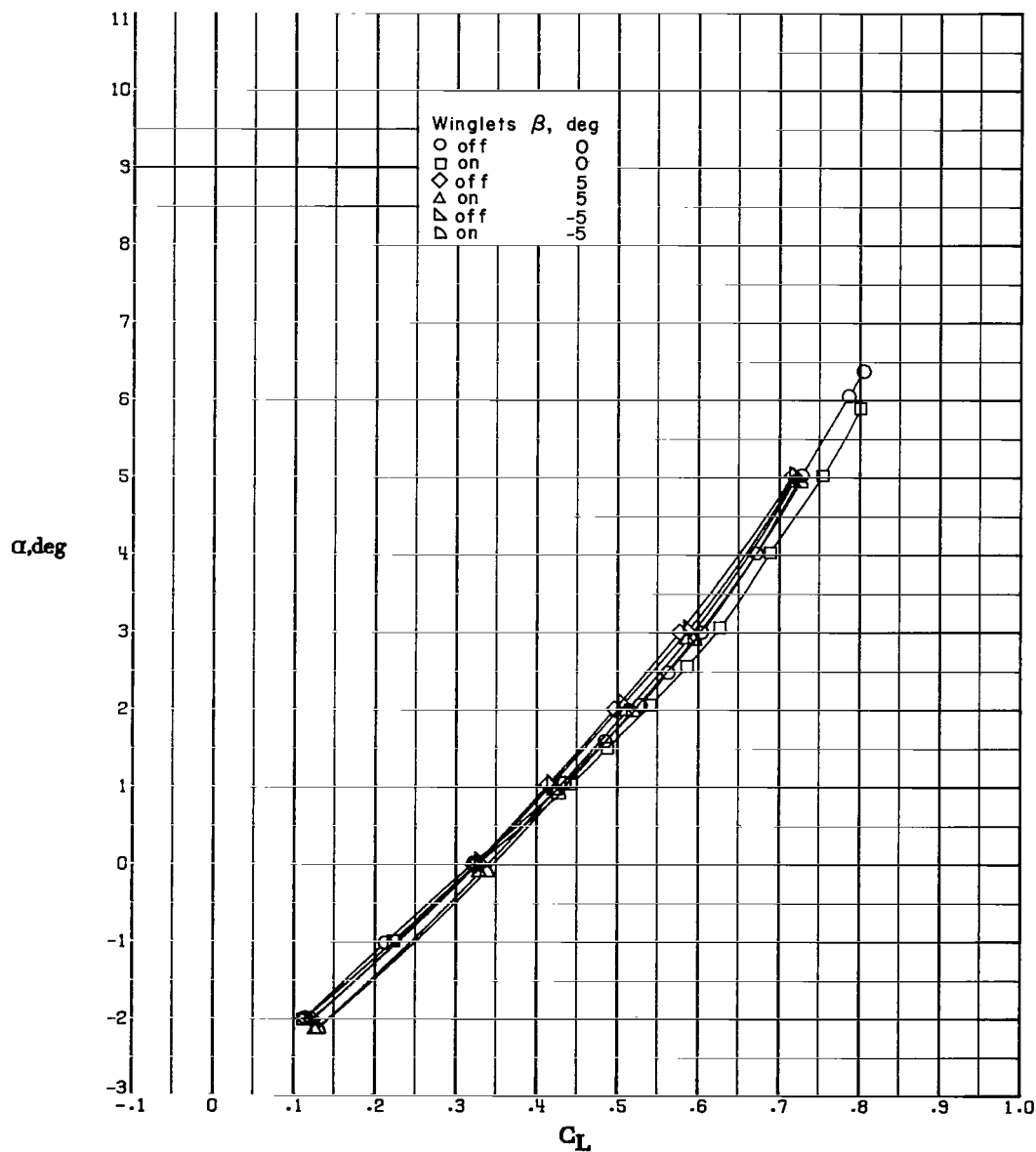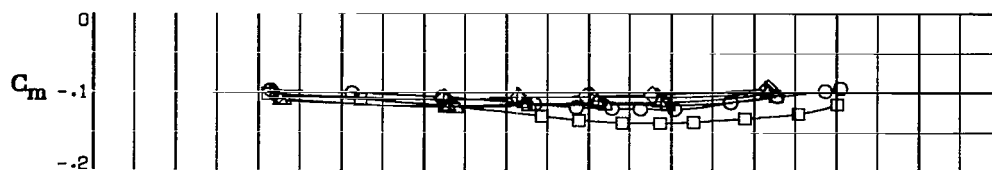
Figure 6.- Continued.

(h) $M_\infty = 0.82$; $R = 16.7 \times 10^6$ per m $(5.1 \times 10^6$ per ft).

Figure 6.- Continued.
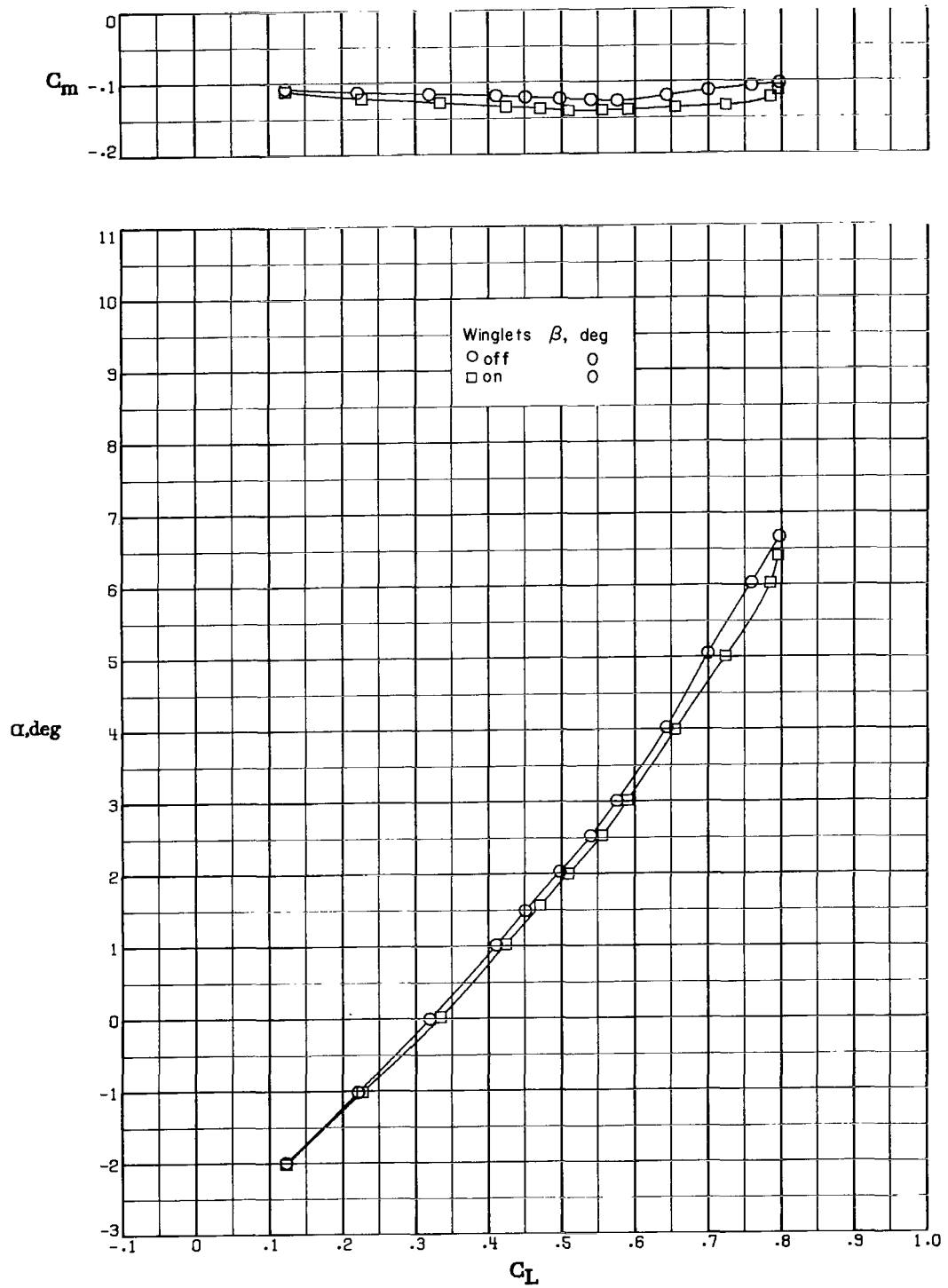
(i) $M_\infty = 0.85$; $R = 16.1 \times 10^6$ per m (4.9×10^6 per ft).

Figure 6.- Continued.
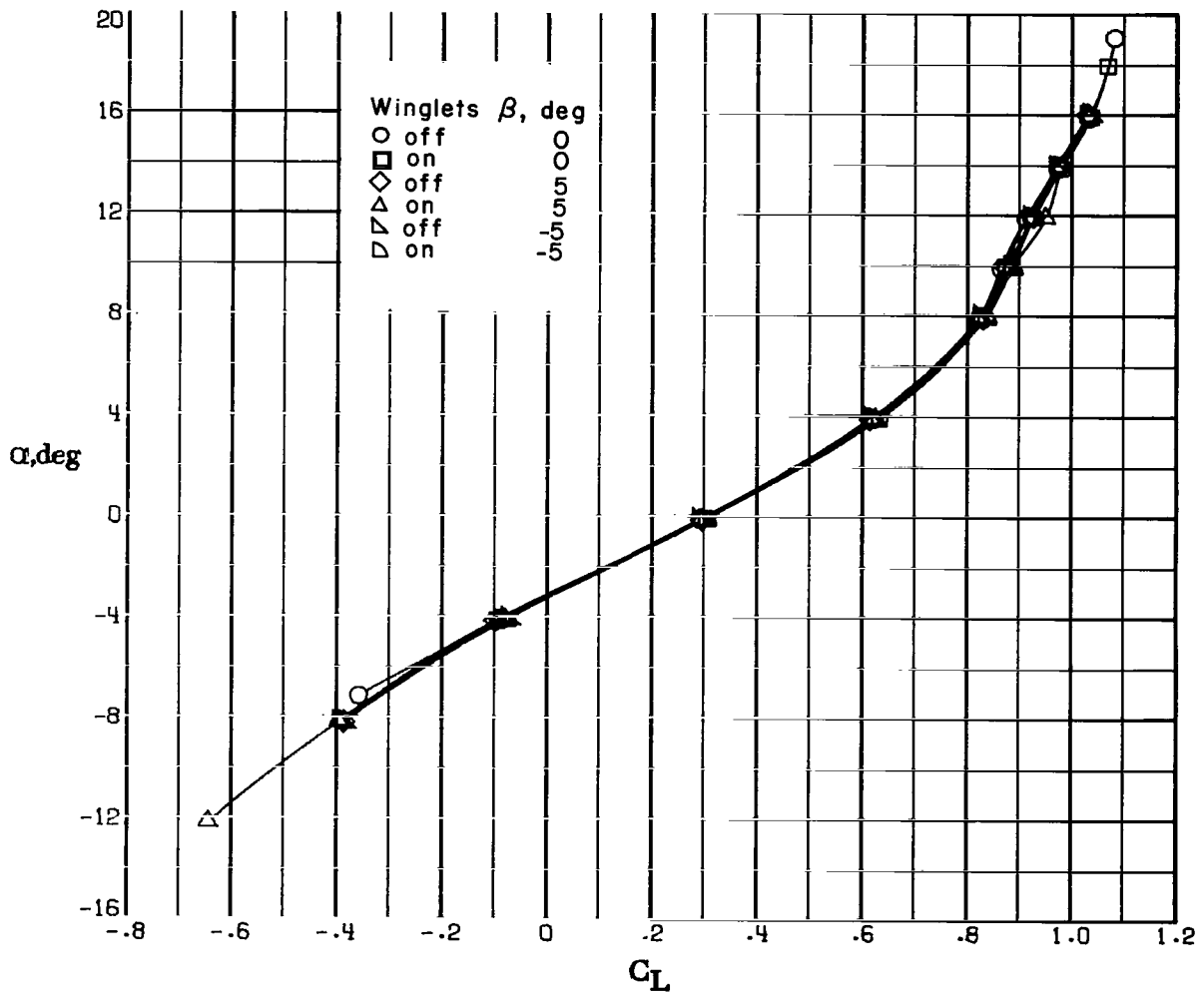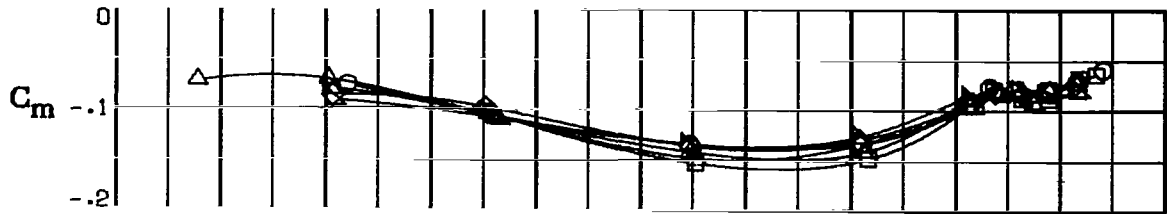
(j) $M_\infty = 0.90$; $R = 10.8 \times 10^6$ per m $(3.3 \times 10^6$ per ft).
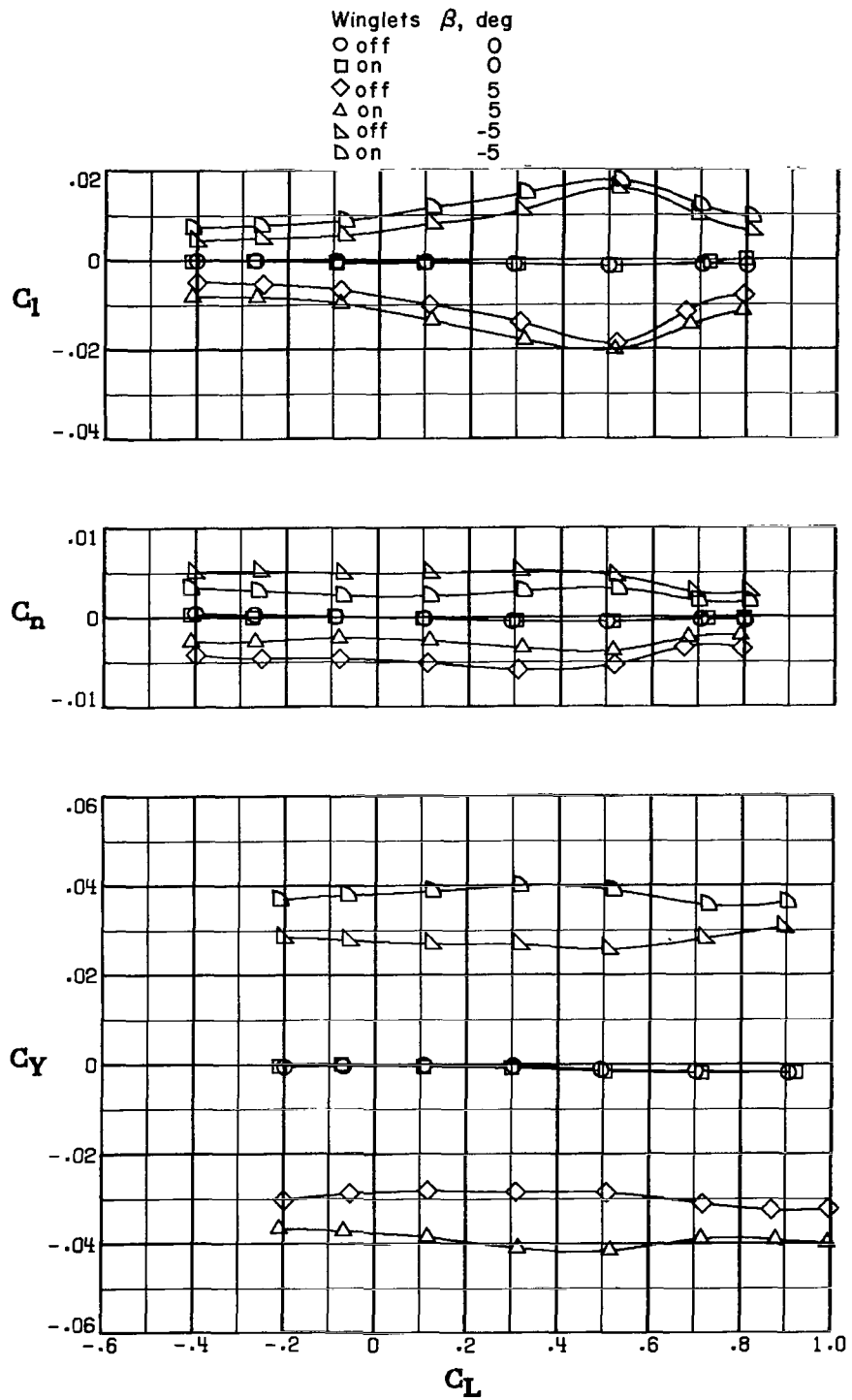
Figure 6.- Continued.

(k) $M_\infty = 0.90$; $R = 15.7 \times 10^6$ per m $(4.8 \times 10^6$ per ft).
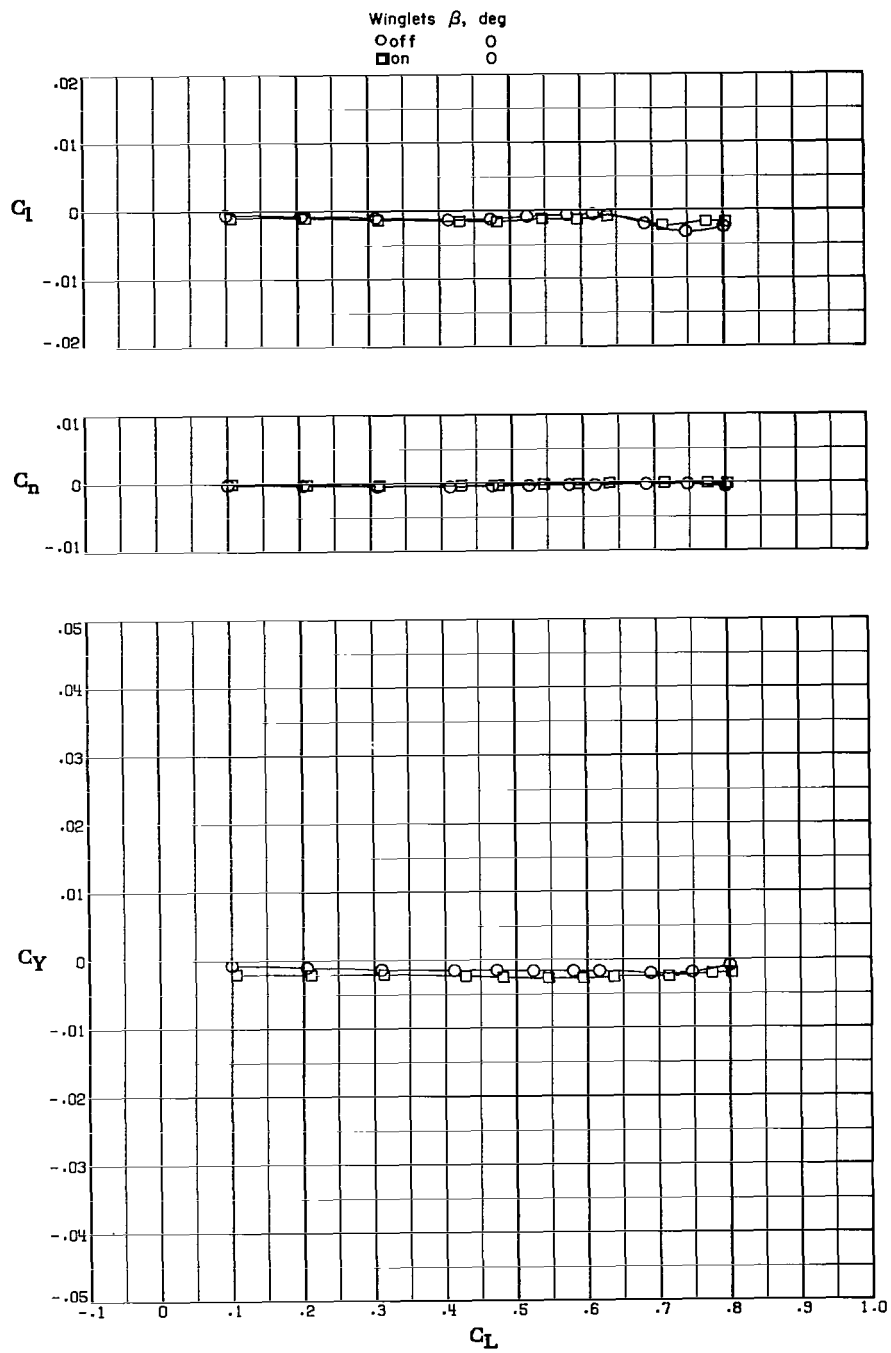
Figure 6.- Continued.

(1) $M_\infty = 0.95$; $R = 10.8 \times 10^6$ per m (3.3×10^6 per ft).
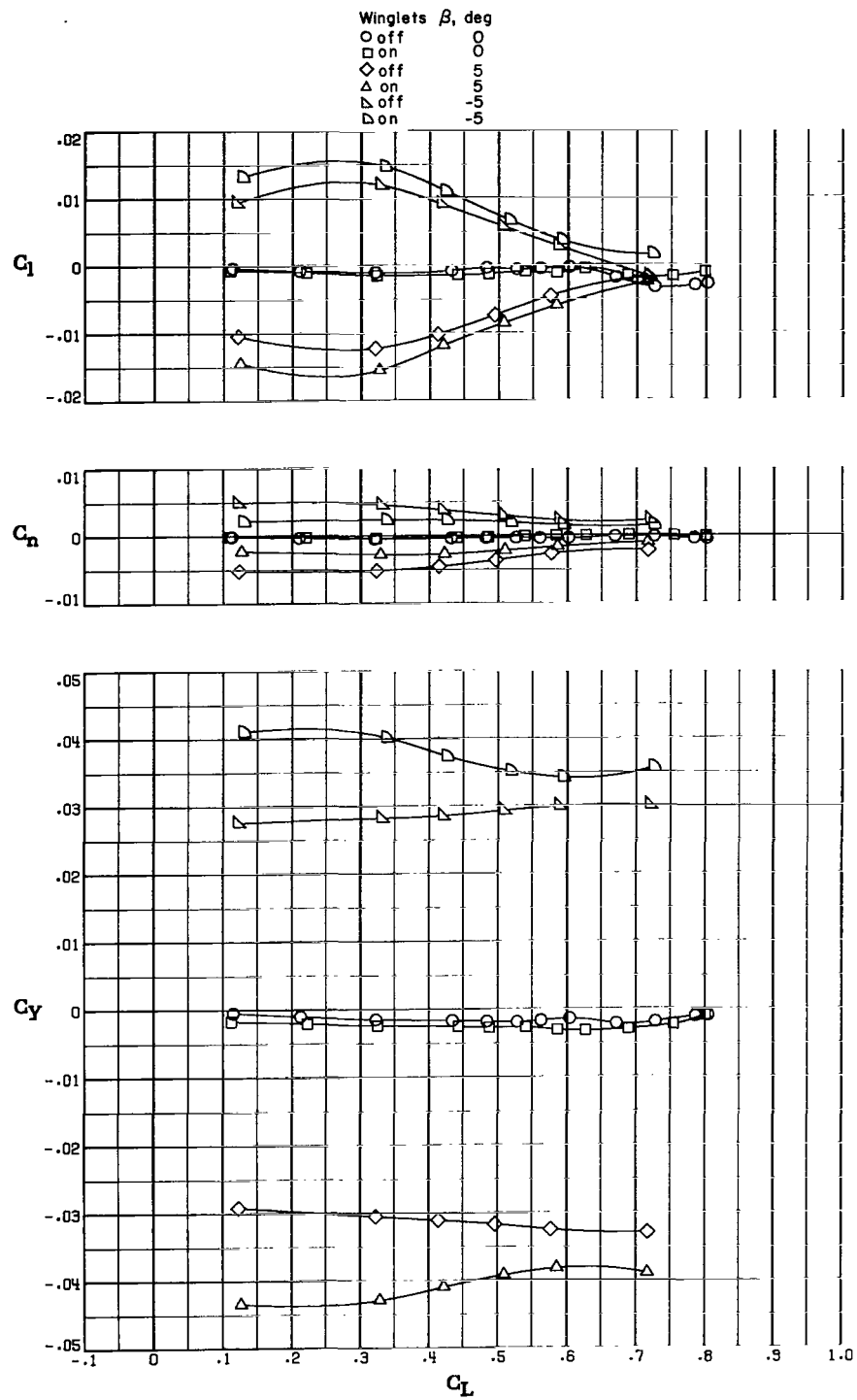
Figure 6.- Continued.
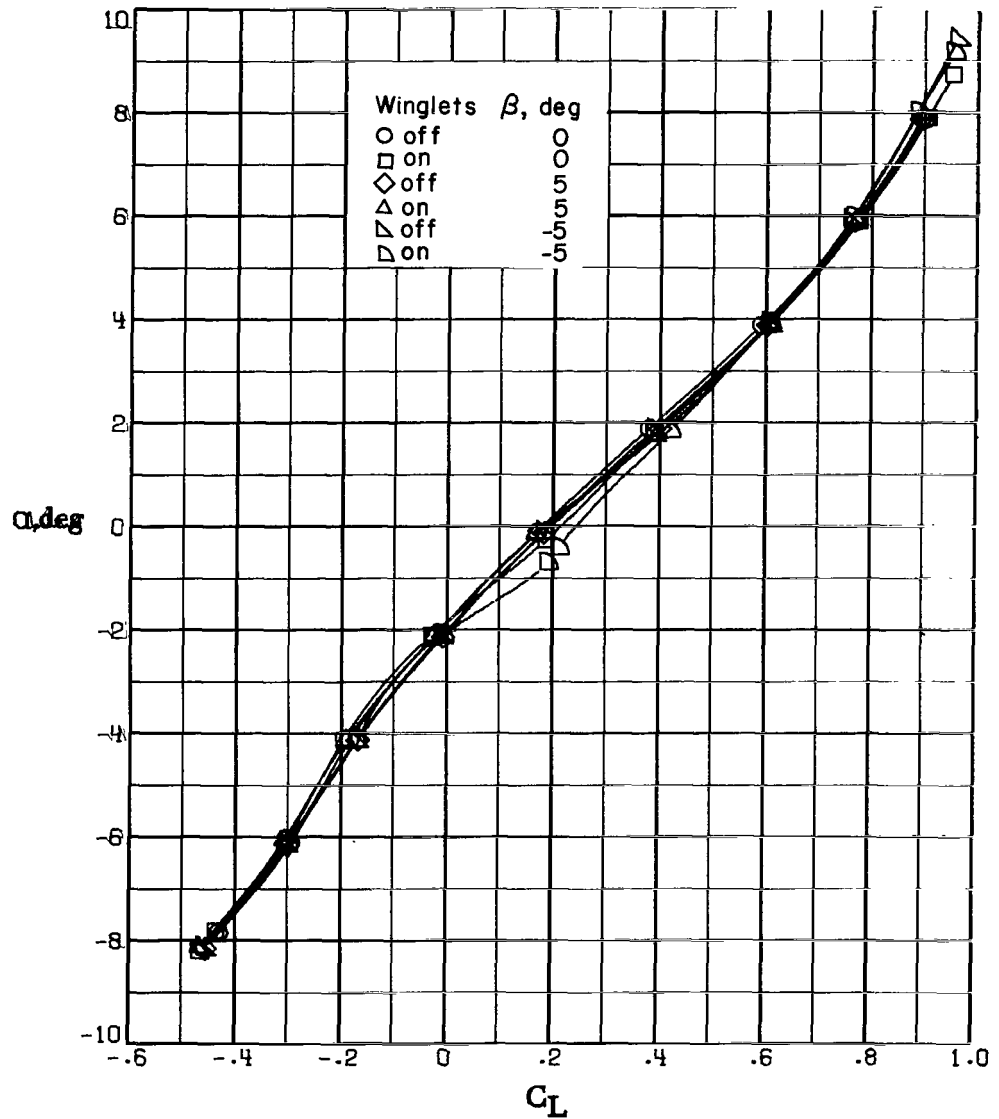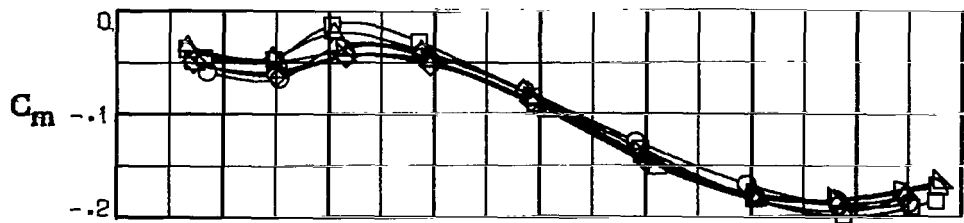
(m) $M_\infty = 0.95$; $R = 12.5 \times 10^6$ per m (3.8×10^6 per ft).

Figure 6.- Concluded.
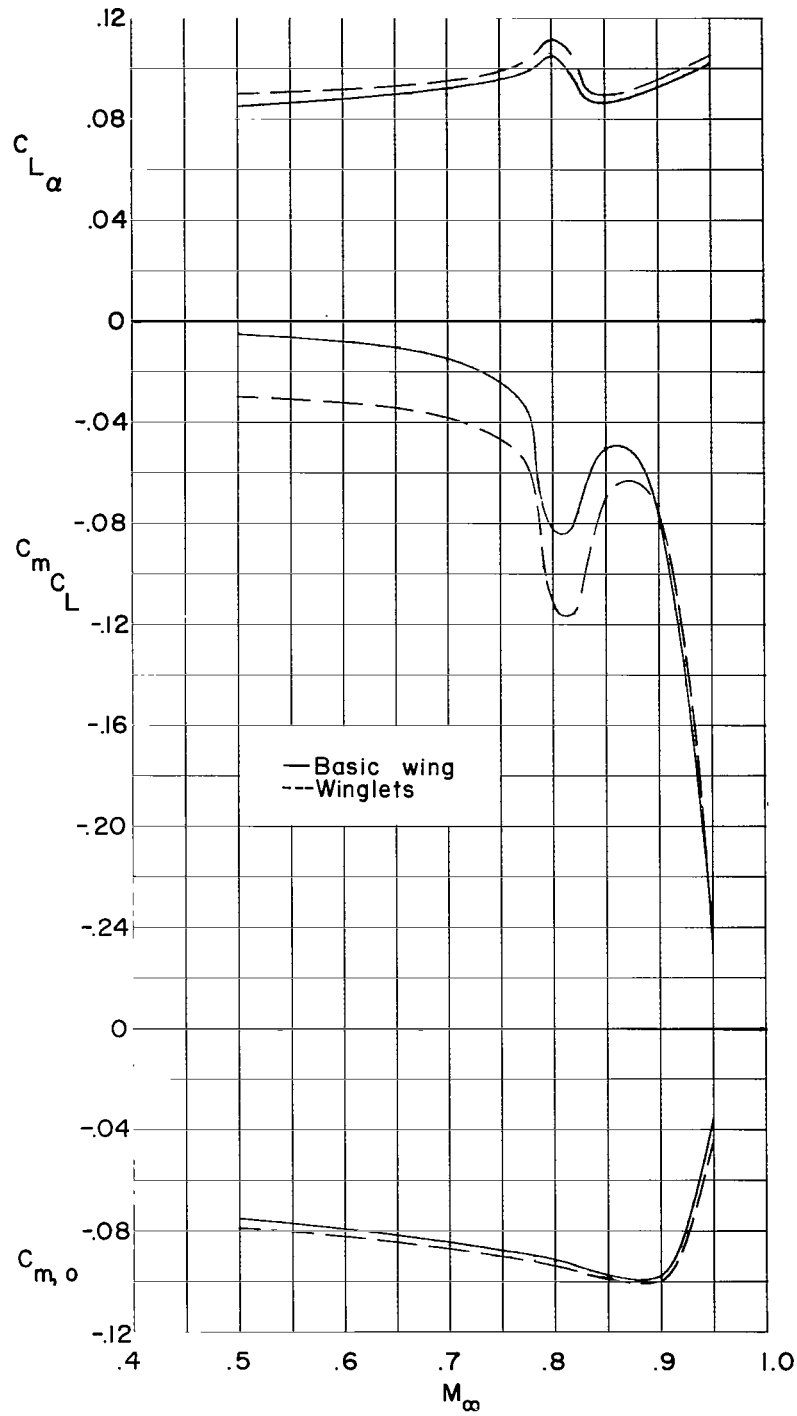
(a) High Reynolds number range.

Figure 7.- Summary of static longitudinal aerodynamic characteristics.
$\beta = 0^O$; $C_L = 0.44$.

(b) Low Reynolds number range.

Figure 7.- Concluded.
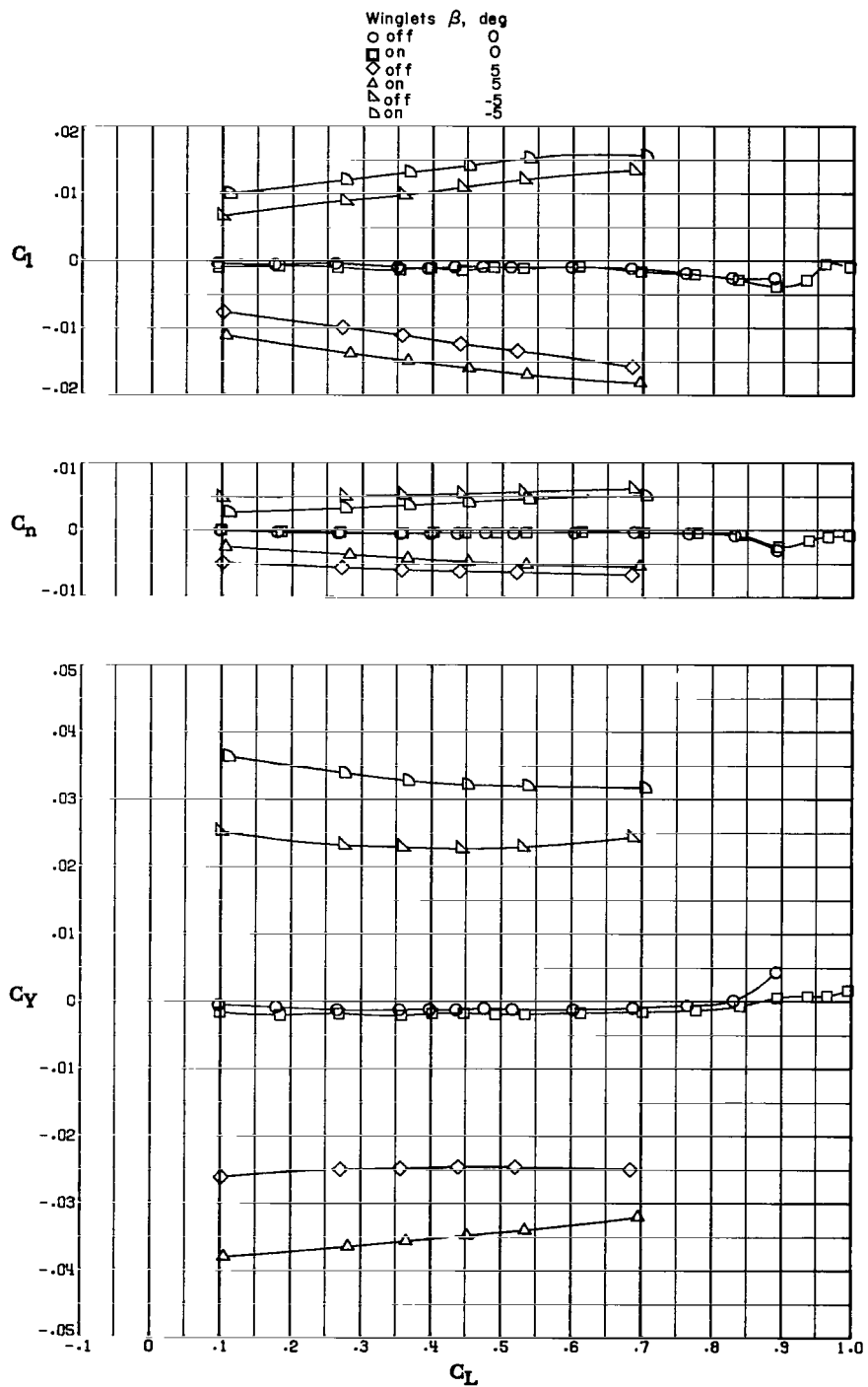
(a) $M_\infty = 0.50$; $R = 14.4 \times 10^6$ per m (4.4×10^6 per ft).

Figure 8.- Variation of rolling-moment, yawing-moment, and side-force coefficients with lift coefficient.

(b) $M_\infty = 0.70$; $R = 10.8 \times 10^6$ per m (3.3×10^6 per ft).

Figure 8.- Continued.

Winglets β, deg
|		
◯	off	0
◻	on	0
◇	off	5
△	on	5
◁	off	-5
◮	on	-5
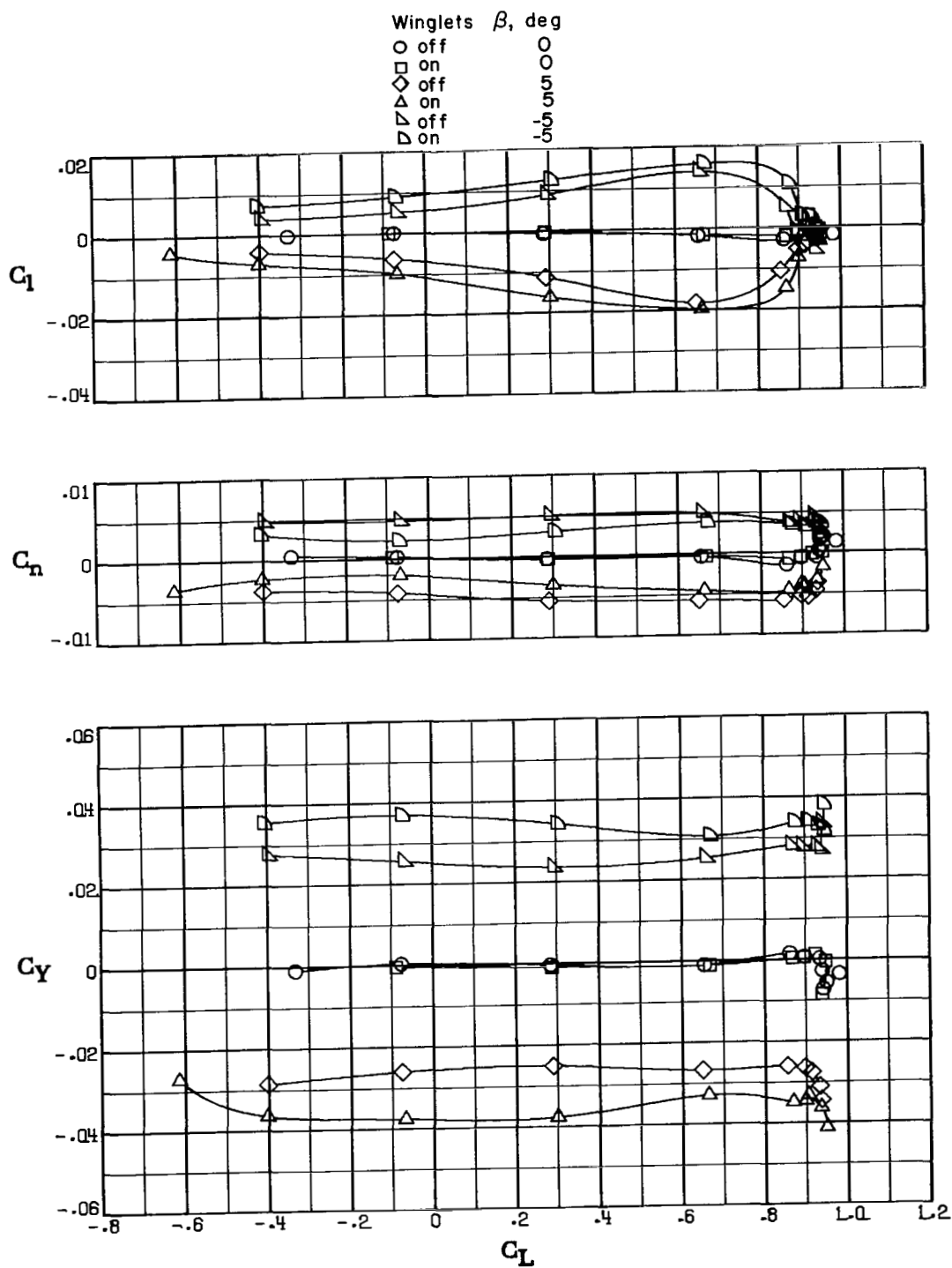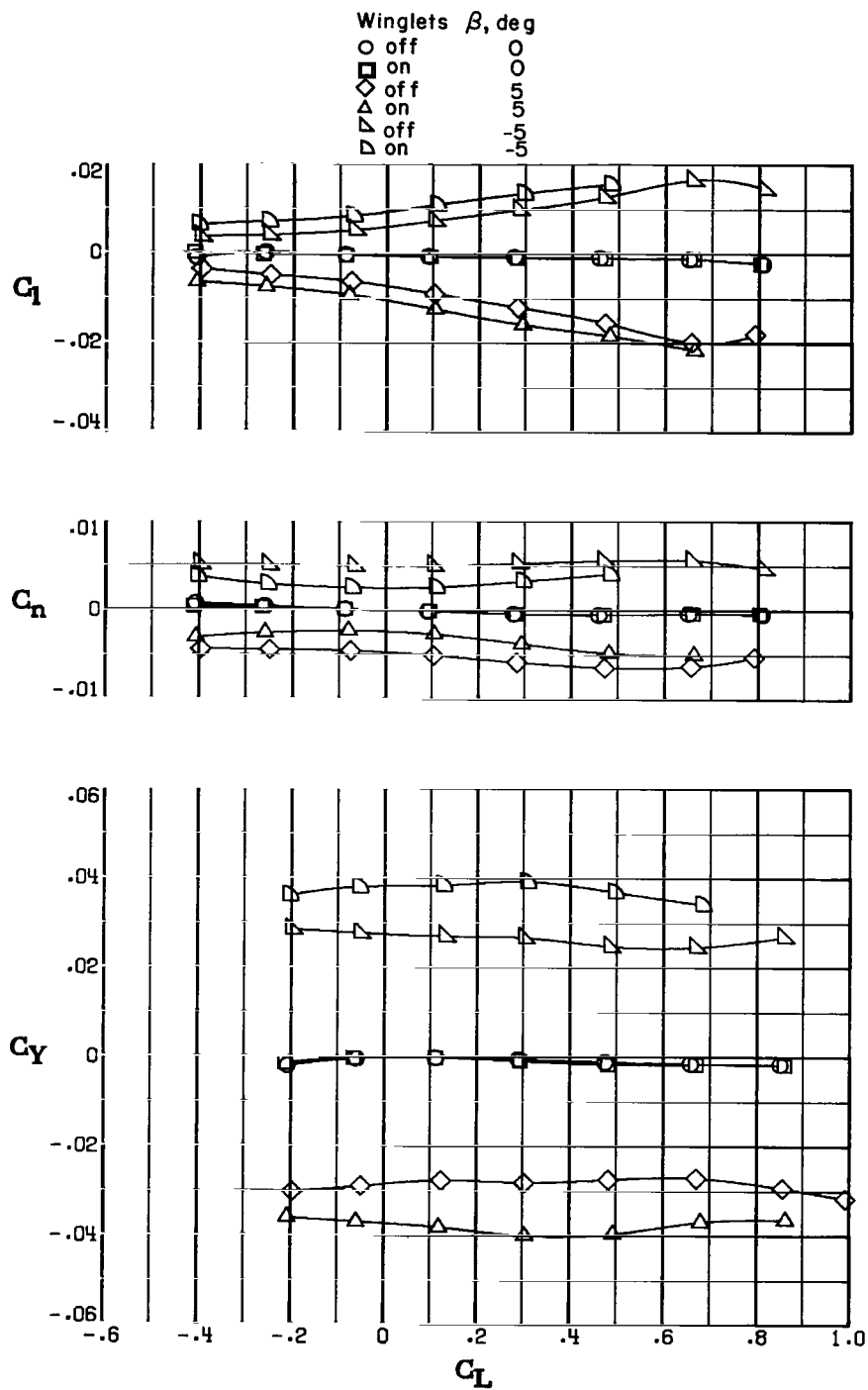
(c) $M_\infty = 0.70$; $R = 18.7 \times 10^6$ per m (5.7 $\times$ 10^6 per ft).
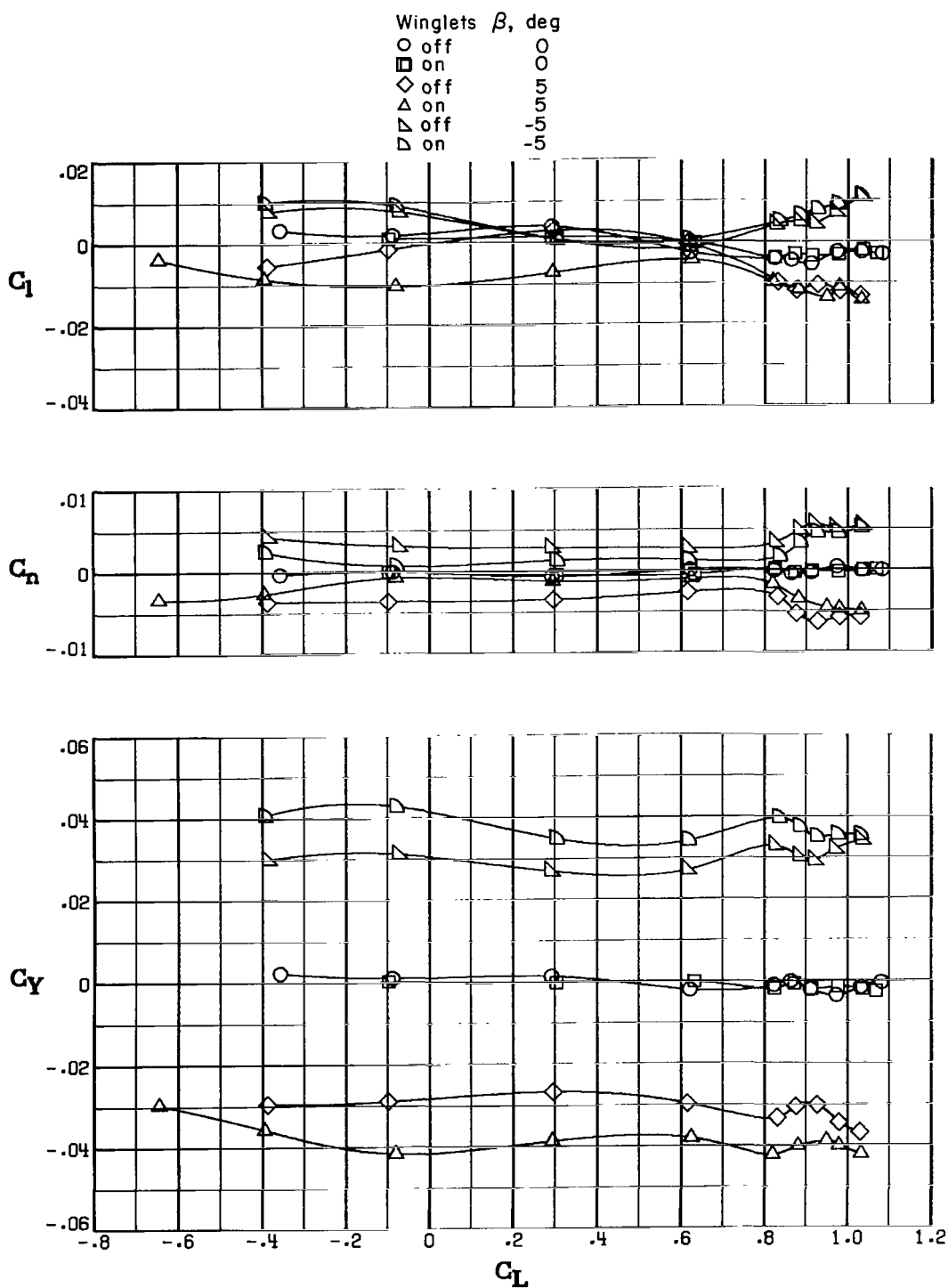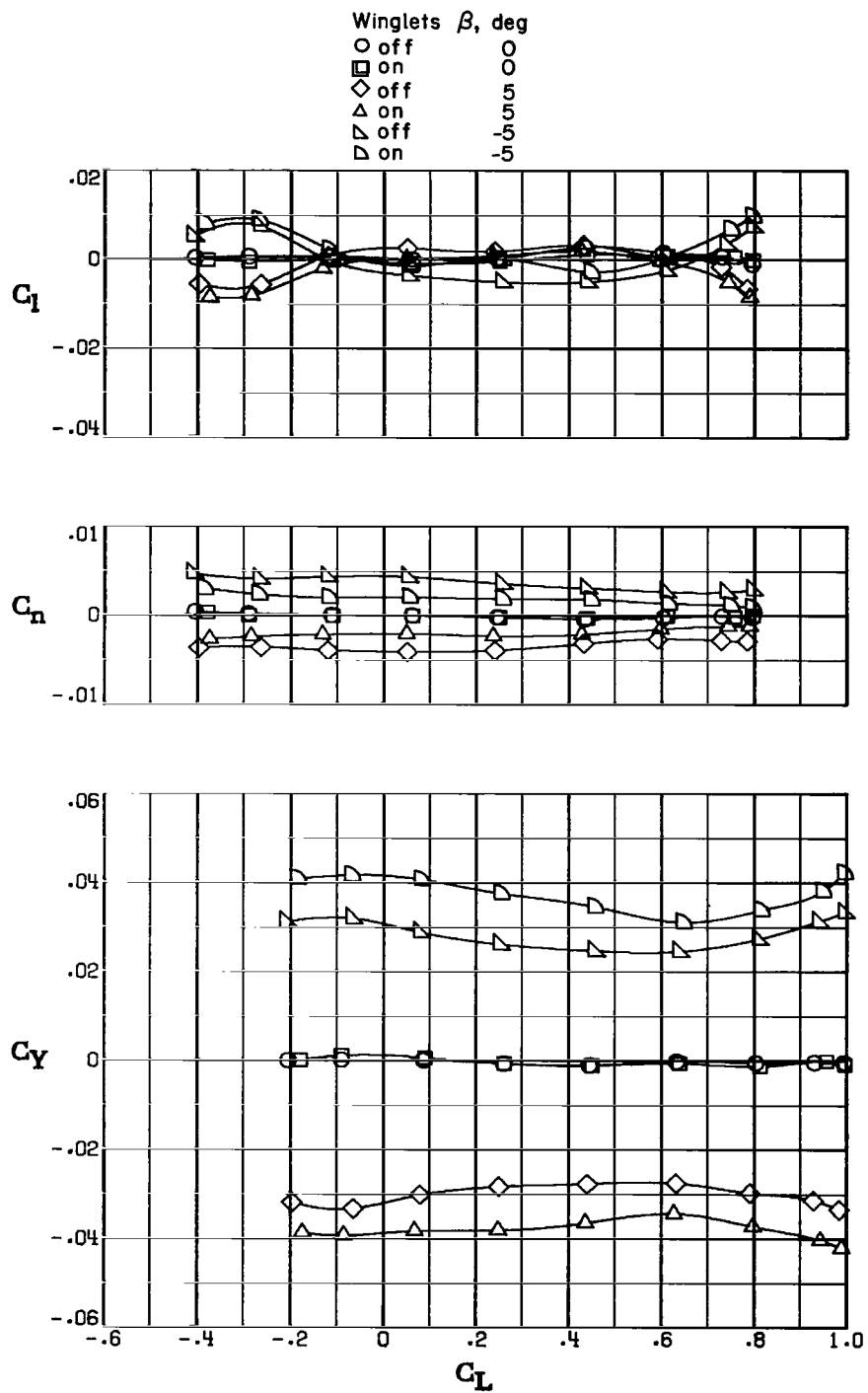
Figure 8.- Continued.

49

(d) $M_\infty = 0.75$; $R = 17.7 \times 10^6$ per m $(5.4 \times 10^6$ per ft).

Figure 8.- Continued.

(e) $M_\infty = 0.78$; $R = 10.8 \times 10^6$ per m (3.3×10^6 per ft).
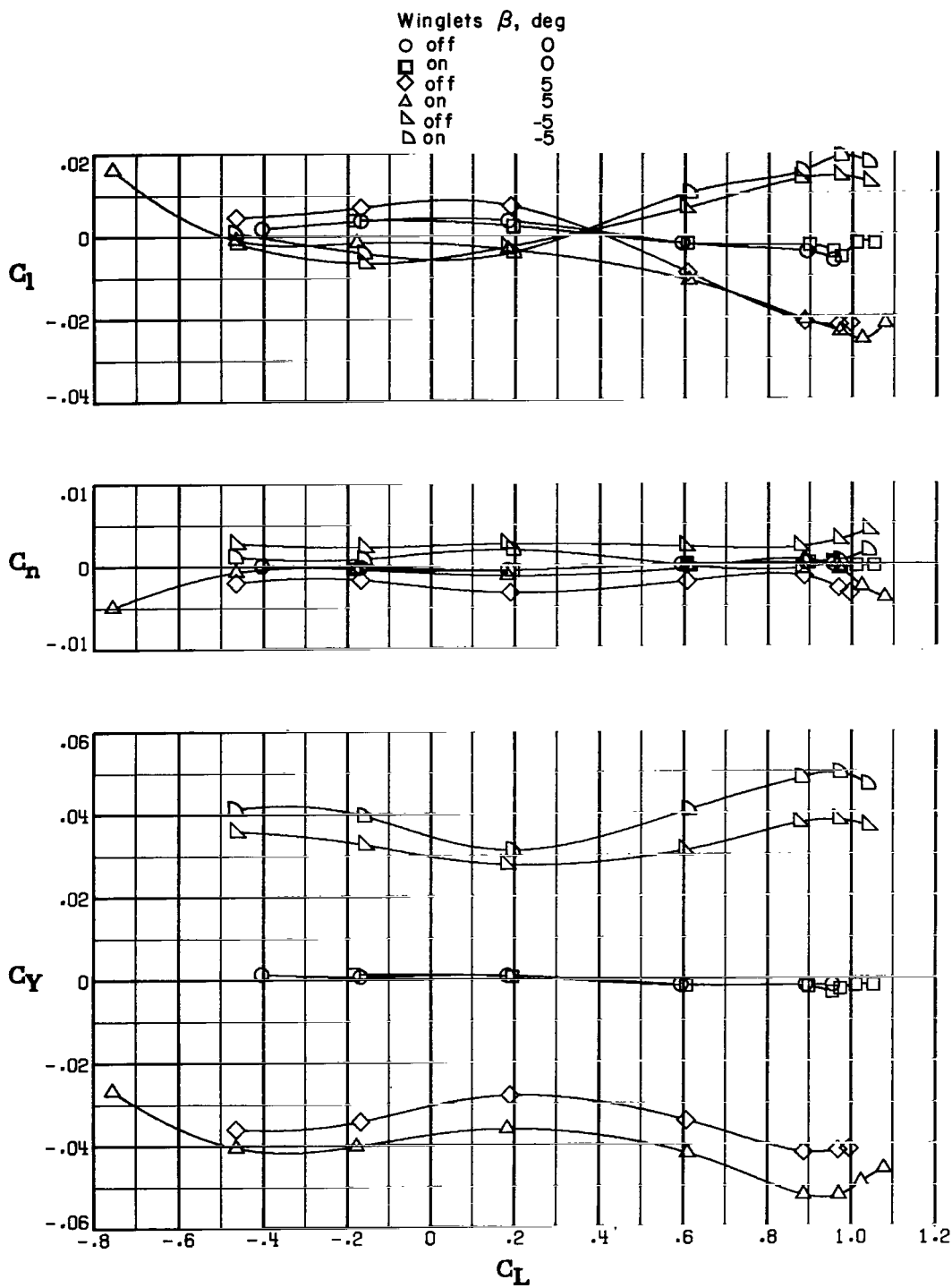
Figure 8.- Continued.

51

Winglets β, deg
○ off   0
□ on   0
◇ off   5
△ on   5
◁ off   -5
◻ on   -5

(f) $M_\infty = 0.78$; $R = 17.1 \times 10^6$ per m (5.2×10^6 per ft).

Figure 8.- Continued.

(g) $M_\infty = 0.80$; $R = 17.1 \times 10^6$ per m (5.2×10^6 per ft).

Figure 8.- Continued.

(h) $M_\infty = 0.82$; $R = 16.7 \times 10^6$ per m (5.1×10^6 per ft).

Figure 8.- Continued.
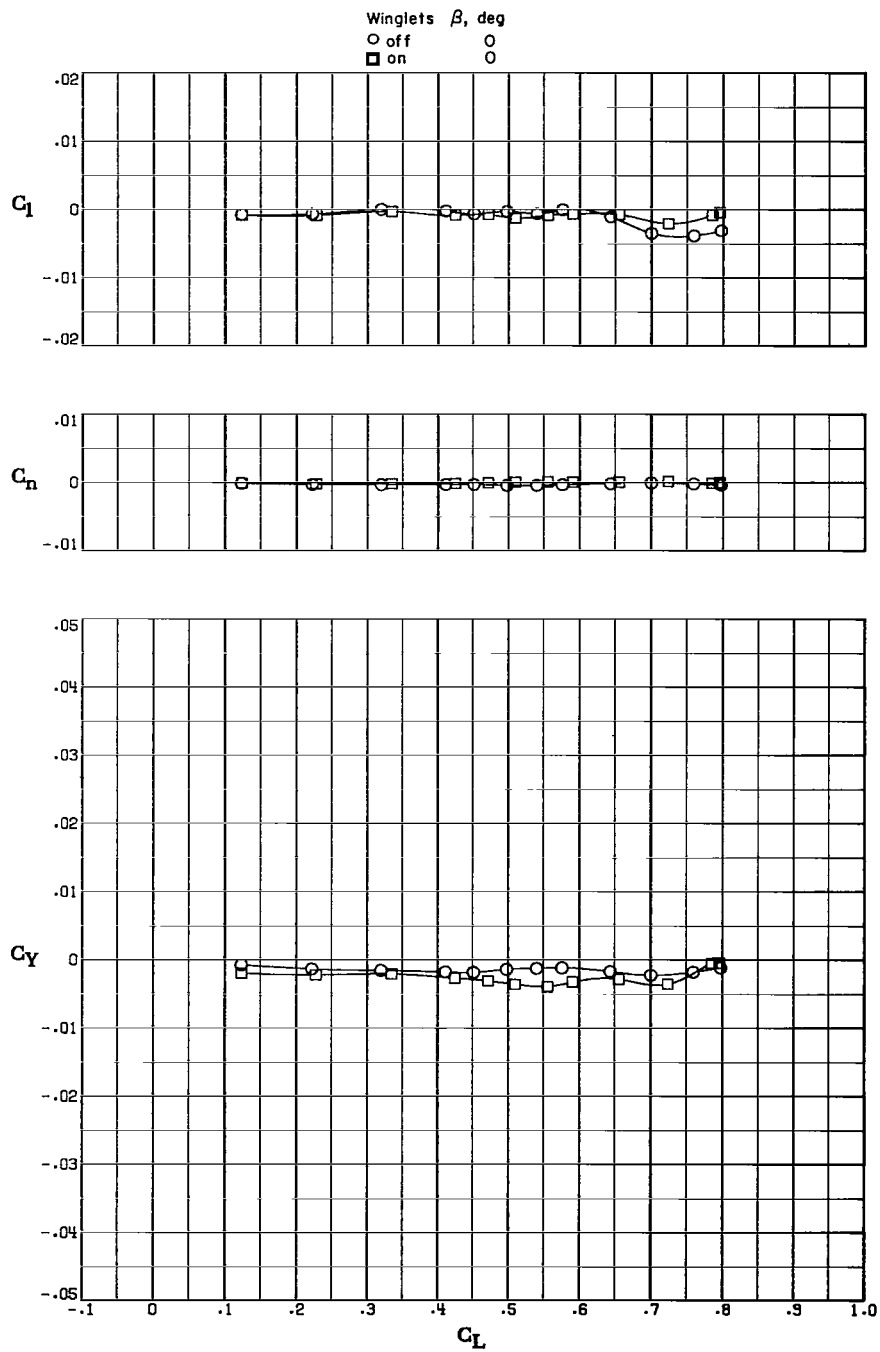
(i) $M_\infty = 0.85$; $R = 16.1 \times 10^6$ per m (4.9×10^6 per ft).

Figure 8.- Continued.

(j) $M_\infty = 0.90$; $R = 10.8 \times 10^6$ per m (3.3×10^6 per ft).
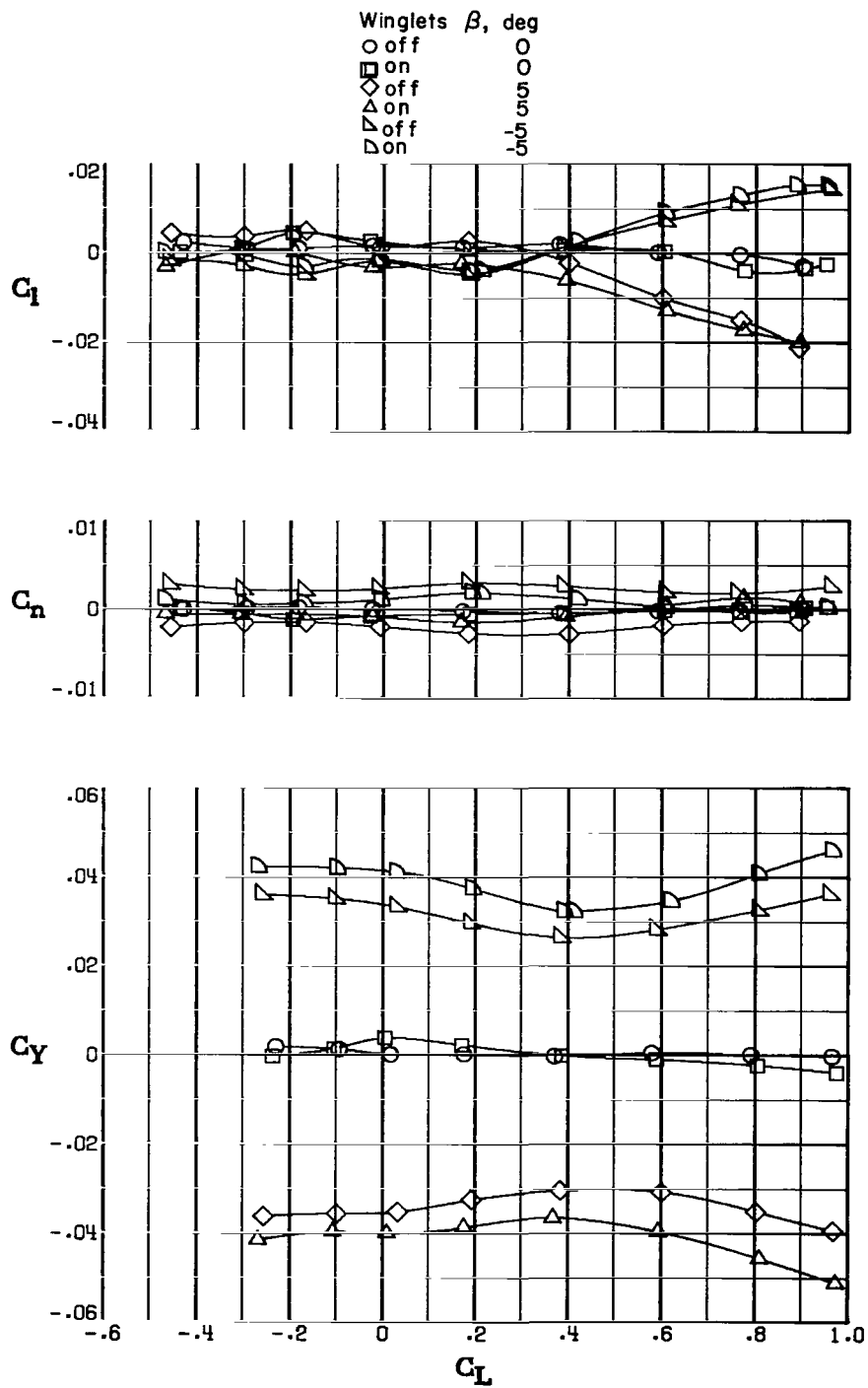
Figure 8.- Continued.

(k) $M_\infty = 0.90$; $R = 15.7 \times 10^6$ per m (4.8×10^6 per ft).
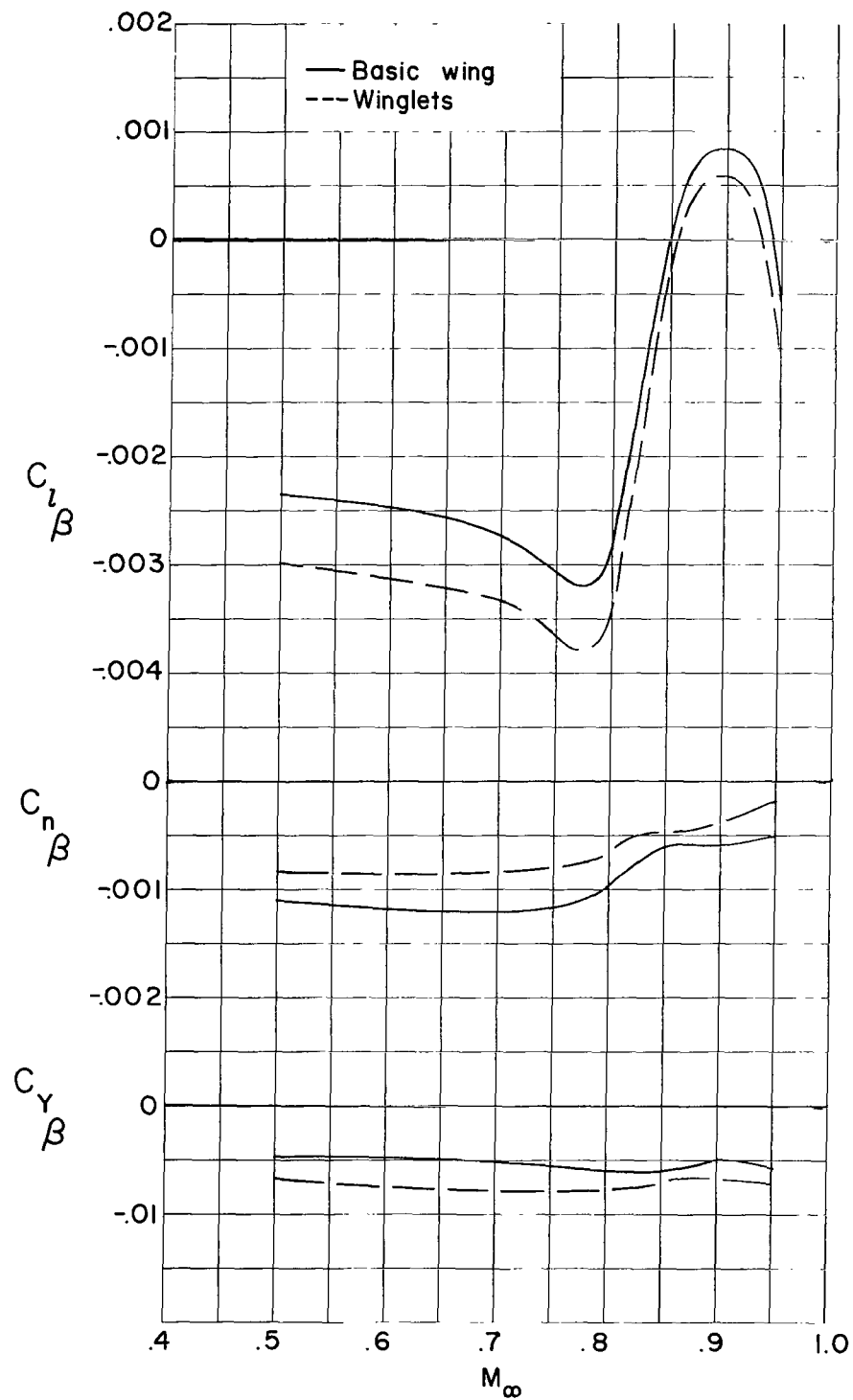
Figure 8.- Continued.

(1) $M_\infty = 0.95$; $R = 10.8 \times 10^6$ per m $(3.3 \times 10^6$ per ft).
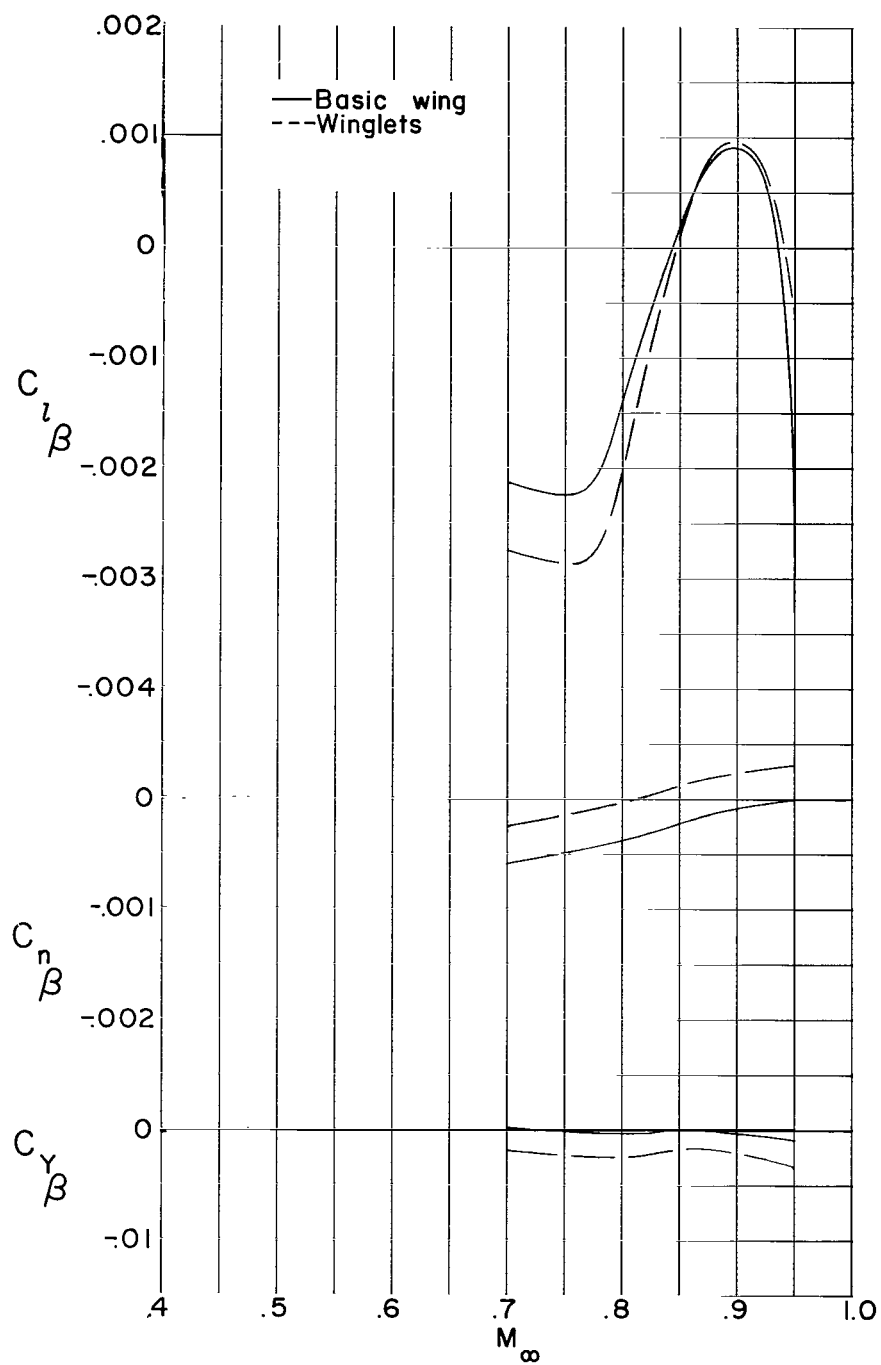
Figure 8.- Continued.

(m) $M_\infty = 0.95$; $R = 12.5 \times 10^6$ per m (3.8×10^6 per ft).

Figure 8.- Concluded.

(a) High Reynolds number range.

Figure 9.- Summary of static lateral-directional aerodynamic characteristics. $C_L = 0.44$.

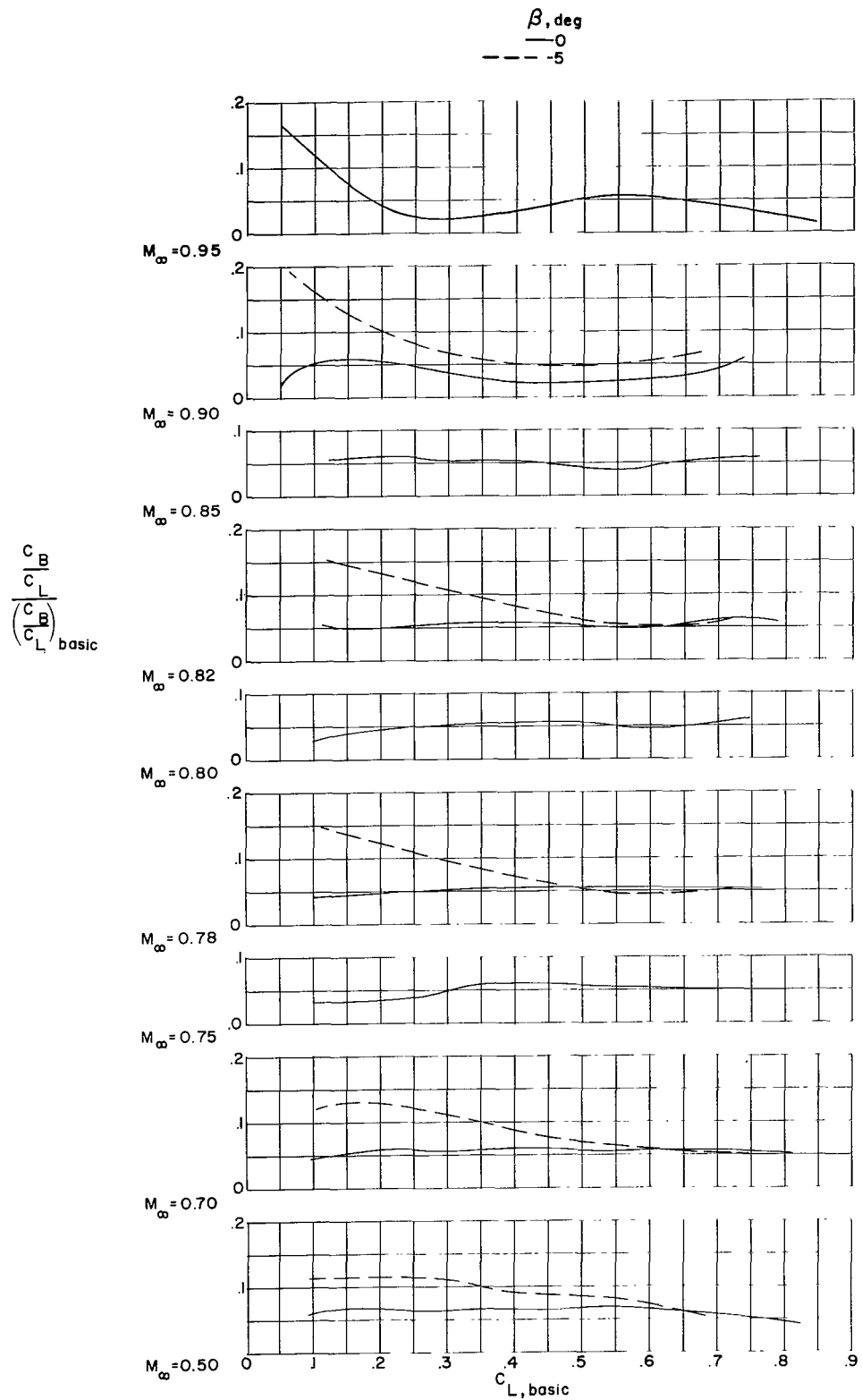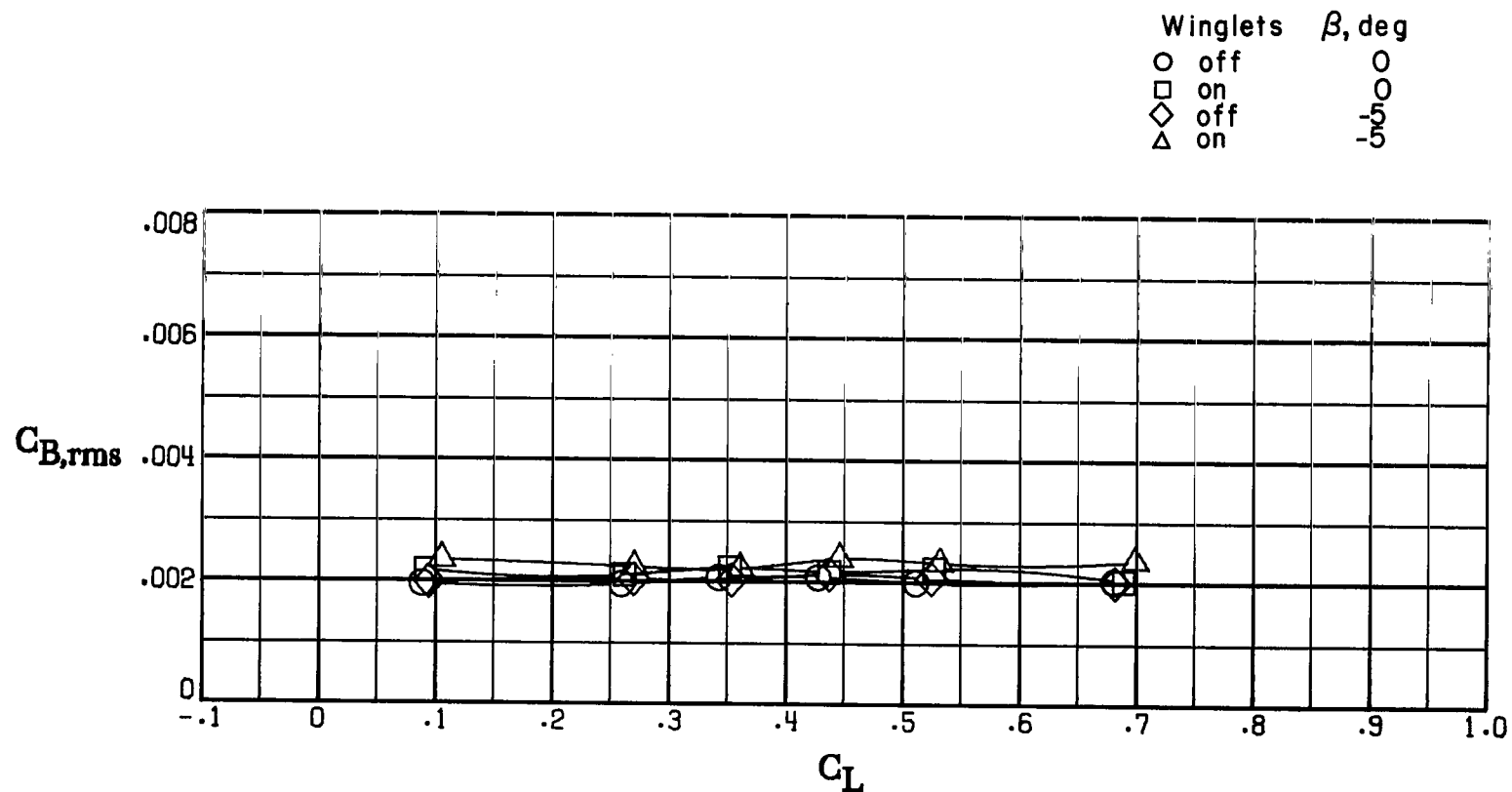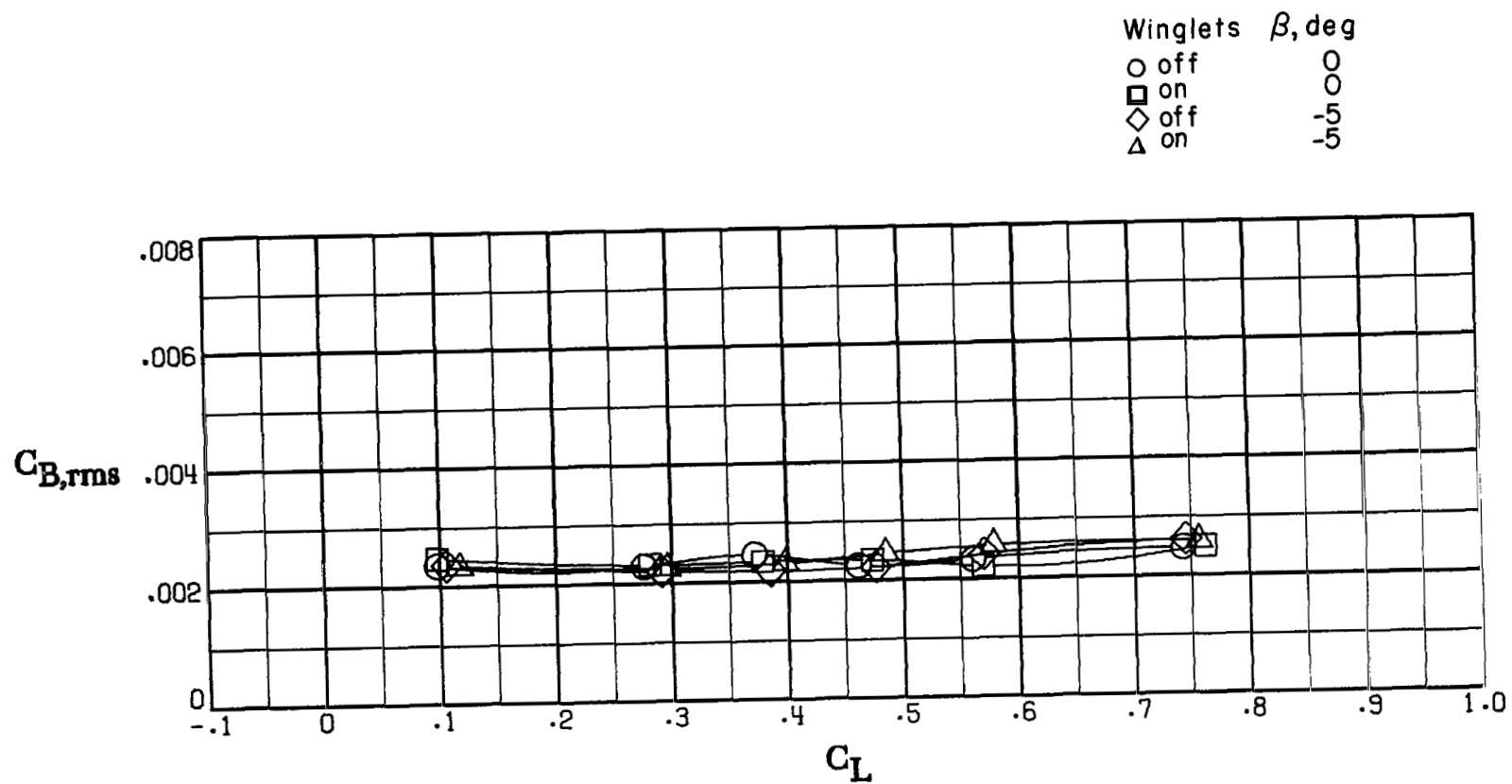(b) Low Reynolds number range.

Figure 9.- Concluded.

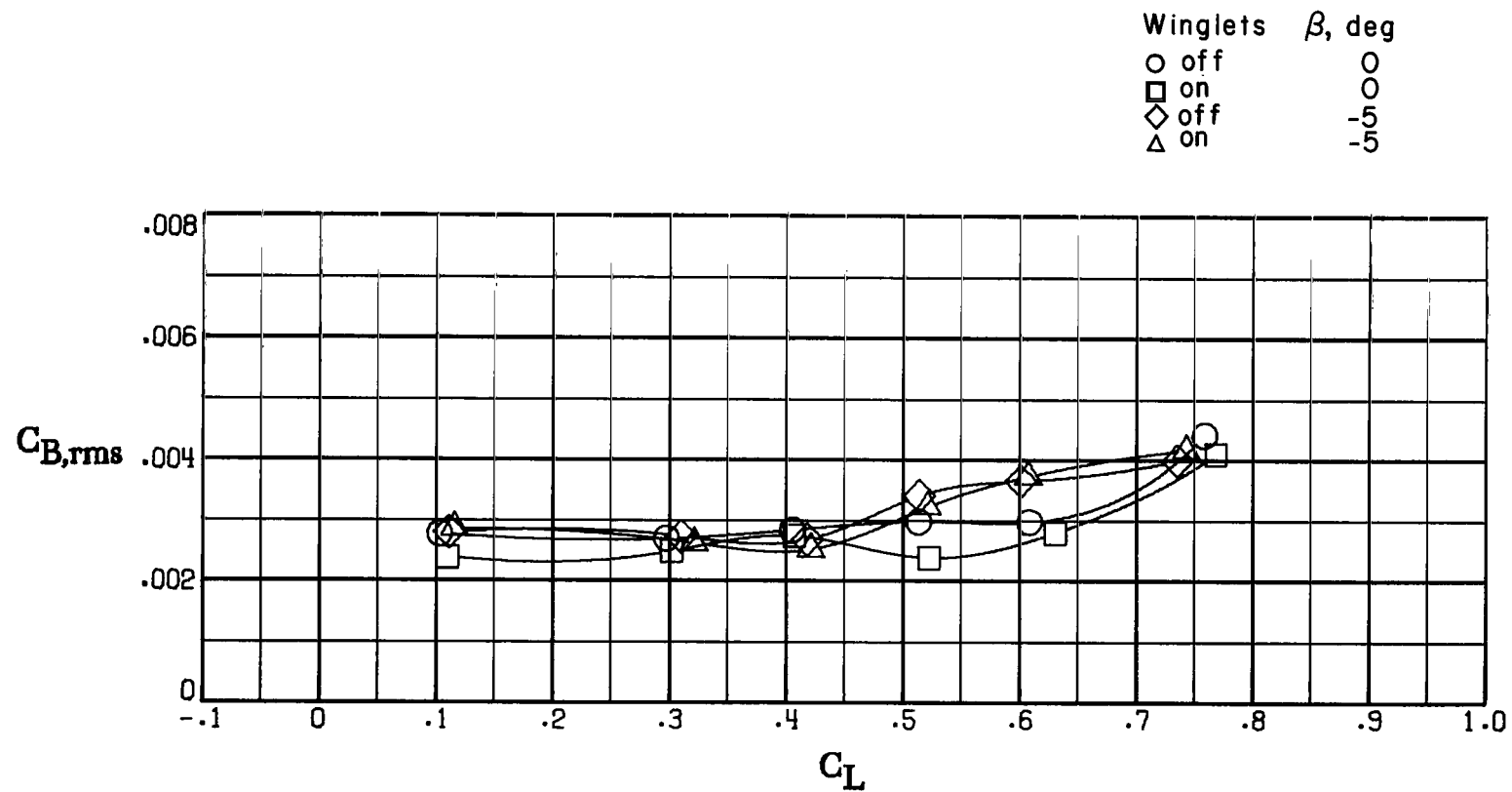Figure 10.- Variation of incremental bending-moment coefficient with lift coefficient.

(a) $M_\infty = 0.50$; $R = 14.4 \times 10^6$ per m $(4.4 \times 10^6$ per ft$)$.

Figure 11.- Variation of wing root-mean-square bending-moment coefficient with lift coefficient.

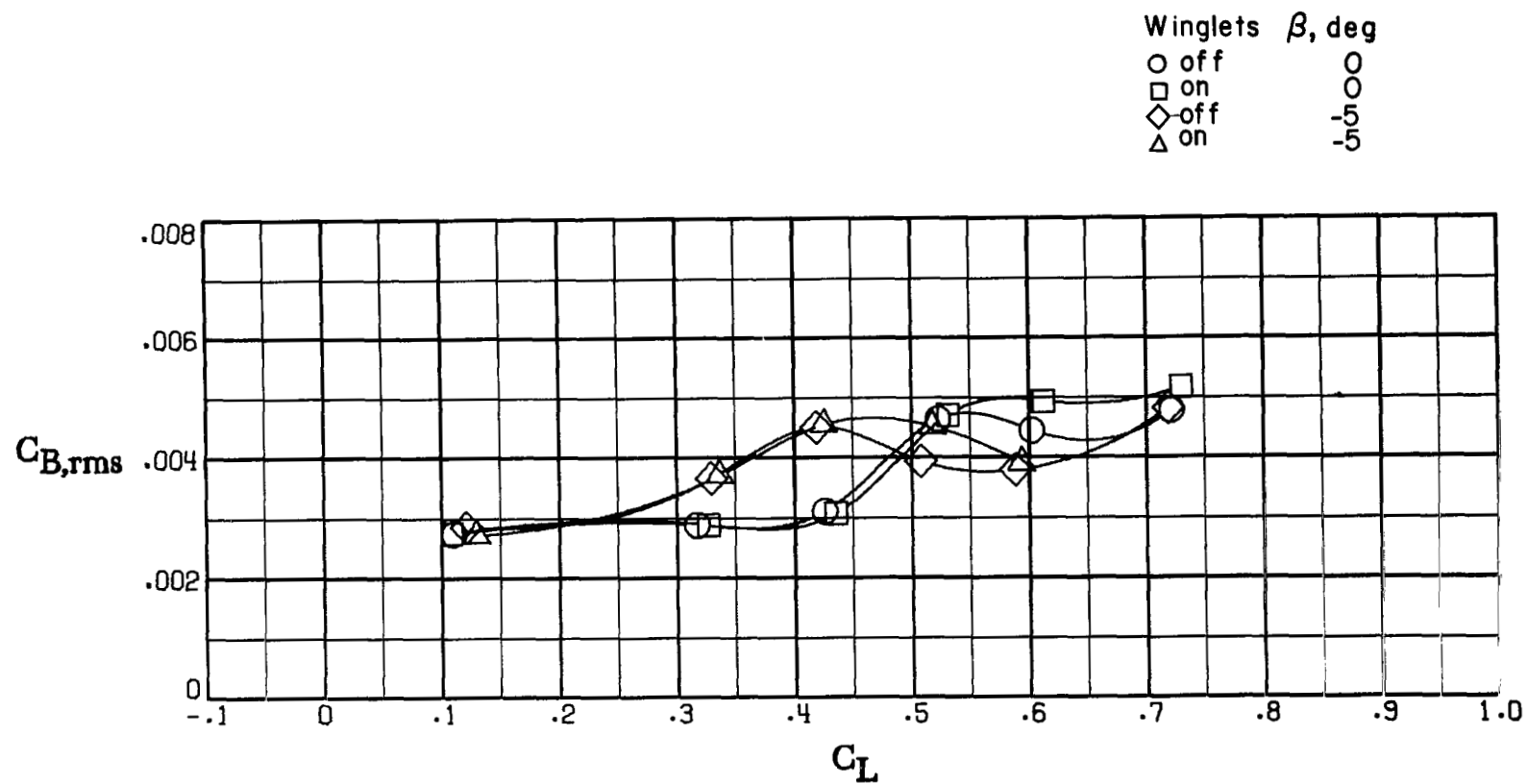| Winglets	β, deg
○ off	0
▢ on	0
◇ off	-5
△ on	-5

(b) $M_\infty = 0.70$; $R = 18.7 \times 10^6$ per m (5.7×10^6 per ft).
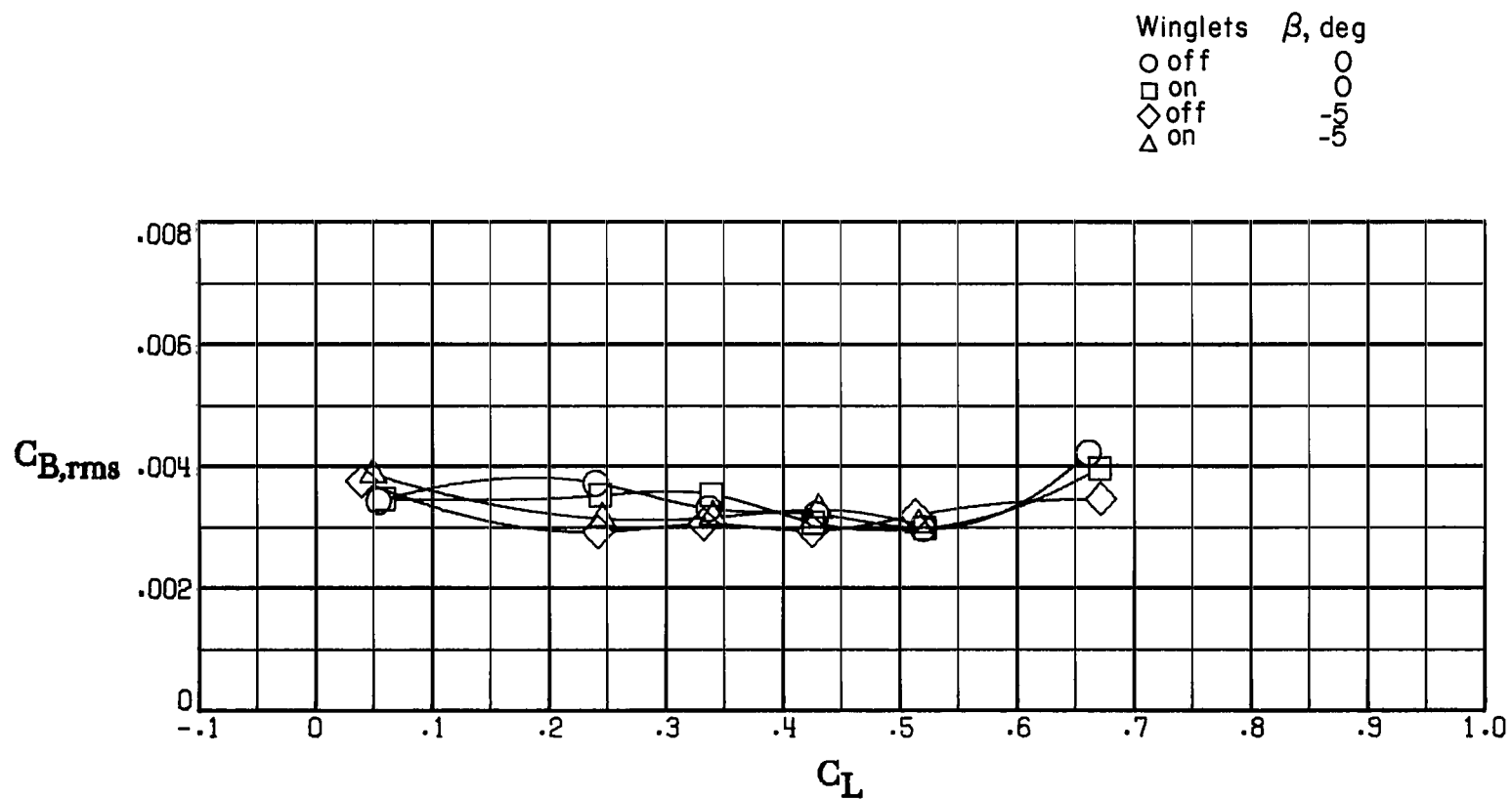
Figure 11.- Continued.

(c) $M_\infty = 0.78$; $R = 17.1 \times 10^6$ per m $(5.2 \times 10^6$ per ft).
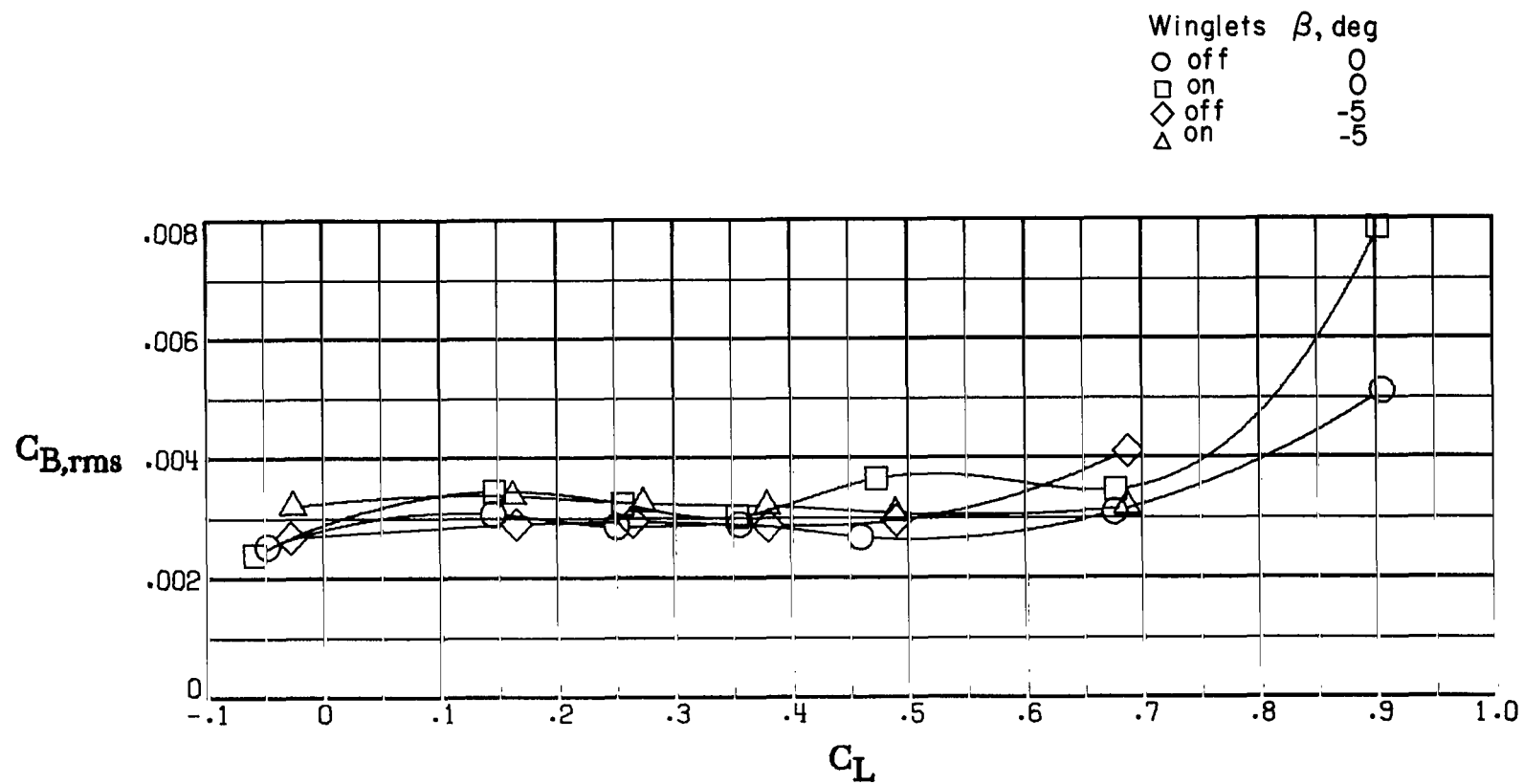
Figure 11.- Continued.

(d) $M_\infty = 0.82$; $R = 16.7 \times 10^6$ per m $(5.1 \times 10^6$ per ft).

Figure 11.- Continued.

(e) $M_\infty = 0.90$; $R = 15.7 \times 10^6$ per m $(4.8 \times 10^6$ per ft$)$.

Figure 11.- Continued.

(f) $M_\infty = 0.95$; $R = 12.5 \times 10^6$ per m $(3.8 \times 10^6$ per ft$)$.

Figure 11.- Concluded.

1. Report No. NASA TP-1163	2. Government Accession No.	3. Recipient's Catalog No.
4. Title and Subtitle EFFECT OF WINGLETS ON A FIRST-GENERATION JET TRANSPORT WING. V - STABILITY CHARACTERISTICS OF A FULL-SPAN WING WITH A GENERALIZED FUSELAGE AT HIGH SUBSONIC SPEEDS		5. Report Date March 1978
		6. Performing Organization Code
7. Author(s) Peter F. Jacobs		8. Performing Organization Report No. L-11982
9. Performing Organization Name and Address NASA Langley Research Center Hampton, VA 23665		10. Work Unit No. 505-11-13-02
		11. Contract or Grant No.
12. Sponsoring Agency Name and Address National Aeronautics and Space Administration Washington, DC 20546		13. Type of Report and Period Covered Technical Paper
		14. Sponsoring Agency Code

15. Supplementary Notes

16. Abstract

This paper presents the effects of winglets on the static aerodynamic stability characteristics of a KC-135A jet transport model at high subsonic speeds. The investigation was conducted in the Langley 8-foot transonic pressure tunnel using 0.035-scale wing panels mounted on a generalized research fuselage.

Data were taken over a Mach number range from 0.50 to 0.95 at angles of attack ranging from -12° to 20° and sideslip angles of 0°, 5°, and -5°. The model was tested at two Reynolds number ranges to achieve a wide angle-of-attack range and to determine the effect of Reynolds number on stability.

Results of the investigation indicate that adding the winglets to the basic-wing configuration produces small increases in both lateral and longitudinal aerodynamic stability and that the model stability increases slightly with Reynolds number. The winglets do increase the wing bending moments slightly, but the buffet onset characteristics of the model are not affected by the winglets.

17. Key Words (Suggested by Author(s)) Winglets Induced drag Drag due to lift Stability	18. Distribution Statement Unclassified - Unlimited Subject Category 02		
19. Security Classif. (of this report) Unclassified	20. Security Classif. (of this page) Unclassified	21. No. of Pages 68	22. Price* $5.25

THIRD-CLASS BULK RATE

2   1 1U,A,   031378 S00903DS
DEPT OF THE AIR FORCE
AF WEAPONS LABORATORY
ATTN: TECHNICAL LIBRARY (SUL)
KIRTLAND AFB NM 87117

NASA

erable (Section 158
Postal Manual) Do Not Return